Þekkingarnet Þingeyinga

NorthQuake 2022

The 4th International Workshop on Earthquakes in North Iceland

Húsavík 18-20 October 2022

December 2022

Desember 2022

Útgefandi/Publisher: Þekkingarnet Þingeyinga / Husavik Academic Centre

Forsíðumynd(Frontpage picture):

Húsavíkurhöfn /Húsavík Harbour. Mynd / Photo: Rafnar Orri Gunnlaugsson

Ábyrgð/Director:
Óli Halldórsson

Ritstjórn/Editors:
Sigurjón Jónsson, Benedikt Halldórsson, Helena Eydís Ingólfsdóttir

ISBN 978-9935-405-70-8

Contents

Inngangur

Undirbúningur og styrktaraðilar

Frumkvæði að ráðstefnunni kom frá sömu aðilum og höfðu frumkvæði að fyrri ráðstefnum. Fræðilegur undirbúningur ráðstefnunnar var í höndum undirbúningsnefndar sem var svona skipuð:

- Sigurjón Jónsson, nefndarformaður, KAUST (sigurjon.jonsson@kaust.edu.sa)
- Benedikt Halldórsson, Háskóli Íslands og Veðurstofa Íslands (skykkur@hi.is)
- Kristín Jónsdóttir, Veðurstofa Íslands (kristin.jonsdottir@vedur.is)
- Páll Einarsson, Háskóli Íslands, (palli@hi.is)

Þekkingarnet Þingeyinga sá um skipulag og framkvæmd ráðstefnunnar í samstarfi við undirbúningnefndina. Fyrir hönd Þekkingarnetsins unnu Helena Eydís Ingólfsdóttir og Huld Hafliðadóttir, að undirbúningi, kynningu og framkvæmd ráðstefnunnar sem og að frágangi þessa ráðstefnurits.

Eftirtaldir aðilar styrktu ráðstefnuhaldið: Síminn, Forsætisráðuneytið, Náttúruhamfaratrygging Íslands, Norðurþing, Veðurstofa Íslands, Landsvirkjun, PCC BakkiSilicon, Landsnet, Sparisjóður Suður Þingeyinga, Warm Arctic ehf.

Um ráðstefnuritið

Þetta ráðstefnurit samanstendur af ágripum og stuttum greinum um það efni sem fjallað var um í erindum á ráðstefnunni. Alls voru 26 erindi á ráðstefnunni þá þrjá daga sem fyrirlestrahaldið stóð.

Ef vitnað er til ágripa í þessu ráðstefnuriti má gera það eins og í dæmunum hér að neðan:

Renier Viltres, Hannes Vasyura-Bathke and Sigurjón Jónsson. Earthquake source estimation of the main events of the 2020 North Iceland earthquake sequence. Í ágripahefti Northquake 2022 ráðstefnunnar, Sigurjón Jónsson o.fl. (ritstj.). Þekkingarnet Þingeyinga, 19-23, 2022.

eða

Viltres, R., H. V. Bathke and S. Jónsson, Earthquake source estimation of the main events of the 2020 North Iceland earthquake sequence. In Proceedings of the NorthQuake 2022 workshop (Ed. S. Jónsson et al.), Húsavík Academic Centre,19-23, 2022.

Introduction

Preparation and support

The members of the scientific committee for the Northquake 2019 workshop were:

- Sigurjón Jónsson, KAUST (sigurjon.jonsson@kaust.edu.sa)
- Benedikt Halldórsson, Univ. of Iceland & the Icelandic Met Office (skykkur@hi.is)
- Kristín Jónsdóttir, The Icelandic Met Office (kristin.jonsdottir@vedur.is)
- Páll Einarsson, University of Iceland, (palli@hi.is)

The Húsavík Academic Centre planned, advertised and ran the workshop together with the scientific committee, as well as preparing this workshop proceedings volume. On behalf of the Húsavík Academic Centre, Helena Eydís Ingólfsdóttir and Huld Hafliðadóttir played the main roles in preparing the workshop.

Finacial support for the workshop was provided by the Síminn, Prime Minister Office, The Natural Catastrophe Insurance of Iceland, Norðurþing, The Icelandic Met. Office, Landsvirkjun, PCC BakkiSilicon, Landsent, Sparisjóður Suður Þingeyinga and Warm Arctic ehf.

About the Workshop Proceedings

This workshop proceedings volume consists of extended abstracts of the contributions presented at the Northquake 2022 workshop. A total of 26 contributions were presented during the three days of the workshop.

Citations to abstracts published in this proceedings volume should be as follows:

Name of authors, contribution title. In Proceedings of the NorthQuake 2022 workshop (Ed. S. Jónsson et al.), Húsavík Academic Centre, pp-pp, 2022.

Example: Viltres, R., H. V. Bathke and S. Jónsson, Earthquake source estimation of the main events of the 2020 North Iceland earthquake sequence. In Proceedings of the NorthQuake 2022 workshop (Ed. S. Jónsson et al.), Húsavík Academic Centre, 19-23, 2022.

Workshop program

Monday, 17 October, 2022	
20:00-21:30	**Registration and Icebreaker**

Tuesday, 18 October, 2022	
9:00-10:00	**Registration and Coffee**
10:00-10:20	**NorthQuake 2022 Opening and Introduction**
	Earthquake Geology and Tectonics **Session chairs: Benedikt Halldórsson and Kristín Jónsdóttir**
10:20-10:40	**Investigating Holocene deformation on the Húsavík Flatey Fault** Rémi Matrau, Yann Klinger, Jonathan Harrington, Thorvaldur Thordarson, Ármann Höskuldsson, Esther R. Gudmundsdóttir, Ulas Avsar and Sigurjón Jónsson
10:40-11:00	**Postglacial faulting within the Skjálfandi Bay** Bryndís Brandsdóttir, Robert S. Detrick, Neal W. Driscoll, Jeffrey A. Karson, Gunnar B. Guðmundsson and Kristín Jónsdóttir
11:00-11:20	**Húsavík-Flatey fault behavior and outstanding data gaps based on insight from major strike slip faults** Gregory P. De Pascale
11:20-11:40	**Insights into two decades of continuous and campaign GPS data in North Iceland** Alejandra Barreto, Renier Viltres, Rémi Matrau, Benedikt G. Ófeigsson and Sigurjón Jónsson
11:40-12:00	**Country-wide InSAR mapping and deformation signals observed in North Iceland** Sigurjón Jónsson and Yunmeng Cao
12:00-13:30	**Lunch**
	Earthquake Seismology **Session chairs: Páll Einarsson og Sigurjón Jónsson**
13:30-13:50	**Recent earthquake activity in the Tjörnes Fracture Zone** Kristín Jónsdóttir
13:50-14:10	**Earthquake source estimation of the main events of the 2020 North Iceland earthquake sequence** Renier Viltres, Hannes Vasyura-Bathke and Sigurjón Jónsson
14:10-14:30	**Seismic monitoring of Krafla, Þeistareykir and Námafjall high-temperature geothermal fields, NE-Iceland** Þorbjörg Ágústsdóttir, Egill Á. Gudnason, Rögnvaldur L. Magnússon, Karl Gunnarsson and Anette K. Mortensen
14:30-15:00	**Coffee break**
15:00-15:20	**On Bayesian applications in statistical seismology: Spatial model for earthquake magnitudes** Atefe Darzi, Birgir Hrafnkelsson and Benedikt Halldorsson
15:20-15:40	**A new Bayesian epidemiological spatiotemporal aftershock sequence model the 2000 and 2008 aftershock sequences in Southwest Iceland** Atefe Darzi, Birgir Hrafnkelsson, Benedikt Halldorsson and Kristín S. Vogfjörð
15:40-16:20	**Discussion**
17:00-18:00	**Field trip to Skjólbrekka and Grjóthals for residents of Húsavík (in Icelandic)**

Wednesday, 19 October, 2022	
Engineering Seismology – Physics-based Approaches to Seismic Hazard **Session chairs: Kristín Jónsdóttir and Sigurjón Jónsson**	
9:00 – 9:20	**Towards a physics-based fault system model for the Tjörnes Fracture Zone** Benedikt Halldorsson, Farnaz Bayat, and Milad Kowsari
9:20 – 9:40	**On the exploration of seismic ground motion amplitudes in North Iceland from dynamic rupture modeling of Húsavík-Flatey Fault Zone earthquake scenarios** Bo Li, Alice-Agnes Gabriel, Thomas Ulrich, Claudia Abril, Benedikt Halldorsson, Lukas Krenz and Michael Bader
9:40 – 10:00	**Modeling potential earthquake-tsunami scenarios from earthquake rupture simulations on the Húsavík-Flatey Fault Zone, North Iceland** Fabian Kutschera, Sara Aniko Wirp, Bo Li, Thomas Ulrich, Alice-Agnes Gabriel, Claudia Abril and Benedikt Halldorsson
10:00-10:30	**Coffee break**
10:30 – 10:50	**A new physics-based fault system model for the Southwest Iceland bookshelf zone** Farnaz Bayat, Milad Kowsari and Benedikt Halldorsson
10:50 – 11:10	**Simulation of finite-fault earthquake catalogues for Monte Carlo hazard assessment** Milad Kowsari, Benedikt Halldorsson and Farnaz Bayat
11:10 - 11:30	**Validation of CyberShake in the Southwest Iceland transform zone - towards application in the Tjörnes Fracture Zone** Otilio Rojas, Marisol Monterrubio-Velasco, Juan E. Rodríguez, Scott Callaghan, Benedikt Halldorsson, Claudia Abril, Milad Kowsari, Farnaz Bayat, Kim Olsen and Josep de la Puente
Engineering Seismology – Engineering Approaches to Seismic Hazard **Session chairs: Bjarni Bessason and Páll Einarsson**	
11:40 – 12:00	**The first seismic wave amplification functions for key geological units in Iceland** Benedikt Halldorsson, Sahar Rahpeyma, Birgir Hrafnkelsson and Atefe Darzi
12:00 – 12:20	**New ground motion models for the extreme near-fault region of strike-slip earthquakes** Farnaz Bayat, Milad Kowsari and Benedikt Halldorsson
12:20 – 12:40	**The implications of the new European Seismic Hazard Model 2020 for Iceland** Benedikt Halldorsson, Milad Kowsari, Farnaz Bayat, Claudia Abril, Atefe Darzi, Bjarni Bessason and Jónas Þór Snæbjörnsson
12:40 – 14:10	**Lunch**
13:15 – 14:00	**Panel discussion for local students and career opportunities in engineering and natural sciences (in Icelandic)**
14:10 – 14:40	**Discussions**
15:00 – 17:30	**Field trip to Út-Kinn – Landslides from October 2021 or Skjólbrekka and Grjótháls**

Thursday, 20 October, 2022	
Earthquake Engineering – Seismic Risk and Societal Effects **Session chairs: Benedikt Halldórsson og Sigurjón Jónsson**	
9:00 – 9:20	**Earthquake Desk Exercise** Kristín Jónsdóttir
9:20 – 9:40	**Foundation types of buildings in Húsavík in the context of seismic hazard** Brynjar Örn Arnarson and Benedikt Halldórsson
9:40 – 10:00	**Statistical empirical vulnearbility model for low-rise Icelandic buildings** Bjarni Bessason, Rajesh Rupakhety and Jón Örvar Bjarnason
10:00 – 10:20	**High spatial resolution loss estimation using new vulnerability models for Iceland** Atefe Darzi, Bjarni Bessason, Benedikt Halldorsson, Sergio Molinad, Alireza Kharazian and Mojtaba Moosapoor
10:20 – 10:50	**Coffee break**
10:50 – 11:10	**Numerical modeling of U-shaped Reinforced Concrete Walls** Ching-Yi Tsai, Bjarni Bessason and Rajesh Rupakhety
11:10 – 11:30	**Social resilience in the aftermath of a natural disaster** Tinna Halldórsdóttir
11:30 – 11:50	**Introducing MEDiate Horizon 2021 project in Iceland for Disaster-Resilient Society 2021 and the unique system dynamics approach to multihazard risk management.** Sólveig Þorvaldsdóttir
NorthQuake 2022 – Panel Discussion and Closing **Session chairs: Helena Eydís Ingólfsdóttir and Huld Hafliðadóttir**	
12:00 – 13:00	**Lunch and NorthQuake 2022 Panel Discussion and Closing (in Icelandic)** Sigurjón Jónsson, Benedikt Halldórsson, Kristín Jónsdóttir, Sólveig Þorvaldsdóttir, Katrín Sigurjónsdóttir, Bjarni Bessason

Investigating Holocene deformation on the Húsavík-Flatey Fault

Rémi Matrau[1], Yann Klinger[2], Jonathan Harrington[1], Thorvaldur Thordarson[3], Armann Hoskuldsson[3], Esther R. Gudmundsdottir[3], Laura Parisi[1], Margherita Fittipaldi[1], Ulas Avsar[4] and Sigurjón Jónsson[1]

[1] *King Abdullah University of Science and Technology (KAUST), Thuwal, Saudi Arabia*
[2] *Université de Paris, Institut de Physique du Globe de Paris, CNRS, Paris, France*
[3] *Institute of Earth Sciences, University of Iceland, Reykjavik, Iceland*
[4] *Middle East Technical University (METU), Ankara, Turkey*

The Tjörnes Fracture Zone in northern Iceland is an Oceanic Fracture Zone accommodating the eastward offset of the oceanic ridge over Iceland due to its interaction with the Icelandic mantle plume (*Saemundsson et al, 1974*). The Tjörnes Fracture Zone accommodates 18 mm/yr of plate motion, and is composed of two main lineaments, the Grímsey Oblique Rift to the north, a set of en-echellon, left stepping, normal faults and volcanic systems, and the Húsavík Flatey Fault (HFF) to the south, a 100 km-long strike, right lateral, transform fault, with a normal component due to the obliquity of the fault to spreading direction. Most of the HFF is located offshore, only the 20 km-long easternmost section of the HFF is located onshore (Fig. 1). To search for evidence of past earthquakes on the HFF, we excavated paleoseismological trenches along the fault and we analyzed periglacial landforms and morphologies to constrain the slip rate of the HFF during the Holocene period.

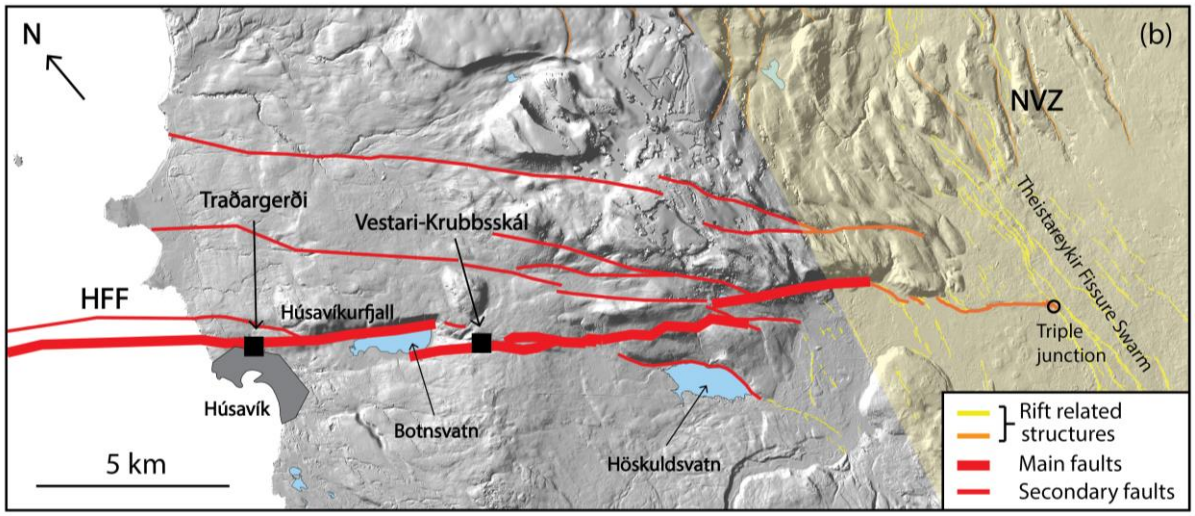

Figure 1: Map of the onshore section of the Húsavík Flatey Fault (HFF). The black squares show the locations of the two study areas.

We excavated a total of 11 trenches in two locations along the HFF, five in Vestari Krubbsskál, a pull-apart basin 5 km east of Húsavík and one in Traðargerði, an alluvial fan directly north of Húsavík (Fig. 1). We used tephras in Vestari Krubbsskál and Traðargerði, together with

birch wood samples from Traðargerði to constrain the timing of past earthquakes. The presence of the tephra layer Askja-S (10800 BP) at the bottom of the trenches suggests that both locations cover the entire Holocene period.

Trenches at both sites show clear dip-slip displacement (Fig. 2), well correlated with their larger scale topographies (pull-apart basin in Vestari Krubbsskál and 45 m-high fault scarp in Traðargerði). However, dip-slip in the context of transform motion is only secondary deformation. The main deformation is accommodated by strike slip motion, which is visible in the trenches in the form of change of thickness of the layers. We mapped layers and faults on all trench walls to identify seismic events and build a catalogue of Holocene earthquakes (Fig. 2). We identified eight events in the last 6000 years, based on upward terminations of cracks and retrodeformations of the layers. Four events are common to the two sites (E1, E1b, E2 and E3), two are only seen in Traðargerði (E2b and E4) and the two youngest events are only seen in Vestari Krubbsskál (E4b and E5).

Figure 2: Field pictures of the excavation of trench Tr1 in Traðargerði. Left. SW looking view of Tr1. Bottom right. NW looking view of Tr1. Top right NW looking view of secondary trenches just east of the main trench Tr1.

Our interpretation of the trench logs yields fewer major earthquakes than expected from the records of the last 300 years. This suggests that large earthquakes (M > 7) are probably rare and the typical earthquakes of the HFF have magnitudes of 6 to 7 (e.g., 1872) producing limited topsoil deformation. Despite some gaps in the earthquake catalogue for the Holocene period, we calculate a return time of the largest earthquake of 500 to 600 years. These gaps could be related to alternating seismic activity, from one structure to another (i.e., Grimsey Oblique Rift and HFF). One lineament accommodates most of the deformation for a period while the other one goes quiet, as illustrated by the slip rate of each structure. In addition, we mapped post glacial morphologies along the HFF, that are offset by faulting activity, and we measured the cumulative displacements of these

offsets. Although we did not directly date these post glacial landforms, our interpretation of these displacements, combined with relative ages, suggests that the Holocene slip rate is slower than the present-day geodetic slip rate (6 to 9 mm/yr.), in the order of 4 to 5 mm/yr.

References

Metzger, S., and S. Jónsson, Plate boundary deformation in North Iceland during 1992–2009 revealed by InSAR time-series analysis and GPS, *Tectonophysics*, **634**, 127-138, https://doi.org/10.1016/j.tecto.2014.07.027, 2014.

Saemundsson, K., Evolution of the axial rifting zone in Northern Iceland and the Tjornes fracture zone. *Bulletin of the Geological Society of America*, **85(4)**, 495-504, 1974.

NorthQuake 2022 - The 4th International Workshop on Earthquakes in North Iceland
Húsavík, North Iceland, 18-20 October 2022

Postglacial faulting within the Skjálfandi Bay

Bryndís Brandsdóttir[1], Robert S. Detrick[2], Neal W. Driscoll[3], Jeffrey A. Karson[4], Gunnar B. Guðmundsson[5] and Kristín Jónsdóttir[5]

[1]*Institute of Earth Sciences, Science Institute, University of Iceland (bryndis@hi.is)*
[2]*Incorporated Research Institutions for Seismology (IRIS), Washington DC, USA*
[3]*Scripps Institute of Oeanography, San Diego, California, USA*
[4]*Department of Earth Sciences, Syracuse University, Syracuse, New York, USA*
[5]*Icelandic Meteorological Office, Reykjavík, Iceland*

The Tjörnes Fracture Zone (TFZ) is a complex transform fault zone linking the Northern Volcanic Zone (NVZ) on land with the offshore Kolbeinsey Ridge. The transform zone is roughly 150 km long (E-W) by 50-75 km wide (N-S) incorporating three major N-S trending pull-apart basins bounded by a complex array of normal and oblique-slip faults. The Skjálfandi Bay is the southern extension of the central basin, Skjálfandadjúp. Seismicity within the Skjálfandi Bay is mostly confined to its western margin and the Húsavík-Flatey fault system (HFFS) across the southern part of the bay. The HFFS extends eastwards into the NVZ and westwards into the southern Eyjafjörður basin. The main strands of the HFFS can be traced offshore from Húsavík across Skjálfandi in both CHIRP and multibeam data as two WNW-trending, south-facing fault scarps. Several smaller WNW-trending faults are located sub-parallel of the main HFFS, many of which are delineated by pockmarks on the seafloor. Pockmark lineaments in northeastern Skjálfandi are elongated NE-SW, and WNW-ESE in the western part of the bay. The NE-SW pockmarks appear to be aligned along sediment covered marginal faults of the Skjálfandi graben whereas the northwestern pockmark field seems to be linked to WNW-ESE –trending strike-slip faults with little or no vertical displacement. The inferred pattern of WNW-ESE strike-slip faults and NE-SW basin-bounding faults matches results from adjacent areas of the Tjörnes Peninsula and Flateyjarskagi. Paleoearthquake records can be derived from high-resolution seismic reflection profiles of active fault-growth sequences where long-term rate of sedimentation exceeds the rate of vertical fault displacement. Dense profiles across strike-slip faults within Skjálfandi indicate both increasing and decreasing vertical slip during several earthquake sequences in the last ~12000 years.

NorthQuake 2022 - The 4th International Workshop on Earthquakes in North Iceland
Húsavík, North Iceland, 18-20 October 2022

Insights into Two Decades of Continuous and Campaign GPS Data in North Iceland

Alejandra Barreto[1], Renier Viltres[2], Rémi Matrau[1], Benedikt G Ófeigsson[3], Sigurjón Jónsson[1]

[1]*Physical Science and Engineering Division, King Abdullah University of Science and Technology, Saudi Arabia. (maria.pereabarreto@kaust.edu.sa)*
[2]*ITES - Institut Terre et Environnement Strasbourg, Université de Strasbourg, Strasbourg, France.*
[3]*Icelandic Meteorological Office, Reykjavík, Iceland.*

The Tjörnes Fracture Zone (TFZ) is one of the two transform zones in Iceland capable of generating earthquakes of magnitude ~7 (Einarsson, 1991; 2008). It is therefore fundamental to assess the seismic hazard that the TFZ poses in North Iceland. Understanding the magnitude and the recurrence of large earthquakes is a starting point for such assessments. Large earthquakes in the TFZ concentrate in its two main sub-parallel structures: the Húsavík-Flatey Fault (HFF) and the Grímsey Oblique Rift (GOR) (Einarsson, 2008). However, accounts from historical earthquakes in the region are limited and information about their locations and sizes are not accurate. The earliest known earthquake in the TFZ occurred in 1262 close to Flatey Island. Other large earthquakes in 1755, 1838, and 1872 took place on the HFF, most likely, but the information is limited (Thorgeirsson, 2011).

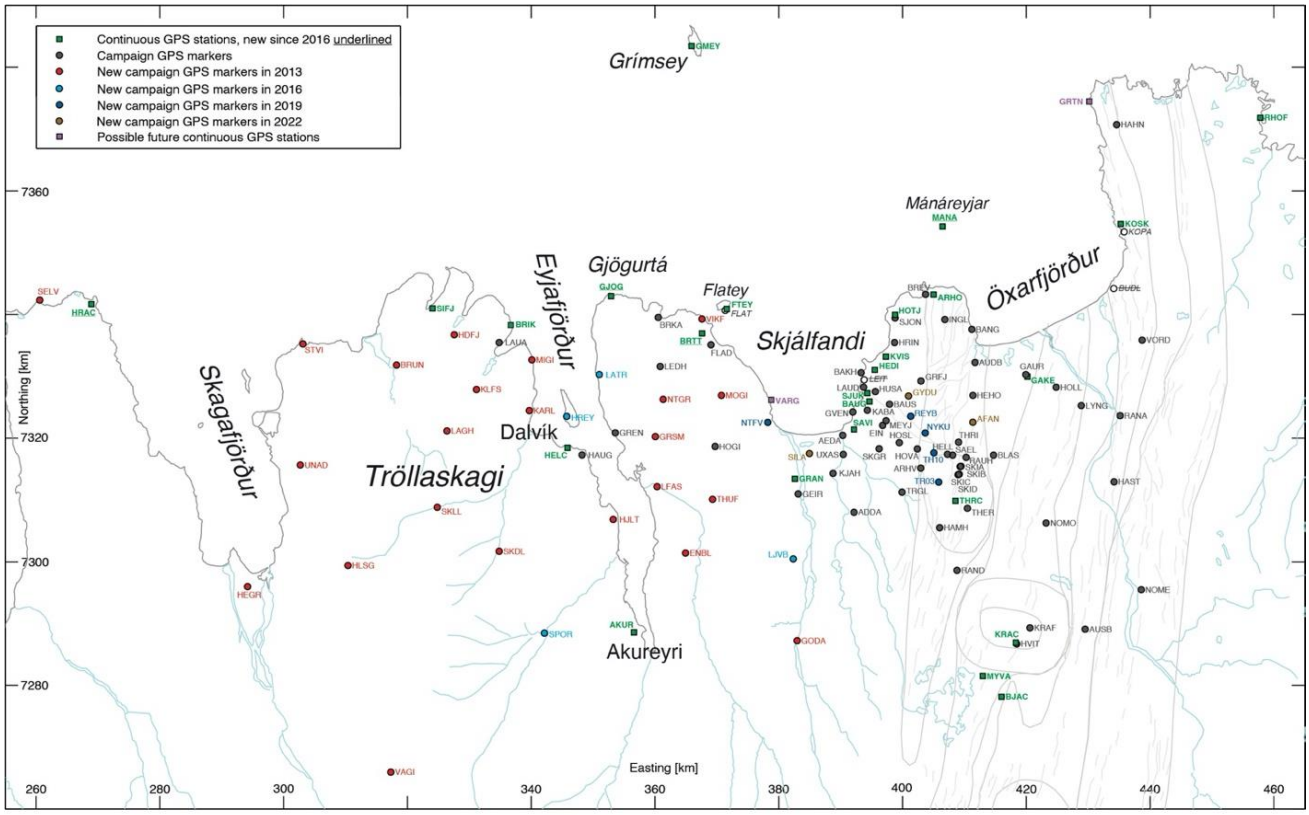

Figure 1. Map of GPS stations in North Iceland. Continuous GPS sites are represented by squares, whereas campaign markers are represented by squares, color-coded by the year they were added to the network.

Therefore, the use of geodetic observations of interseismic strain accumulation plays a key role in constraining the rate of strain accumulation and moment release of the fault zone, consequently providing key inputs for assessing the regional seismic hazard.

Our geodetic GPS network in North Iceland covers an area of roughly 200 km by 130 km in size and includes more than 20 continuous GPS (cGPS) and 92 campaign-style eGPS stations (Fig. 1). The continuous data now span up to ~21 years from 2001 to 2022. The first stations installed were AKUR on the North American (NA) plate and RHOF in Eurasia (EU) in 2001. The last cGPS installations were stations BRTT in Flateyjardalur in 2019 and BRIK in Ólafsfjörður in 2020. The first eGPS network focused on the HFF was put in place in 1995 (*Jouanne et al., 1999*) and since then the network has been expanded towards Tröllaskagi and Skagafjörður and remeasured on several occasions (*Jouanne et al., 2006; Metzger et al., 2013; Metzger and Jónsson, 2014; Jónsson et al., 2016; 2019*). Currently data are available for 1997, 1999, 2002, 2007, 2009, 2010, 2011, 2013, 2016, 2019, and 2022. In addition, several stations within the nationwide ISNET reference station network are also in our study area and ISNET data exist from measurements in 1993, 2004 and 2016 (*Valsson, 2016*).

Here we present the most up to date velocity field for North Iceland combining continuous and campaign data collected until August 2022 (Fig. 2). The velocity field is presented with respect to the NA plate (i.e., the average velocities on the NA plate are set to zero) with velocities gradually increasing towards the east to roughly 18 mm/year (to the ESE) on the EU plate. Velocities just south of the HFF, on the NA plate, are small but show systematic eastward movement that increases as one crosses the HFF near Húsavík. At the northern tip of the Tjörnes peninsula the velocities are rougly at half the total rate seen at the easternmost stations on the EU plate.

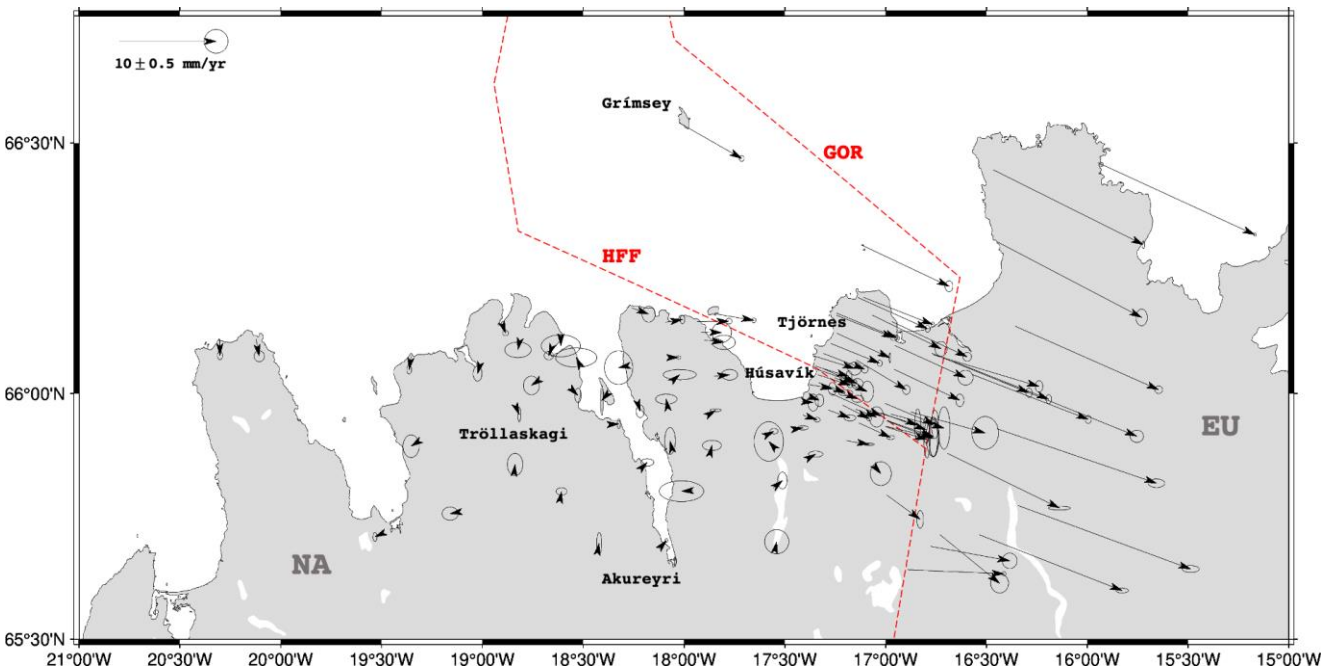

Figure 2. Interseismic GPS velocity vectors for North Iceland using campaign and continuous data for the past 20 years, plotted with respect to the North American plate, with vector ellipses indicating 95% confidence level.

The new results provide the first information about possible internal deformation on Tröllaskagi peninsula, within which the so-called Dalvík Lineament or Dalvík Zone has been proposed.

Significant seismicity occurs south of the HFF in this area and several major earthquakes have taken place, such as the 1934 Dalvík and 1963 Skagafjörður earthquakes (Stefánsson et al., 2008). The GPS velocities in Tröllaskagi, however, do not show clear systematic deformation pattern with relative velocities smaller than 4 mm/year. This indicates that the majority of the moment release is focused on the HFF and GOR, but not to the south of HFF. This appears to suggest that major earthquakes south of the HFF may be less frequent than the earthquake activity in the past 200 years may imply. Longer GPS time-series will help in determining better the low strain rates on Tröllaskagi peninsula.

Our future work includes studying signal transients in the GPS time series and removing them to better isolate the secular tectonic signal, which will improve the network-wide interseismic velocity field in North Iceland. We will then use back-slip and block modeling modeling of the interseismic deformation field to provide updated information about the fault locking depth and slip rate of the HFF. We anticipate the new results will help us address questions regarding the distribution of elastic and inelastic deformation across the TFZ, the partitioning of slip between its main structures, and to further constrain the fault parameters of the HFF.

References

Einarsson, P., Earthquakes and present-day tectonism in Iceland, Tectonophysics **189**, 261-279, 1991.

Einarsson, P., Plate boundaries, rifts and transforms in Iceland, Jökull **58**, 35-58, 2008.

Jónsson, S., S. Metzger & B. Ófeigsson, Rate of moment accumulation on the Húsavík-Flatey Fault from GPS, In: Proc. of the 2nd workshop on earthquakes in North Iceland (ed. R. Stefánsson et al.), Húsavík Academic Centre, 17-19, 2016.

Jónsson, S., R. Matrau, R. Viltres & B. Ófeigsson, An update of GPS measurements in North Iceland, In: Proc. of the NorthQuake 2019 workshop (ed. S. Jónsson et al), Húsavík Academic Centre, 107-110, 2019.

Jouanne, F., T. Villemin, V. Ferber, C. Maveyraud, J. Ammann, O. Henriot & J.L. Got, Seismic risk at the rift-transform junction in North Iceland, Geophys. Res. Lett., **26**, 3689-3692, 1999.

Jouanne, F., T. Villemin, A. Berger & O. Henriot, Rift-transform junction in North Iceland: rigid blocks and narrow accommodation zones revealed by GPS 1997-1999-2002, Geophys. J. Int., **167**, 1439-1446, 2006.

Metzger, S., S. Jónsson and H. Geirsson, Locking depth and slip-rate of the Húsavík Flatey fault, North Iceland, derived from continuous GPS data 2006-2010, Geophys. J. Int., **187**, 564-576, 2011.

Metzger, S., S. Jónsson, G. Danielsen, S. Hreinsdóttir, F. Jouanne, G. Giardini, T. Villemin, Present kinematics of the Tjörnes Fracture Zone, North Iceland, from campaign and continuous GPS measurements, Geophys. J. Int. **192**, 441-455, 2013.

Metzger, S. and S. Jónsson, Plate boundary deformation in North Iceland during 1992-2009 revealed by InSAR time-series analysis and GPS, Tectonophysics **634**, 127-138, 2014.

Stefánsson, R., G.B. Gudmundsson & P. Halldórsson, Tjörnes Fracture Zone. New and old seismic evidences for the link between the North Iceland rift zone and the Mid-Atlantic ridge, *Tectonophysics*, **447**, 117-126, 2008.

Thorgeirsson, Ó., Historical earthquakes in North Iceland (in Icelandic), Húsavík Academic Centre report, 54pp, 2011.

Valsson, G.Þ., Results from the ISNET2016 campaign and a new dynamic reference frame for Iceland (in Icelandic, with English summary), The Land Survey of Iceland, 66pp, 2016.

NorthQuake 2022 - The 4th International Workshop on Earthquakes in North Iceland
Húsavík, North Iceland, 18-20 October 2022

Country-wide InSAR Mapping of Iceland and Deformation Signals Observed in North Iceland

Sigurjón Jónsson[1] and Yunmeng Cao[1,2]

[1]*King Abdullah University of Science and Technology (KAUST), Saudi Arabia (sigurjon.jonsson@kaust.edu.sa)*
[2]*Now at GNS, New Zealand*

Large-scale deformation mapping with Interferometric Synthetic Aperture Radar (InSAR) has become feasible with more frequent and regular satellite radar data acquisitions and developments in data processing methods. InSAR deformation mapping of entire countries, using multiple years of data, are increasingly being produced for mapping tectonic deformation, subsidence due to groundwater pumping, and creeping landslides, e.g., in Turkey (*Weiss et al.*, 2020), Italy (e.g., *Zinno et al.*, 2020), and Norway (*Dehls et al.*, 2019). Countrywide deformation mapping of Iceland from InSAR was first reported by *Drouin & Sigmundsson* (2019) using four years (2015-2018) of Sentinel-1 radar data. We improve on these results by using seven years of data (2015-2021), by reducing atmospheric signals using a two-step correction approach (*Cao et al.* 2021), and by employing more advanced processing methods, yielding full displacement time-series, instead of just average velocities (*Cao et al.*, 2022).

The InSAR data processing consisted of selecting all the available Sentinel-1 radar data from three parallel and overlapping descending and three parallel and overlapping ascending orbit tracks, yielding complete countrywide coverage for both look directions. To avoid winter snow, only data acquired during Summer and Fall months (May-October) for the years 2015 to 2021 were selected. The total number of satellite passes for each of the six orbit tracks is about 170, meaning that over 1000 data sets were used, from which we processed about 8700 interferograms. Due to the quantity of data, we multilooked the interferograms to about 100 m × 100 m pixels and solved for the time-series of each of the six data sets, which involved SBAS time series processing of the data from each year, with careful bridging of data between successive years. Atmospheric signals were reduced in the InSAR data by carefully interpolating information from global atmospheric models according to the methods of *Cao et al.* (2021). In the next step of the analysis, we inverted for near-east and near-vertical time-series, using all the available information (2-4 data sets at each location), assuming that north ground displacements are minimal. The resulting average near-east ground velocities are shown in Fig. 1.

Large-scale deformation in Iceland is dominated by plate motion between the North-American and Eurasian plates and by glacio-isostatic adjustment. The east displacement rates clearly show the location of the plate boundary between the two plates from Reykjanes, through the South Iceland Seismic Zone, and the Eastern and Northern Volcanic Zones. The width of the plate-boundary zone varies from being relatively narrow in Reykjanes to more distributed deformation in the Eastern Volcanic Zone. The glacio-isostatic uplift reaches a maximum of 3 cm/year in central Iceland and appears to accelerate during the observation period (*Cao et al.*, 2022).

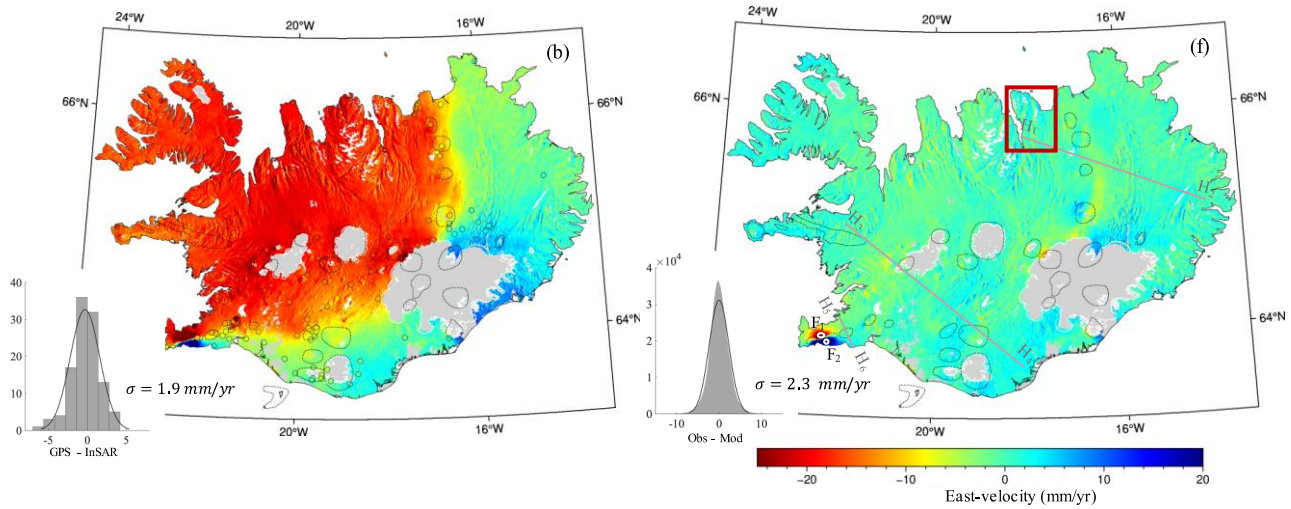

Figure 1. Left: Observed near-east displacement rates (2015-2021) with respect to the Eurasian plate. The histogram shows comparisons with east velocities at continuous GPS stations (circles). Right: Residual near-east displacement rates after removing modelled plate motions and glacio-isostatic adjustment rates. The histogram shows the residual distribution with standard deviation of 2.3 mm/year. Red rectangle shows the area covered in Fig. 2.

We can explain almost all of the large-scale deformation with a model of the plate motion, plate-boundary deformation and glacio-isostatic adjustment (Fig. 1). In northern Iceland, the plate boundary deformation is well modelled although the data do not provide much resolution of the deformation around the Húsavík-Flatey fault. To capture its interseismic deformation, the local GPS measurements provide better constraints (*Metzger and Jónsson*, 2014; *Barreto et al.*, 2022). Only local deformation signals remain in the residual displacement rate map (Fig. 1), most notably related to the Fagradalsfjall intrusion activity in Reykjanes in 2021. In addition, several central volcanoes (such as Torfajökull and Askja) and geothermal areas (such as Hellisheiði and Nesjavellir) exhibit significant displacements, some of which are transient during the observation period.

Widespread slope movements are also evident in the residual deformation map (Fig. 1). Almost all east-facing slopes are moving eastward and west-facing slopes westward. This deformation is seen all over Iceland where there are significant slopes and amounts to a few mm/year. At first, one might expect that these signals have something with due do with inaccuracies in the data processing, e.g., due to errors in the digital elevation model (DEM) or due to mis-alignment of the DEM and the radar data. However, the deformation map is produced from six independent data sets, each covering different parts of the country, so DEM related problems or processing issues cannot explain the observed deformation patters. The results therefore show that slope movements occur on all over Iceland, most likely due to relatively stable soil and landslide creep.

The slope movements are found in both geologically younger and older parts of Iceland. For example, they can be seen in the Western Fjords, in Esja and Skarðsheiði in southwestern Iceland, and in Húnavatnssýslur, Skagafjörður and Tröllaskagi in North Iceland (Fig. 1). They are not as clearly visible in the Eastern Fjords of Iceland, as most slopes in this region are either north- or south-facing, meaning the near-east displacement map does not capture the slope-parallel motion. They are, however, clearly seen in Fljótsdalshérað in eastern Iceland and on mountain ridges east of the Northern Volcanic Zone.

Near the Húsavík-Flatey fault, the most notable slope motions are seen on Flateyjarskagi,

the peninsula between Eyjafjörður and Skjálfandi Bay (Fig. 2). The peninsula has two major north-trending valleys, Fjörður and Flateyjardalur and west-facing slopes of these valleys, as well as Látraströnd on the eastern side of Eyjafjörður, show systematic westward motion. Similarly, the east-facing slopes of the valleys and slopes in Út-Kinn and Náttfaravíkur, on the eastern side of the peninsula, clearly have eastward motion. The motion is commonly 5-10 mm/year on many of the slopes and does not show strong seasonality, although this is not well resolved by the InSAR data, which only include data from Summer and Fall. Somewhat higher displacement rates are found on known landslides (>10 mm/year), such as on the Yzta-Vík landslide in Eyjafjörður (*Jónsson,* 2008).

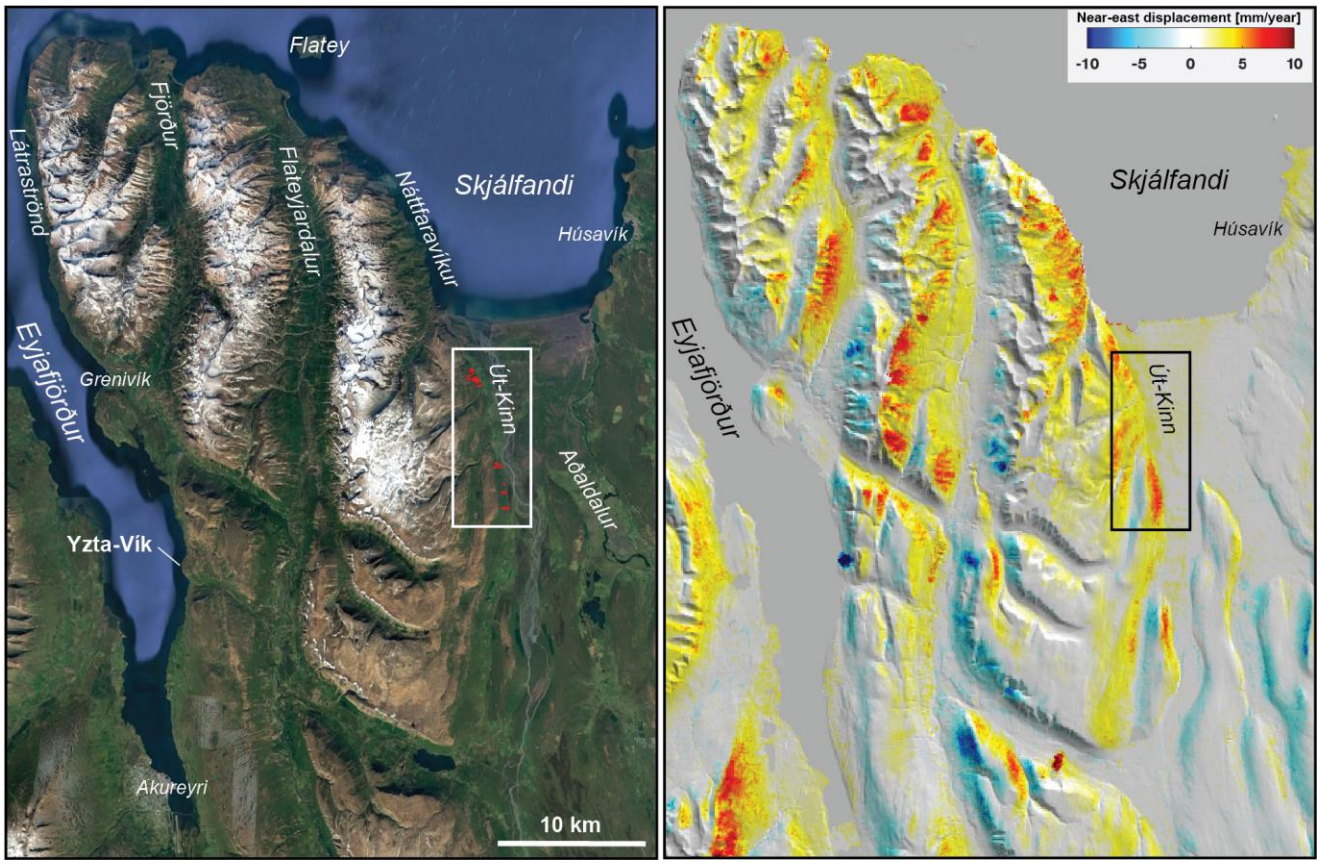

Figure 2. Slope movements in Flateyjarskagi between Eyjafjörður and Skjálfandi Bay. Left: Google Earth image with the main valleys and place names indicated and the Út-Kinn (box) landslides marked in red. Right: Near-east velocities after removing effects of plate motions, showing 5-10 mm/year slope creep on many east- and west-facing slopes.

The area of Út-Kinn was hit by unusual amount of local rain fall in early October 2021, resulting in several slope failures on vegetated and soil-covered slopes, leaving behind barren bedrock slopes and piles of mud and debris at the foot of the affected slopes, covering the farm lands below. Luckily the mudslides did not cause any injuries or significant structural damage. The radar data span several years before the slope failures í Út-Kinn and they show widespread slope motion, like on many other slopes in Iceland. However, the exact areas of the slope failures in Fall of 2021 do not show up as moving any faster than other slopes in the area or any anomalous motion during the years before the slope failures. There is nothing in the radar data that point to the exact locations that failed and all of the east-facing slopes appear to have been equally likely to fail, if the steady motion observed in the InSAR data is taken as indicative of potential future sudden slope failure if exposed to intensive rain.

In Summary, our results show that InSAR data are effective to map country-wide ground velocities and velocity changes as well as local deformation signals and transients at volcanoes and geothermal areas. The results also show that slopes all over Iceland are subject to steady gravitational soil creep amounting to several mm/year, with higher rates observed in many areas where geomorphologically landslides can be identified in the landscape.

References

Barreto, A., R. Viltres, R. Matrau, B.G. Ófeigsson & S. Jónsson, Insights into two decades of continuous and campaign GPS data in North Iceland, In *Proc. to the NorthQuake 2022 workshop* (this volume), 2022.

Cao, Y., S. Jónsson & Z. Li, Advanced InSAR tropospheric corrections from global atmospheric models that incorporate spatial stochastic properties of the troposphere, *J. Geophys. Res.*, **126**, e2020JB020952, 2021.

Cao, Y., S. Jónsson, & S. Hreinsdóttir, P., Iceland kinematics from InSAR, *J. Geophys. Res. (submitted)*, 2022.

Dehls, J.F., Y. Larsen, P. Marinkovic, T. R. Lauknes, D. Stodle, & D. A. Moldestad, A national InSAR deformation mapping/monitoring service in Norway – from concept to operations. In proc. to *IGARSS 2019*, 5461-5464, 2019.

Drouin, V., & F. Sigmundsson, Countrywide observations of plate spreading and glacial isostatic adjustment in Iceland inferred by Sentinel-1 radar interferometry, *Geophys. Res. Lett.*, **46**, 8046-8055, 2019.

Jónsson, S., *A survey of active landslide movement in central-north Iceland from satellite radar interferometry*, Icel. Met. Office report, 75pp, 2008.

Metzger, S. & S. Jónsson, Plate boundary deformation in North Iceland during 1992-2009 revealed by InSAR time-series analysis and GPS, *Tectonophysics* **634**, 127-138, 2014.

Weiss, J.R. et al., High-resolution surface velocities and strain for Anatolia from Sentinel-1 InSAR and GNSS data, *Geophys. Res. Lett.*, **47**, e2020GL087376, 2020.

Zinno, I. et al., National scale surface deformation time series generation through advanced DInSAR processing of Sentinel-1 data within a cloud computing environment, *IEEE Trans. on Big Data*, **6(3)**, 558-571, 2020.

Recent earthquake activity in the Tjörnes Fracture Zone

Kristín Jónsdóttir

[1] *Icelandic Meteorological Office*

The Natural Hazards Monitoring at the Icelandic Meteorological Office (IMO) operates 24/7 to be able to respond to crises such as the onset of a volcanic eruption or a significant earthquake. A seismic bulletin of last week's countrywide reviewed earthquake activity is released every Tuesday from IMO.

There has been considerable earthquake activity in Northern Iceland and the Tjörnes Fracture Zone (TFZ) in recent years. Since 2019, there have been three major earthquake swarms: Between the 15th of march and 15th of April in 2019 in Öxarfjörður west of Kópasker; 19th of June to 19th of October in 2020 at the junction of the Eyjafjörður Graben and the Húsavík-Flatey Fault and in September 2022 east of Grímsey. The most significant earthquake occurred on the 21st of June in 2020 during the seismic crises in the Eyjafjarðaráll graben. Being only 27 km north of Tröllaskagi Peninsula it was widely felt in northern Iceland, triggered landslides but caused only minor damage. This event is the largest event ever recorded with the SIL seismic network (national digital seismic network). The earthquake swarms in the TFZ are signified by intense seismicity with many events of similar size and repeated main shock – aftershock type activity. Sometimes a clear migration of seismicity is seen along the faults.

There are clear synergies between the Grímsey Oblique Rift (GOR) and the Reykjanes Oblique Rift. Thus, it is important to pay attention to the lessons learned during recent unrest on the Reykjanes Peninsula, where repeated magma intrusions and widespread earthquake activity was observed. One important outcome is that earthquake locations can be tricky to interpret when it comes to intrusive activity, as they may be the result of stress triggering on tectonic faults up to tens of kilometers away from the intrusion itself. In order to identify any patterns of stress triggering (e.g. caused by magma intrusions) on the GOR, improved precision of earthquake locations are needed at IMO.

A new study diving into the Surtsey eruption tremor, recorded on old seismographs in the seventies, shows that the submarine eruption triggered strong enough tremor to be recorded up to 137 km away from the eruption. This is an important finding for the operational monitoring of submarine volcanoes. Given that the strength of the Surtseyjan tremor is a common feature, the SIL seismic network should capably record any eruption tremor from the volcanic systems on the GOR.

NorthQuake 2022 - The 4th International Workshop on Earthquakes in North Iceland
Húsavík, North Iceland, 18-20 October 2022

Earthquake source estimation of the main events of the 2020 North Iceland earthquake sequence

Renier Viltres[1], Hannes Vasyura-Bathke[2], and Sigurjón Jónsson[3]

[1]*Institut Terre et Environnement de Strasbourg (ITES), Université de Strasbourg, France (renierldgv@unistra.fr)*
[2]*GFZ German Research Centre for Geosciences, Telegrafenberg, 14473 Potsdam, Germany (vasbath@gfz-potsdam.de)*
[3]*King Abdullah University of Science and Technology (KAUST), Saudi Arabia (sigurjon.jonsson@kaust.edu.sa)*

North Iceland was rocked in June 2020 by the most powerful earthquake sequence since the 1976 M6.2 Kópasker earthquake occurred at the start of the Krafla rifting episode (*Stefánsson et al.*, 2019). The offshore earthquake sequence started on June 19th, 2020, with more than 7000 events recorded within the first week (*IMO*, 2020). Similar to other seismic swarms in the area, the earthquake activity was characterized by a lack of a clear mainshock-aftershock pattern (*Jónsdóttir et al.*, 2020). The swarm accounted for three events of magnitude above M5.0, one of them of M6.0, and triggered intense rockfall in the neighboring coastal area (*IMO*, 2020; Fig. 1). Furthermore, the mainshocks not only radiated seismic energy that was recorded at teleseismic distances but also produced measurable static offsets at GPS stations located in North Iceland (Fig. 2a).

Two of the largest events (M5.4, M5.7) occurred ~4h apart on June 20th and were located close to the junction of the Húsavík-Flatey fault (HFF) and Eyjafjarðaráll graben (Fig. 1a). The largest earthquake of magnitude M6.0 struck on the following day and was located ~35 km to the NE of Siglufjörður (*IMO*, 2020; Fig. 1a). The earthquake activity suggests a tectonic origin for the main events of the sequence, with faulting within two distinct tectonic settings, i.e., WNW-ESE oriented right-lateral (or N-S oriented left-lateral) strike-slip for the first two large earthquakes and N-S oriented normal faulting for the M6.0 earthquake. However, the offshore location of the events in addition to the limitation of distinguishing between fault planes using waveform data makes it difficult to constrain the orientation and geometry parameters of the rupturing source faults. In addition, seismic swarms can often precede large earthquakes in this area and may release a significant amount of the strain aseismically (*Passarelli et al.*, 2018). Therefore, good constraints on the tectonic structures involved and quantification of the ratio of seismic/aseismic energy release are crucial for the seismic hazard assessment of Húsavík and other communities in North Iceland.

Here we estimate the source parameters of the three main events of the June 2020 earthquake sequence by combining GPS-derived coseismic offsets with teleseismic waveforms using Bayesian inference. The datasets include measurements from 20 continuous and 10 survey GPS stations from the North Iceland geodetic network (*Barreto et al.*, 2022) and seismic waveform recordings from stations located at distances up to 4000 km from the earthquakes (Fig. 2).

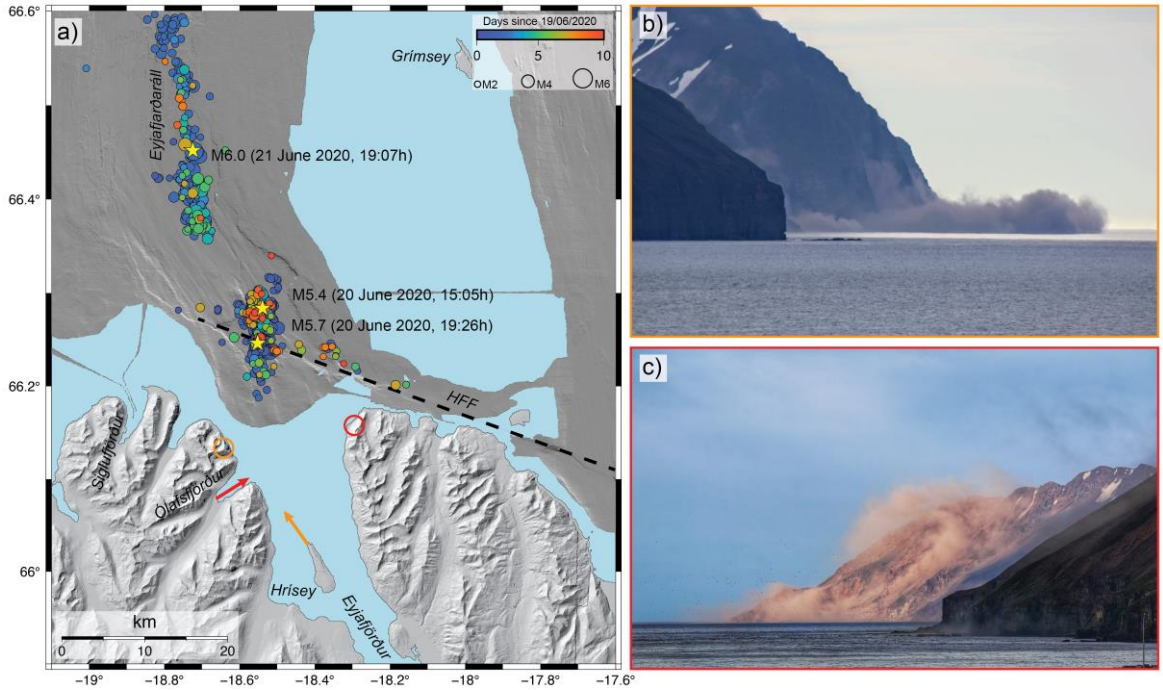

Figure 1. a) Locations of earthquakes of magnitude 2.0 and above nucleating during the first 10 days of the 2020 North Iceland earthquake sequence (Icelandic Met Office) with the three main events marked as yellow stars. B, c) Photographs of rockfall triggered by the magnitude 5.7 earthquake on June 20th. Circles and arrows in a) show the location of the rockfall and the looking directions from where the pictures were taken on Hrísey Island (by Unnur Sæmundsdóttir) and in Ólafsfjörður (by Sigurgeir Haraldsson), respectively.

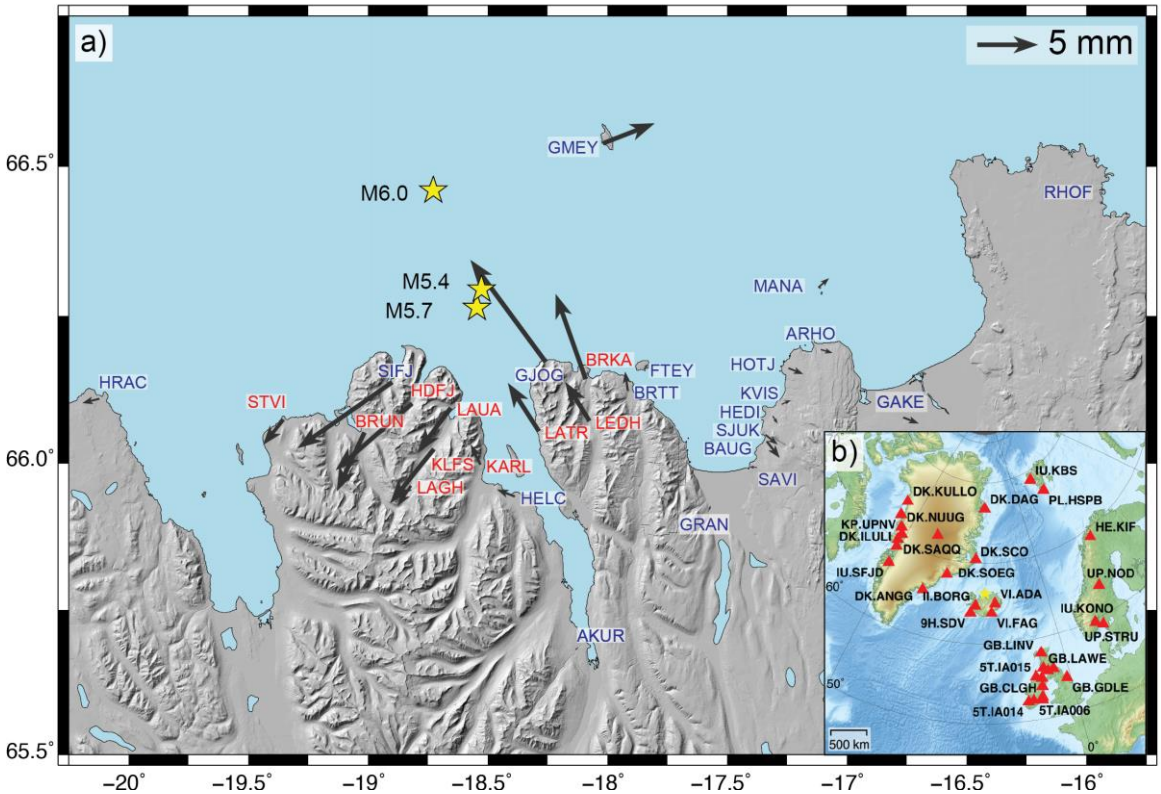

Figure 2. Cumulative coseismic displacements (black vectors) at continuous (blue-labels) and survey (red-labels) GPS stations for the three main events of the earthquake sequence. b) Locations of seismic stations used in this study.

We used the GAMIT/GLOBK analysis software (*Herring et al.*, 2018) to produce daily

station position time series from the geodetic GPS data following the first two steps described by *Floyd et al.* (2010) and *Kogan et al.* (2012). Previous to the coseismic offset estimation, outliers were removed from the time series using the 3-σ rule, and then a trajectory model containing a linear trend and a Heaviside step-function term at the averaged date of the three main earthquakes (*Equation* 1) was fitted to each of the horizontal components:

$$P(t) = a + b \cdot t + c_i \cdot H(t - t_i) + \varepsilon(t) \quad (1)$$

The trajectory model parameter estimation was performed using the Hector software package (*Bos et al.,* 2013) assuming that the noise within the GPS time series was well described by a combination of white and flicker components. For each event, we selected P waveforms providing the best signal-to-noise ratio and azimuthal coverage from an initial pool of 73 seismic stations (Fig. 2b). The raw waveforms were then resituated to true ground velocity, rotated into the radial (R), transverse (T), and vertical (Z) components, and bandpass-filtered from 100s to 10s to decrease high-frequency noise effects (*Steinberg et al.,* 2020). For the earthquake source model parameter estimation, the vertical component (Z) was used to fit the P waveforms and non-Toeplitz covariance matrices were adopted to better account for measurement and theory errors (*Dettmer et al.,* 2007; *Vasyura-Bathke et al.,* 2021). Before the Bayesian inference, Green's function stores were precalculated to ensure numerical efficiency when creating synthetic observations for any given source-receiver configuration. In this step, we used the PSGRN/PSCMP (*Wang et al.,* 2006) and the QSSP (*Wang et al.,* 2017) software packages for the static and transient data, respectively, and used an updated local velocity model defined after *Abril et al.* (2021).

We estimated the earthquake source parameters using both double-couple and finite-fault sources. Our double-couple solutions are generally consistent with previous estimates, i.e., from the Icelandic Meteorological Office (IMO) and the Global Centroid Moment Tensor (GCMT) catalogue. However, our estimated magnitudes and event depths are systematically smaller compared with the IMO and GCMT solutions, particularly for the M5.4 and M5.7 events (Fig. 1a, Fig. 3). Shallow event depths of 4-9 km probably result from the use of a local velocity model in our Bayesian inference and are significantly shallower than the event depths of 9-10 km in the IMO data and the fixed depths of 12 km in the GCMT catalogue. For the largest earthquake of the sequence (M6.0, 21/06/2020) we note that the best double-couple solution is sensitive to the seismic/geodetic station selection, suggesting a non-double-couple component that needs further consideration. The estimated earthquake magnitudes using seismic + geodetic data require a larger moment release for the second event of the sequence (M5.7), compared with the solution obtained using seismic data alone. Since the GPS-derived coseismic offsets include the combined effects of the major events, this result may indicate that a part of the moment was released aseismically. Furthermore, the geodetic data do not resolve well whether the M5.4 and M5.7 earthquakes occurred on WNW-ESE striking faults, similar to the HFF, or on SSW-NNE striking conjugate faults. The trend of some of the events during the sequence, in particular after the M5.7 earthquake (see *IMO*, 2020, Fig. 1a), suggests that the second mainshock occurred on a SSW-NNE striking fault. Similarly, the data do not uniquely determine whether the M6.0 normal-faulting earthquake occurred on a west- or east-dipping fault, although its location on the east flank of the Eyjafjarðaráll graben indicates that the source fault dips to the west.

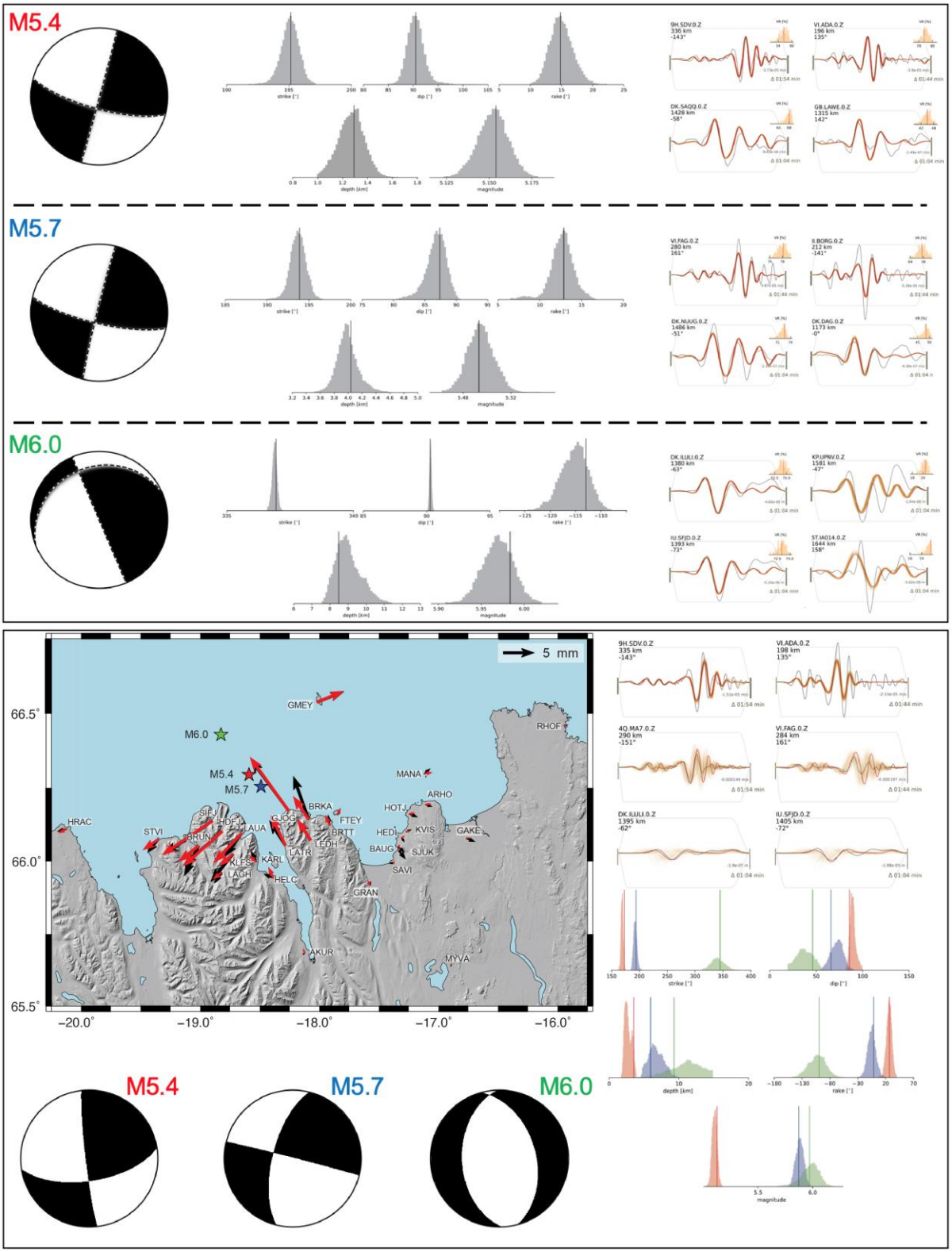

Figure 3. Estimated double-couple source parameters using seismic data only (top) and seismic + GPS data (bottom). The parameters defining the double-couple sources with maximum a posteriori probability (MAP) are represented in form of beachballs. Histograms show the one-dimensional marginal posteriors for the double couple parameters with vertical lines marking the MAP solution. Waveform fits at selected seismic stations are represented by the grey (observed) and red (predicted) solid lines. The brown shadings show 200 randomly selected synthetic waveforms from the posterior predictive distribution. Black/red arrows show the observed/predicted coseismic offsets, respectively.

References

Abril, C., A. Tryggvason, Ó. Gudmundsson, & R. Steffen, Local earthquake tomography in the Tjörnes Fracture Zone (North Iceland), J. Geophys. Res.: Solid Earth **126**, e2020JB020212, doi: 10.1029/2020JB020212, 2021.

Barreto, A., R. Viltres, R. Matrau, B.G. Ófeigsson & S. Jónsson, Insights into two decades of continuous and campaign GPS data in North Iceland, In *Proc. to the NorthQuake 2022 workshop* (this volume), 2022.

Bos, M. S., R. M. S. Fernandes, S. D. P. Williams, and L. Bastos. Fast error analysis of continuous GNSS observations with missing data, J. Geod. **87**, no. 4, 351-360, doi: 10.1007/s00190-012-0605-0, 2013.

Dettmer, J., S. E. Dosso, and C. W. Holland, Uncertainty estimation in seismoacoustic reflection travel time inversion, J. Acoust. Soc. Am. **122**, no. 1, 161-176, doi: 10.1121/1.2736514, 2007.

Floyd, M. A., H. Billiris, D. Paradissis, G. Veis, A. Avallone, P. Briole, J.-M. Nocquet, K. Palamartchouk, B. Parsons, and P. C. England, . A new velocity field for Greece: Implications for the kinematics and dynamics of the Aegean, J. Geophys. Res. **115**, no. B10, doi: 10.1029/2009JB007040, 2010.

Herring, T. A., R. W. King, M. A. Floyd, and S. C. McClusky, Documentation for the GAMIT/GLOBK GNSS Analysis Software, release 10.7 [Computer software manual] Cambridge, 2018.

IMO – The Icelandic Met Office, A strong earthquake swarm offshore North Iceland. https://en.vedur.is/about-imo/news/a-strong-earthquake-swarm-offshore-north-iceland, 2020.

IMO – The Icelandic Met Office. https://skjalftalisa.vedur.is/#/page/map. Last access on 01/10/2022, 2022.

Jónsdóttir, K., G. B. Guðmundsson, L. Passarelli, S. Jónsson, Y. Cubuncu, T. Lecocq, C. Caudron, & F. Rodriguez Cardozo. Recent seismic swarms in the Tjornes fracture zone, N-Iceland, EGU General Assembly Conference Abstracts, doi: 10.5194/egusphere-egu2020-19267, 2020.

Kogan, L., S. Fisseha, R. Bendick, R. Reilinger, S. McClusky, R. King, and T. Solomon, Lithospheric strength and strain localization in continental extension from observations of the East African Rift, J. Geophys. Res. **117**, no. B3, doi: 10.1029/2011JB008516, 2012.

Passarelli, L., Rivalta, E., Jónsson, S., Hensch, M., Metzger, S., Jakobsdóttir, S. S., Maccaferri, F., Corbi, F., T. Dahm, Scaling and spatial complementarity of tectonic earthquake swarms, *Earth and Planetary Science Letters* **482**, 62-70**,** doi: 10.1016/j.epsl.2017.10.052, 2018.

Stefánsson, R. & G.B. Guðmundsson, Kópasker earthquake in 1976: About pre-activity, location and post-activity, *In: Proc. of the NorthQuake 2019 workshop* (ed. S. Jónsson et al.), Húsavík Academic Centre, 28-33, 2019.

Steinberg, A., H. Sudhaus, S. Heimann, and F. Krüger, Sensitivity of InSAR and teleseismic observations to earthquake rupture segmentation, *Geophys. J. Int.* **223**, no. 2, 875-907, doi: 10.1093/gji/ggaa351, 2020.

Vasyura-Bathke, H., J. Dettmer, R. Dutta, P. M. Mai, and S. Jónsson, Accounting for theory errors with empirical Bayesian noise models in nonlinear centroid moment tensor estimation, *Geophys. J. Int.* **225**, no. 2, 1412–1431, doi: 10.1093/gji/ggab034, 2021.

Wang, R., S. Heimann, Y. Zhang, H. Wang, and T. Dahm. Complete synthetic seismograms based on a spherical self-gravitating Earth model with an atmosphereocean-mantle-core structure, Geophys. J. Int. **210**, no. 3, 1739–1764, doi: 10.1093/gji/ggx259 2017.

Wang, R., M. F. Lorenzo, and F. Rot, PSGRN/PSCMP - a new code for calculating co- and post-seismic deformation, geoid and gravity changes based on the viscoelastic- gravitational dislocation theory, *Comput. Geosci*. **32**, no. 4, 527-541, doi: 10.1016/j.cageo.2005.08.006, 2006.

NORTHQUAKE 2022 - The 4th International Workshop on Earthquakes in North Iceland
Húsavík, North Iceland, 18-20 October 2022

Seismic monitoring of Krafla, Þeistareykir and Námafjall high-temperature geothermal fields, NE-Iceland

Thorbjörg Ágústsdóttir[1], Egill Á. Gudnason[1], Rögnvaldur L. Magnússon[1], Karl Gunnarsson[1], Anette K. Mortensen[2] and Philippe Jousset[3]

[1] *ÍSOR, Iceland GeoSurvey, Kópavogur, Iceland (thorbjorg.agustsdottir@isor.is, egill.arni.gudnason@isor.is)*
[2] *Landsvirkjun, Reykjavík, Iceland (Anette.Mortensen@landsvirkjun.is)*
[3] *GFZ, German Research Centre for Geosciences, Potsdam, Germany (pjousset@gfz-potsdam.de)*

Geothermal fields in Iceland, specifically the high-temperature fields, are located in tectonically active areas that naturally experience seismicity. Iceland has successfully utilised their bountiful energy resource, both for electrical power production and space heating. Iceland GeoSurvey (ÍSOR) has monitored the developed geothermal fields in Krafla, Þeistareykir and Námafjall with permanent seismic stations for Landsvirkjun (LV) for nearly a decade.

The geometry of the seismic network in the Krafla and Námafjall areas has remained the same since 2015 and 2017, respectively. From 2017 to 2020, the German Research Centre for Geosciences (GFZ) operated 13 seismic stations (120s) in Þeistareykir (*Toledo et al., 2022*), as a part of a larger deployment effort to monitor the exploitation activity in Þeistareykir, and in 2021, three of the GFZ stations were added to the permanent LV/ÍSOR seismic network in the Þeistareykir area. To date, the LV/ÍSOR seismic network consists of 21 permanent stations (1, 5 and 120s), supplemented with 6 stations from the Icelandic Meteorological Office (5s); in total 27 stations are used for the monitoring of the three geothermal fields (*Guðnason et al., 2021*). All seismic data is streamed in real-time to ÍSOR, and subsequently, automatic locations of earthquakes are available to Landsvirkjun.

For automatic earthquake detection and location, and day to day monitoring of the geothermal fields, ÍSOR uses the SeisComP software, where the majority of events are manually refined. To date, over 40,000 manually refined events are in the ÍSOR catalogue for the three geothermal fields. In the yearly reports prepared for LV, ÍSOR has observed increased but variable seismic rate in production and injection areas, while it can be challenging to distinguish between natural and induced seismicity. In some cases, the shallow seismicity at <3km depth is linked to either production or injection. Seasonal fluctuations are observed in both seismicity rate and magnitude range in some areas, with varying b-values above 1 and low Vp/Vs ratios.

Seismicity rate is highest in Krafla, at least an order of magnitude higher than in Þeistareykir and Námafjall, but in general the majority of the events across the geothermal fields are less than M_L 1. Nevertheless, seismicity maps the fracture permeability and fault orientation in all the geothermal areas. Seismicity within the Krafla caldera is to a large extent extremely shallow, located at less than 2 km depth, clustered within the main wellfield and the adjacent fissure swarm. Detailed mapping of the brittle-ductile transition (BDT) below the geothermal fields gives important information on the physical state and properties of the crust, including constraints on temperature. This is clear beneath the IDDP-2 well, where the BDT domes up, indicating higher temperatures (*Guðnason et al., 2021*). At Þeistareykir, the seismicity distribution is markedly

deeper, mainly located between 3 and 6 km depth, clustered in the main upwelling area beneath Mt. Bæjarfjall and within the fissure swarm.

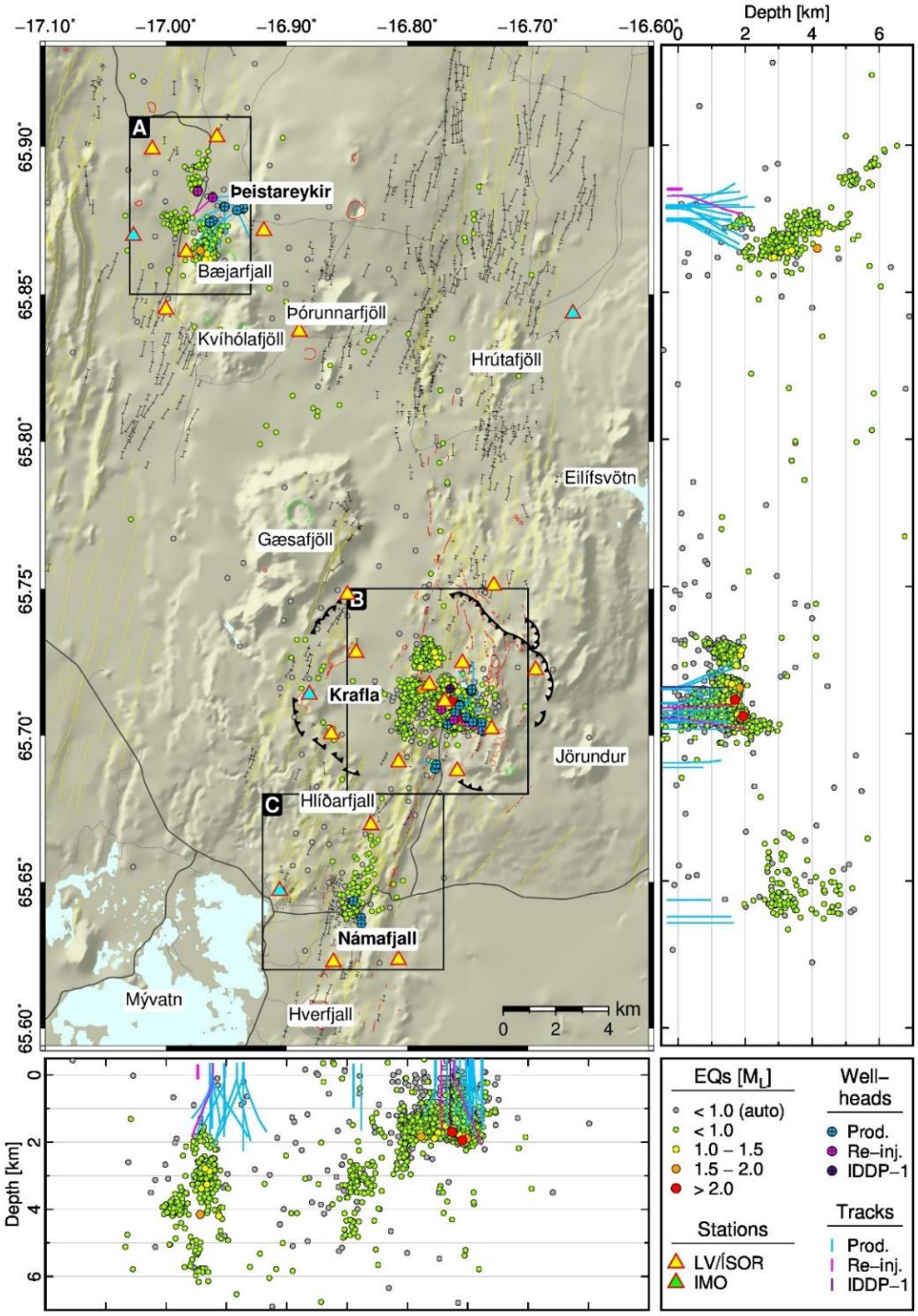

Figure 1. Refined earthquake locations in the Krafla, Þeistareykir and Námafjall geothermal areas in 2021, in map and depth view (Figure 2 from Guðnason et al., 2021). Automatic locations (M_L < 1) are in grey and manual locations are colour coded according to magnitude. See legend for different seismic stations, wellheads and well tracks. Mapped geological structures are from the geological map of Sæmundsson et al. (2012). Black boxes mark the outlines of the zoomed-in view of each geothermal area as shown in Figures 3, 5 and 7 of Guðnason et al. (2021).

References

Guðnason, E.Á., Magnússon, R. L., Vilhjálmsson., A. M., Ágústsdóttir, Þ., Gunnarsson, K., Seismic Monitoring in Krafla, Þeistareykir and Námafjall. Report prepared for Landsvirkjun. ÍSOR-2021/049,

http://gogn.lv.is/files/2021/2021-053.pdf, 2021
Sæmundsson, K., Hjartarson, Á., Kaldal, I., Sigurgeirsson, M. Á., Kristinsson, S. G. and Víkingsson, S., Jarðfræðikort af Norðurgosbelti – Nyrðri hluti, 1:100.000. Reykjavík, Iceland GeoSurvey, 2012.
Toledo, T., Obermann, A., Verdel, A., Martins, J. E., Jousset, P., Mortensen, A. K., Erbas, K. and Krawczyk, C. M., Ambient seismic noise monitoring and imaging at the Theistareykir geothermal field (Iceland). *Journal of Volcanology and Geothermal Research*, **429**, 105790. doi.org/10.1016/j.jvolgeores.2022.107590, 2022.

Magnitude of Earthquakes in th Tjörnes Fracture Zone

Birgir Hrafnkelsson[1], Atefe Darzi[2], Benedikt Halldórsson[3]

[1]*University of Iceland, (birgirhr@hi.is)*
[2]*University of Iceland, (atefe@hi.is)*
[3]*University of Iceland and the Icelandic Meteorological Office (skykkur@hi.is)*

The specification of the spatial characterization of earthquake sources in a seismic region and their seismic activity, are two of three key elements of probabilistic seismic hazard assessment, the third one being ground motion modeling. Here, the focus is on the spatial variation in the probability distribution describing the magnitude of earthquakes. The historical annals and earthquake catalogues suggest that the probability distribution for earthquake magnitudes within the South Iceland Seismic Zone (SISZ) and Reykjanes Peninsula Oblique Rift (RPOR) varies across the region (see e.g., Einarsson, 1991, 2014; Sigmundsson et al., 1995; Solnes et al., 1994; Solnes and Halldorsson, 1996; Bayat et al., 2022). Less is known about the spatial variation in the probability distribution for earthquake magnitudes in the Tjörnes Fracture Zone (TFZ). Here, we apply a statistical model to assess how the probability distribution of earthquake magnitudes varies across the TFZ. The statistical model is a Bayesian hierarchical model (e.g., Gelman et al. 2013) that assumes the generalized Pareto distribution (e.g., Coles, 2001) for earthquakes magnitudes above a prespecified threshold. This model was proposed by Darzi et al. (2023), and was motivated by the work of Dutfoy (2021). Data from the Grimsey Oblique Rift (GOR) and Húsavík-Flatey transform Fault Zone (HFFZ), see Jónasson (2021), which stretch from northwest to southeast, were analysed, see Fig. 1. The scale parameter of the generalized Pareto distribution is assumed to vary spatial along the northwest-southeast direction of GOR and HFFZ.

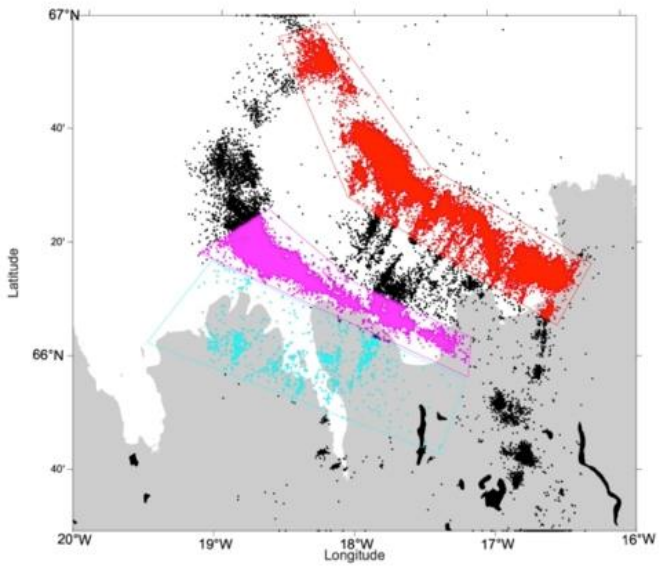

Figure 1. The figure shows earthquakes from the GOR and the HFFZ that were used in the analysis, in red and pink,

respectively. Earthquakes from the Dalvik Zone (blue) were not analysed here.

The results in Darzi et al. (2023) showed that the scale parameter varies along the east-west direction in the case of both the RPOR and the SISZ. An exponential distribution with a spatially varying scale parameter was also considered. The results indicated strongly that this model provides a poor fit to the data, while the fit of the model that assumes the generalized Pareto distribution with spatially varying scale parameter provides a convincing fit. Furthermore, it was argued that the magnitude should have an upper bound. The generalized Pareto distribution can take this assumption into account by restricting its shape parameter to be negative. Fig. 2 shows the upper bound of the earthquake magnitude as a function of longitude a cross the RPOR and the SISZ.

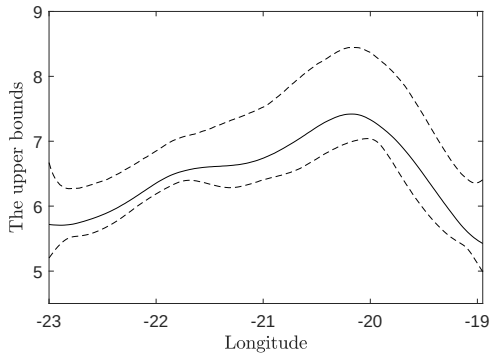

Figure 2. The figure shows the upper bound of the earthquake magnitude as a function of longitude across the SISZ and RPOR regions when assuming the generalized Pareto distribution with scale parameter that varies with longitude. The solid line shows the posterior median while the dashed lines show the 95% posterior interval as a function of longitude.

The results from the analysis of data from the GOR and the HFFZ show that the scale parameter of the generalized Pareto distribution varies with the northwest-southeast direction. The reason for selecting the northwest-southeast direction is due to the fact that the fractures in these regions are lined perpendicular to this direction. An upper bound is assumed for the earthquake magnitudes. The upper bound of the earthquake magnitudes of the HFFZ is uncertain, while the upper bound of the GOR is estimated with less uncertainty, see Fig. 3. The uncertainty decrease with the number of earthquake above 4.0. Due to this uncertainty, the upper bounds should be interpreted with care, especially in the case of the HFFZ.

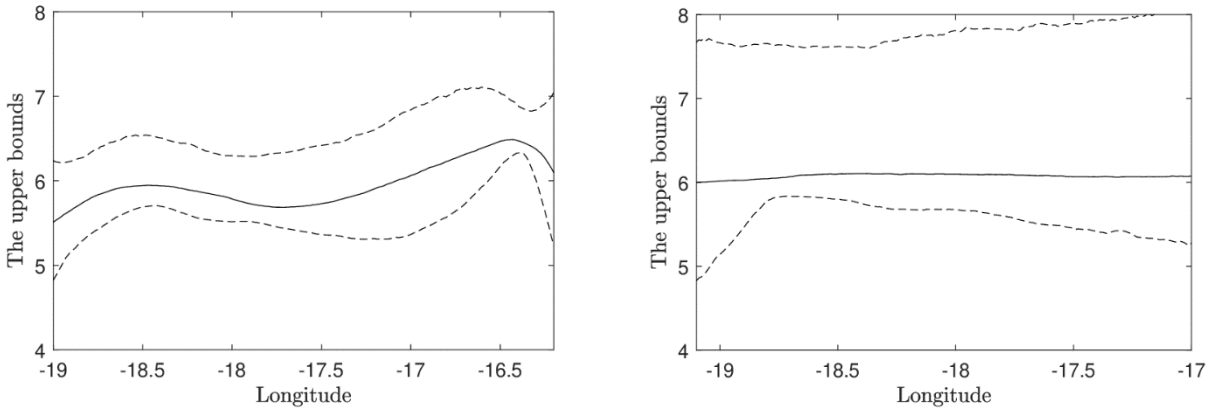

Figure 3. The figure shows the upper bounds of the earthquake magnitude as a function of longitude across the GOR (left panel) and the HFFZ (right panel) when assuming the generalized Pareto distribution with scale parameter that

varies with the northwest-southeast direction. The solid line shows the posterior median while the dashed lines show the 95% posterior interval as a function of longitude.

References

Bayat, F., M. Kowsari and B. Halldorsson, A new 3D finite-fault model of the Southwest Iceland bookshelf transform zone. *Geophysical Journal International*, ggac272, 2022.

Coles, S., *An Introduction to Statistical Modeling of Extreme Values*, Springer, London, 2001.

Darzi, A., B. Hrafnkelsson and B. Halldorsson, Bayesian modeling in engineering seismology: Spatial earthquake magnitude model. In Hrafnkelsson, B., editor, *Bayesian Latent Gaussian Models – with Applications to Geophysics and Environmental Sciences*. Springer, Berlin. To appear in 2023.

Dutfoy, A., Earthquake recurrence model based on the generalized Pareto distribution for unequal observation periods and imprecise magnitudes. *Pure and Applied Geophysics*, **178**, 1549-1561, 2021.

Einarsson, P., Earthquakes and present-day tectonism in Iceland. *Tectonophysics*, **189**, 261-279, 1991.

Einarsson, P., Mechanisms of Earthquakes in Iceland. In Beer, M., K. I. P. E. and Au, I. S.-K., editors, *Encyclopedia of Earthquake Engineering*. Springer, Berlin, 2014.

Gelman, A., J. B. Carlin, H. S. Stern, D. B. Dunson, A. Vehtari and D. B. Rubin, *Bayesian Data Analysis*, Third Edition, Chapman & Hall/CRC Texts in Statistical Science, Taylor & Francis, 2013.

Jónasson, K., B. Bessason, Á. Helgadóttir, P. Einarsson, G. Guðmundsson, B. Brandsdóttir, K. S. Vogfjörd, and K. Jónsdóttir. (2021). A harmonised instrumental earthquake catalogue for Iceland and the Northern Mid-Atlantic Ridge. *Natural Hazards and Earth System Sciences*, **21**, 2197-2214.

Sigmundsson, F., P. Einarsson, R. Bilham, and E. Sturkell, Rift-transform kinematics in south Iceland: Deformation from Global Positioning System measurements, 1986 to 1992. *Journal of Geophysical Research: Solid Earth* **100**, 6235-6248, 1995.

Solnes, J. and B. Halldorsson, Generation of synthetic earthquake catalogs: Applications in earthquake hazard and seismic risk assessment. In *Proceedings of the fifth international conference on seismic zonation (Nice, October 17-19, 1995)*, pages 1131-1140, 1996.

Solnes, J., R. Sigbjörnsson and B. Halldorsson, Assessment of Seismic Risk and Earthquake Hazard Based on Simulated and Upgraded Earthquake Catalogues. In *Proceedings of the 9th International Seminar on Earthquake Prognostics, San José, Costa Rica*, 1994.

A new Bayesian epidemiological spatiotemporal aftershock sequence model the 2000 and 2008 aftershock sequences in Southwest Iceland

Atefe Darzi[1], Benedikt Halldorsson[1,2], Birgir Hrafnkelsson[3] and Kristín S. Vogfjörð[2]

[1]*Faculty of Civil and Environmental Engineering, University of Iceland, Reykjavik, Iceland (atefe@hi.is,skykkur@hi.is)*
[2]*Division of Processing and Research, Icelandic Meteorological Office, Reykjavik, Iceland (vogfjord@vedur.is)*
[3]*Faculty of Physical Sciences, University of Iceland, Reykjavik, Iceland (birgirhr@hi.is)*

Iceland is the most seismically active region in northern Europe. The largest earthquakes in Iceland occur within the two transform fault zones in the country, the more populous of which is the South Iceland Seismic Zone (SISZ). The three largest and most recent earthquakes in SISZ and Reykjanes Peninsula Oblique Rift (RPOR) are 17-June-2000 at 15:40 (M_w6.4), 21-June-2000 at 00:51 (M_w6.5) and 29-May-2008 at 15:45 (M_w6.3) (Fig. 1). All of them were followed by intense aftershock sequences. After a large earthquake, aftershocks tend to cluster in time and space, forming complex seismic sequences that complicate the assessment of the temporal variation of probabilistic seismic hazard of aftershocks greatly. Modelling spatio-temporal aftershock clustering is one of the first steps towards detailed and improved short-term seismic risk forecasting, loss prevention, emergency disaster management and response.

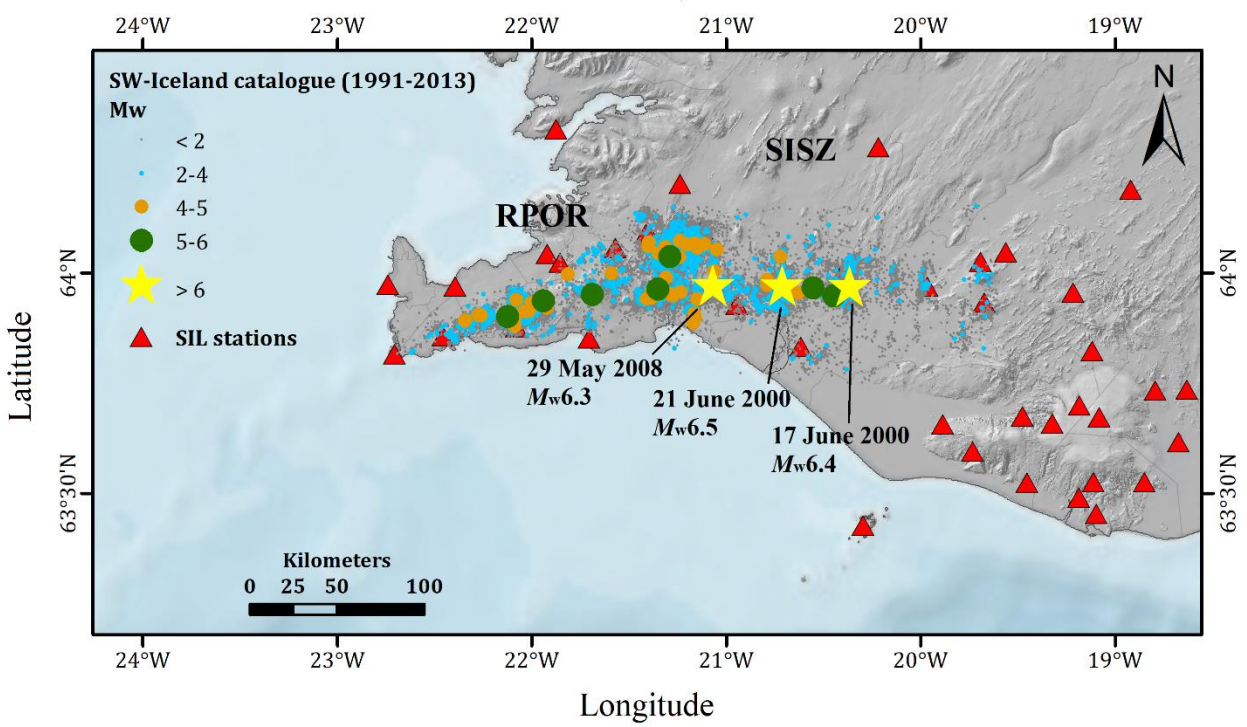

Figure 3. Seismic events in SW-Iceland recorded by the Icelandic seismic network (SIL), operated by the Icelandic Meteorological Office (IMO).

In this study, we perform retrospective experiments to explore daily aftershock forecasting over several stages of the 2000 and 2008 sequences in SISZ by employing an advanced Bayesian spatiotemporal epidemic-type aftershock sequence (ETAS) seismicity model (Ebrahimian and Jalayer 2017). This study provides us with a comprehensive validation of the potential operational earthquake forecasting (OEF) system for south Iceland which is the prerequisite for its practical application. Contrary to the conventional single-point estimation methods, using the Bayesian parameter estimation approach enables us to assign a posterior probability distribution to the ETAS model parameters, thus accounting for the epistemic uncertainty, informing and tuning the model with more and richer information.

In Fig. 2, for several daily forecasting intervals (FI) over the two intense seismic sequences, the number of forecasted earthquakes with $M_w \geq M_{cut}$ (herein 2.0) (median displayed in black square-line) are presented while accounting for the incorporated uncertainties (2^{nd}-98^{th} percentiles shown by grey shaded area) and the results compared with the actual observed earthquakes (red star in Fig. 2). The x-axis shows the time of issuing forecasts.

For the 2008 sequence, an informative set of ETAS parameters obtained from the strong June 2000 sequence was used as mean of prior probability distribution within the Bayesian updating framework (Darzi et al. 2022a, b) while for the 2000 sequence forecasting, a set of generic values were used, both with fix coefficient of variation (CV) of 0.3 (Darzi et al. 2023). In both sequences, for the subsequent daily forecasting analyses, the adaptive inference of posteriors of the ETAS model parameters from the preceding FI is employed as priors for the next FI. The resulting model proved fast parametric convergence and provided a strong forecasting ability of the Bayesian ETAS model, even only a few hours after the mainshocks, and over the subsequent daily intervals (see Darzi et al. 2022a, b, 2023, for a detailed discussion).

As can be seen in Fig. 2, unlike the 2008 sequence, following the 17 June mainshock the intense seismic activity continues over the next couple of days (119 N_{obs} recorded on 18 June 2000 vs. 68 N_{obs} observed on 30 May 2008). For the 2000 sequence, we observe more accurate and confident forecasts, and the median forecasted number of events is almost equal to the observations. This is attributed to the more stable and narrower posterior distributions associated with the June 2000 sequence. Whereas, for the forecasting of 2008 sequence, the median predictions both under- and overpredict the observations in a non-systematic manner as expected due to the wide dispersion of their corresponding ETAS model posteriors. However, it should be noted that the observations based on the 2008 sequence fall in the 96% prediction interval, indicating that the variability in the model is properly modeled. We conclude that each earthquake sequence is an indication of a unique ETAS parametric set and there are no representative regional ETAS parameters for SISZ earthquake sequences, at least at this stage, and further retrospective analyses are needed. We also note that in both sequences, and for all forecasts, the model exhibited a strong spatial forecasting ability, even only a few hours after the mainshock (not presented herein, see Darzi et al. (2022a, b)).

The Bayesian spatiotemporal ETAS model has been implemented within the TURNkey FWCR platform (Forecasting – Early Warning – Consequence Prediction– Response) to facilitate informative earthquake forecasting by taking advance seismicity forecasting framework as well as a multi-sensor earthquake information system. This model can potentially be applied as a regional OEF system for aftershocks, enabled by the real-time magnitude and location capability of the SIL seismic system and its low magnitude of completeness. For future activity, we intend to investigate the uncertainties associated with the quasi-real-time earthquake catalogues registered and streamed

online in SIL monitoring network using the employed Bayesian-based seismicity forecasting framework and exploring the most recent sequence.

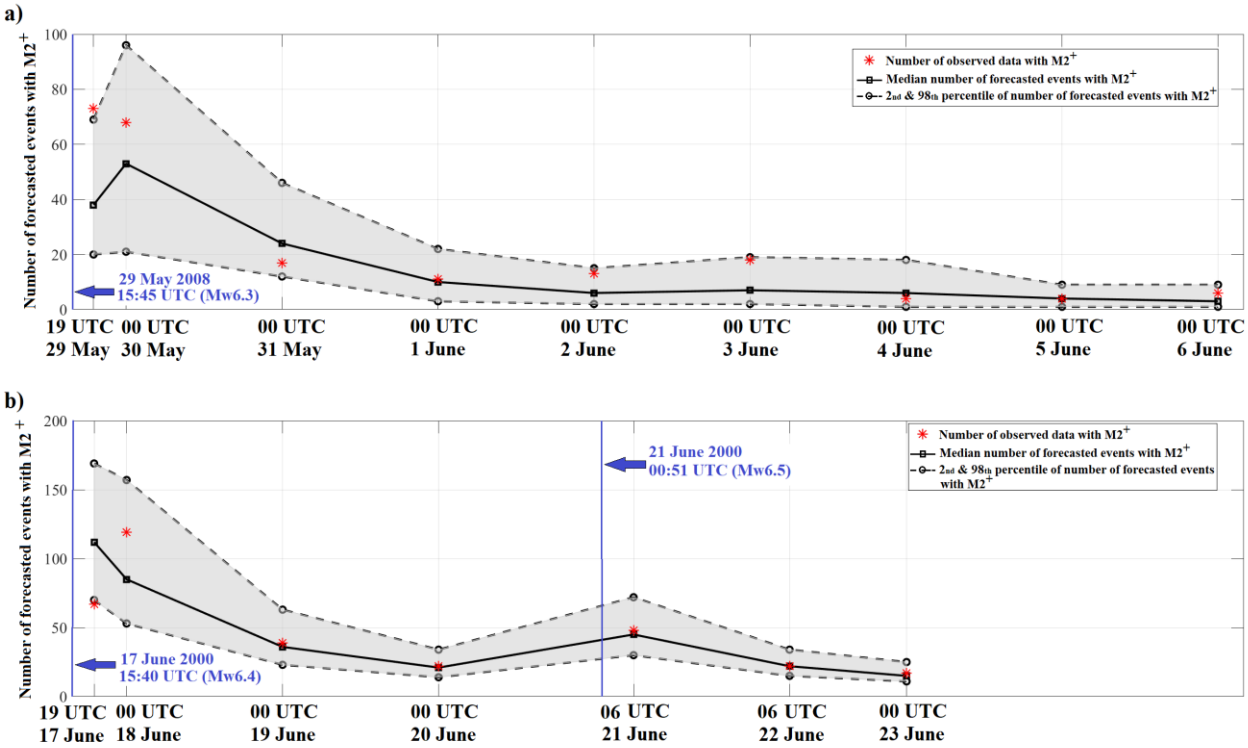

Figure 2. Daily forecasting comparisons during the 2008 (1st panel) and 2000 (2nd panel) seismic sequences.

This study was funded by the H2020 TURNkey project (#821046) and Postdoctoral grant from Icelandic Research Fund (#218255). The Bayesian ETAS model codes are made available on GitHub: https://github.com/HossEbi/Bayesian_ spatiotemporal_ETAS_model_ver1.git

References

Darzi A, B. Halldorsson, B. Hrafnkelsson, et al., Calibration of a Bayesian spatio-temporal ETAS model to the June 2000 South Iceland seismic sequence. *Geophysical Journal International* **232**:1236–1258. https://doi.org/10.1093/gji/ggac387, 2023.

Darzi A, B. Halldorsson, B. Hrafnkelsson, K.S. Vogfjord, Variability of ETAS model parameters for two intense seismic sequences of May 2008 vs. June 2000 in southwest Iceland. In: *Proceedings of the 3rd European Conference on Earthquake and Engineering Seismology (3ECEES)*. Bucharest, Romania, p 10 (Paper No. 5068), 2022a.

Darzi A, B. Halldorsson, B. Hrafnkelsson, K.S. Vogfjörð, Short-term Bayesian ETAS spatiotemporal forecasting of the Ölfus 2008 earthquake sequence in Iceland. *Tectonophysics* **839**:229522, https://doi.org/10.1016/j.tecto.2022.229522, 2022b.

Ebrahimian H, F. Jalayer, Robust seismicity forecasting based on Bayesian parameter estimation for epidemiological spatio-temporal aftershock clustering models. *Sci Rep* **7**:9803. https://doi.org/10.1038/s41598-017-09962-z, 2017.

NorthQuake 2022 - The 4th International Workshop on Earthquakes in North Iceland
Húsavík, North Iceland, 18-20 October 2022

Towards a physics-based fault system model for the Tjörnes Fracture Zone

Benedikt Halldorsson[1,2], Claudia Abril[3], Farnaz Bayat[1], Milad Kowsari[1]

[1]*Faculty of Civil and Environmental Engineering, School of Engineering and Natural Sciences, University of Iceland (skykkur@hi.is (B.H.);, fab14@hi.is, milad@hi.is)*
[2]*Division of Processing and Research, Icelandic Meteorological Office, Iceland (benedikt@vedur.is)*
[3]*Uppsala University, Sweden (claudia.abril@geo.uu.se)*

The Tjörnes Fracture Zone (TFZ) in North Iceland is one of two major transform zones in Iceland, the other being the South Iceland Seismic Zone (SISZ; Einarsson 2014; Stefansson et al. 2008, and references therein). The TFZ connects the active tectonic extension of the Mid-Atlantic Ridge offshore north of Central Iceland to the active tectonic extension in the Northern Volcanic Zone on land in northeast Iceland (Thordarson and Hoskuldsson 2002) (see Figure 11). The recent publication of the ICEL-NMAR harmonized earthquake catalogue captures over a century of significant earthquake occurrence in Iceland complete with revised epicentral locations from local sources and moment magnitude estimates from international monitoring agencies (Jónasson et al. 2021). When plotted on a map of the greater TFZ region, the significant earthquakes (larger than M_w3.5) appear to be almost randomly distributed over a relatively large area, with perhaps a few clusters of varying spatial extents. However, when the recent microseismic catalogue of the National seismic network (SIL, since 1991) is plotted on the map (Bodvarsson et al. 1996), three observations become evident: (1) The microseismicity outlines distinct seismic lineaments (Rögnvaldsson et al. 1998; Stefansson et al. 2008) that are oriented ~NW-SE that coincide with locations of many ICEL-NMAR events; (2) the multiple dense clusters of offshore microseismicity suggests an even more complex seismotectonic character of the TFZ without the clear spatial correlation with many ICEL-NMAR events; and (3) a considerable number of ICEL-NMAR events is located west and south of the southernmost microseismic lineament while not being collocated with dense clusters of microseismicity as in (2) above.

Intense geophysical and seismological research efforts focused on the TFZ have been made over the past couple of decades. A comprehensive overview has been compiled in NorthQuake proceedings published every three years since 2013 (www.hac.is) covering a wide range of topics, key examples of which are: geophysical exploration, surface fault mappings, bathymetry mapping, seismic reflection and seismicity studies (e.g., Brandsdóttir et al. 2005; Magnúsdóttir and Brandsdóttir 2011; Hjartardóttir et al. 2016; Abril et al. 2019a, b; Einarsson et al. 2019; Einarsson and Brandsdóttir 2021); Geodetic measurements, both on permanent stations and campaign measurements across the TFZ, but primarily across the western ends of lineaments A and B (Metzger et al. 2011, 2013; Metzger and Jónsson 2014); Revision of the historical earthquake catalogue for North Iceland (Thorgeirsson 2012), along with very localized seismic and hazard studies (e.g., Halldorsson et al. 2013, 2019; Olivera et al. 2013; Waltl et al. 2013, 2019; Kowsari et al. 2019; Sonnemann et al. 2019).

For the sake of reference, we plot in Fig. 1 the simplified model of seismogenic structures in

the region that had been proposed for use in seismic hazard assessment that was required for site-specific seismic hazard assessment for potential developmental sites of heavy industry and geothermal projects in North Iceland at the time (Björnsson et al. 2007). In this model, the main tectonic lineaments of strike slip faulting are drawn in a simplistic manner as long linear faults (A, B, C, red lines in Figure 1) and normal faulting in the Northern Volcanic Zone and the Mid-Atlantic Ridge (red lines, D-H). While they proposed some segmentation of lineament B, the overall modeling was simplistic, but reflected the status of knowledge at that time, at least that was needed

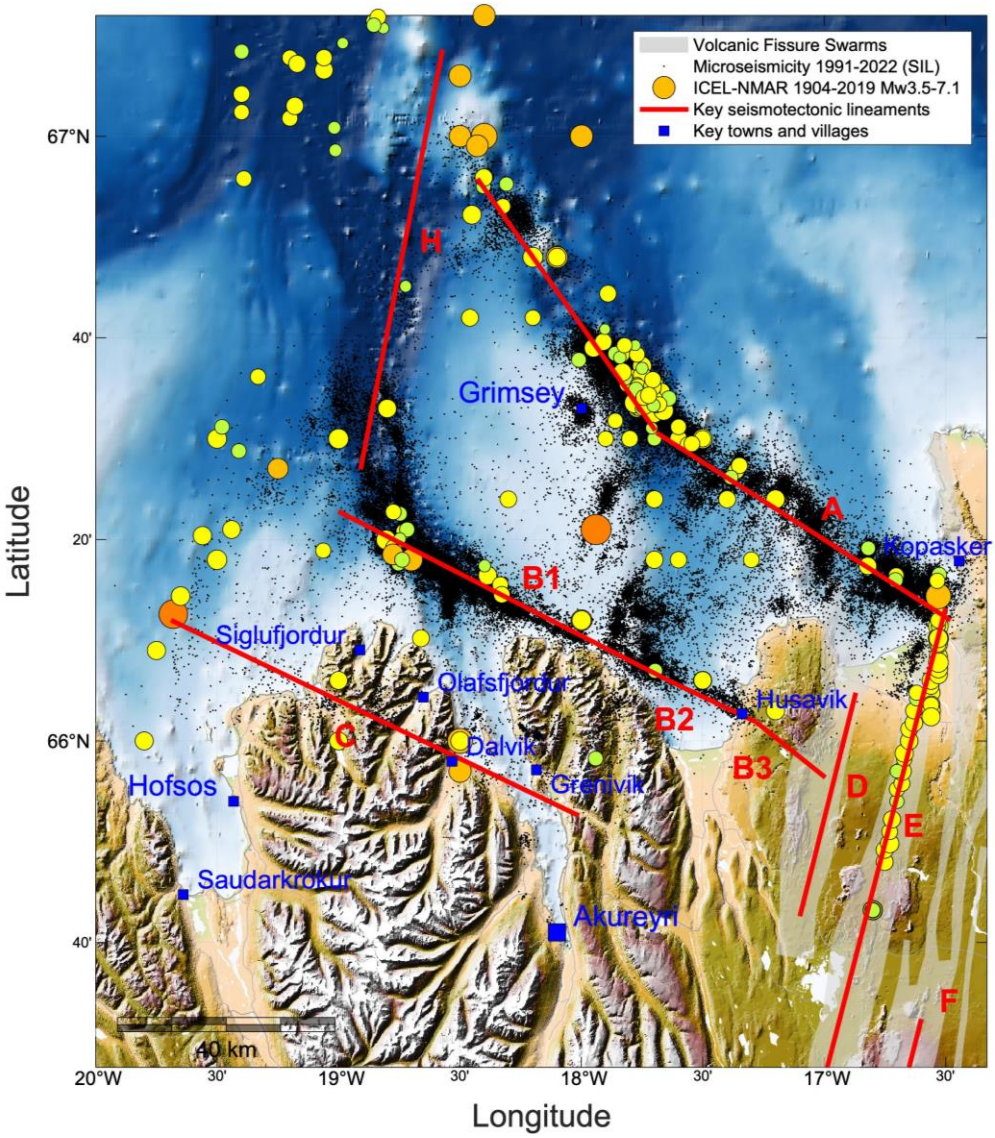

Figure 4. Map of the topography and bathymetry of the larger TFZ region. The black dots denote the microearthquake SIL catalogue, and the larger colored circles denote significant earthquakes from 1904-2019 (ICEL-NMAR) with diameters and color coding denoting relative magnitude differences (Jónasson et al. 2021). Locations of key towns and villages are shown relative to red lines that denote the long axes of the key lineaments in the region. The Grimsey lineament (A), Husavik-Flatey Fault Zone (B), and the Dalvik Lineament (C) are lineaments and/or faults of strike-slip faulting, with normal faulting dominating the rifting lineaments (D-F denote the Þeistareykir, Krafla and Fremrinámur volcanic systems, respectively, in the Northern Volcanic Zone, while H denotes the Mid-Atlantic Ridge that continues north). The lineaments and segmentation of the HFFZ is from an early hazard model of the region (Björnsson et al. 2007).

for application in seismic hazard assessment.

At present, two main facts about the seismotectonic character of the TFZ seem to be widely

accepted: (1) the southeast-northwest lineament outlined by the ICEL-NMAR and microseismic catalogue in the northernmost part of the TFZ referred to as the Grímsey lineament (Stefansson et al. 2008) (A, in Figure 1) and its continuation towards the northwest, the Grímsey oblique rift can be approximated as a mirror image of the SISZ-RPOR system in Southwest Iceland (Einarsson 2014). Namely, the SISZ is the main seismic zone in Southwest Iceland and it has long been known that instead of a long, linear and classic strike-slip fault along its long-axis, it is characterized by the unique bookshelf faulting i.e., an array of short strike-slip faults oriented at right angles to the long-axis of the lineament. Moreover, it has recently been shown to be continuous all along the Reykjanes Peninsula Oblique Rift (RPOR; Steigerwald et al. 2020). This hypothesis is consistent with, and modeled after, the early findings of relative relocations of small seismic sequences in this region that appeared to outline such bookshelf faults (Rögnvaldsson et al. 1998), and such continued efforts at the Icelandic Meteorological Office for miscellaneous sequences since then. Then (2), that the southern lineament outlined by the earthquakes in the ICEL-NMAR catalogue forming a near-straight line from the town of Húsavík, northwest past Flateyjarskagi peninsula and north of Eyjafjörður fjord is a classic right-lateral linear and near-vertical strike-slip fault, the largest such fault in Iceland, referred to as the Húsavík-Flatey Fault Zone (HFFZ) (B, in Figure 1) (Sæmundsson 1974; Rögnvaldsson et al. 1998; Sæmundsson and Karson 2006; Stefansson et al. 2008; Metzger et al. 2011, 2013; Einarsson 2014; Metzger and Jónsson 2014), with a potential (Metzger et al. 2011, 2013; Metzger and Jónsson 2014). A third lineament, the enigmatic Dalvík lineament, which comprises the area towards the southwest of the HFFZ cannot be denied existence, simply on the basis of the multiple damaging earthquakes there in the 20th century of magnitudes larger than 6, with theories of it being also a bookshelf system but of much fewer faults than the Grímsey lineament (Stefansson et al. 2008) (C, in Figure 1).

Moreover, while seismic hazard assessment is generally time-dependent (see e.g., Baker et al. 2021, and references therein) the seismic activity along these lineaments has been shown to be temporally non-uniform. The most significant example is the spatially concentrated linear seismicity in the eastern part of the TFZ region, in the Northern Volcanic zone, which delineates the Krafla rifting episode of 1975-1984. This rifting episode not only triggered the 1976 M_{w}6.3 earthquake near the village of Kópasker on the Grímsey lineament, but it cast a shadow of tectonic stress over the Grímsey and Húsavík lineaments and effectively has locked the eastern part of the HFFZ (Maccaferri et al. 2013). Correspondingly, recent geodetic measurements across the Grímsey and HFFZ lineaments show that at least 2/3 of the transform motion is presently taken up by the Grímsey lineament, with the remainder taken up by the HFFZ (Metzger et al. 2011, 2013), a fact that appears to be consistent with the apparent lack of microseismic earthquakes on the eastern HFFZ.

Most if not all of the detailed view of the seismogenic structure of the TFZ as presented above has been based on land-based measurements. In the past decade however, intense seismic research has focused on offshore measurements. Namely, bathymetry mappings and reflection studies have confirmed the existence of faults along another seismic lineament, that lies between the central part of the HFFZ and towards the bend in the Grímsey Lineament east of Grímsey island (Einarsson et al. 2019). Placing faults in this confined region on basis of measurements have important implications, as the location of the most recent large earthquake in the region, the 1910 M_{w}7.1 earthquake, is largely unknown but given its reported effects in the northern region, it has been placed in the centre of the TFZ (see the approximate location of the large event, between mid-

HFFZ and Grímsey island, in Fig. 1). Then, the North Iceland Experiment project saw the use of fourteen ocean-bottom seismometers in addition to a land-based densification of seismic stations over a few months in 2004 (Riedel et al. 2006). This enabled the detailed analysis of microseismicity on the basis of empirical travel times and local tomography modeling (Abril 2018; Abril and Gudmundsson 2018; Abril et al. 2021). This latest work not only confirms the state of knowledge of the seismotectonic character of the TFZ that had been proposed, but holds the promise of specifying further the detailed fault structure, not only in terms of potential fault locations but also the distribution of seismogenic depths in the region. Such information could facilitate the development of one of the three key elements in the state-of-the-art probabilistic seismic hazard assessment (PSHA), namely, a comprehensive specification of the fault system. On that basis, the fault slip rates can be calculated for the fault system on which basis the seismicity activity rates are established, which is the second key element of PSHA (Bayat et al. 2022). Finally, as the third element, the new hybrid and empirical Bayesian ground motion models (Kowsari et al. 2020) allow us to propagate such seismic activity away from the fault system, to the locations of vulnerable exposure in the region (see Figure 1) and if the local geological conditions require, in that effort we may account for site effects as well (Rahpeyma et al. 2022)

References

Abril C (2018) Seismicity and crustal structure in Iceland. Ph.D. Dissertation, Acta Universitatis Upsaliensis, Uppsala, Sweden

Abril C, Gudmundsson O (2018) Relocating earthquakes with empirical traveltimes. Geophys J Int 214:2098–2114. https://doi.org/10.1093/gji/ggy246

Abril C, Gudmundsson O, Tryggvason A (2019a) Earthquake relocation in the Tjörnes Fracture Zone. In: Proceedings of the Northquake 2019 workshop (Ed. S. Jónsson et al.). Húsavík Academic Centre, Husavik, Iceland, 21-24 May

Abril C, Tryggvason A, Gudmundsson O, Steffen R (2019b) Local earthquake tomography in North Iceland. In: Proceedings of the Northquake 2019 workshop (Ed. S. Jónsson et al.). Húsavík Academic Centre, Husavik, Iceland, 21-24 May

Abril C, Tryggvason A, Gudmundsson Ó, Steffen R (2021) Local Earthquake Tomography in the Tjörnes Fracture Zone (North Iceland). J Geophys Res Solid Earth 126:e2020JB020212. https://doi.org/10.1029/2020JB020212

Baker J, Bradley B, Stafford P (2021) Seismic Hazard and Risk Analysis. Cambridge University Press, Cambridge

Bayat F, Kowsari M, Halldorsson B (2022) A new 3-D finite-fault model of the Southwest Iceland bookshelf transform zone. Geophys J Int 231:1618–1633. https://doi.org/10.1093/gji/ggac272

Björnsson A, Sæmundsson K, Sigmundsson F, et al (2007) Geothermal projects in Iceland at Krafla, Bjarnarflag, Gjástykki and Theistareykir: assessment of geo-hazards affecting energy production and transmission systems emphasizing structural design criteria and mitigation of risk

Bodvarsson R, Rognvaldsson ST, Jakobsdottir SS, et al (1996) The SIL data acquisition and monitoring system. Seismol Res Lett 67:35–46

Brandsdóttir B, Riedel C, Richter B, et al (2005) Multibeam bathymetric maps of the Kolbeinsey Ridge and Tjörnes Fracture Zone, N-Iceland. In: Geophysical Research Abstracts. p A-07219

Einarsson P (2014) Mechanisms of Earthquakes in Iceland. In: Beer M, Kougioumtzoglou IA, Patelli E, Au IS-K (eds) Encyclopedia of Earthquake Engineering. Springer Berlin Heidelberg, Berlin, Heidelberg, pp 1–15

Einarsson P, Brandsdóttir B (2021) Seismicity of the Northern Volcanic Zone of Iceland. Front Earth Sci 9:628967. https://doi.org/10.3389/feart.2021.628967

Einarsson P, Brandsdóttir B, Hjartardóttir ÁR (2019) Seismicity, Faults, and Bathymetry of the Tjörnes Fracture Zone. In: Proceedings of the Northquake 2019 workshop (Ed. S. Jónsson et al.). Húsavík Academic Centre, Husavik, Iceland, 21-24 May

Halldorsson B, Jónsson S, Sigbjörnsson R, Ólafsson S (2013) ICEARRAY II: A multidisciplinary array of geodetic and strong-motion instruments in Húsavík, North Iceland. In: Earthquakes in North Iceland. Collection of lectures from a workshop in Husavik, North Iceland 6 – 8 June 2013. Húsavík Academic Centre, Húsavík, Iceland, p 4

Halldorsson B, Sonnemann T, Kowsari M, et al (2019) On the Scaling of Earthquake Strong-motion in North Iceland. In: Proceedings of the Northquake 2019 workshop (Ed. S. Jónsson et al.). Húsavík Academic Centre, Husavik, Iceland, 21-24 May

Hjartardóttir Á, Einarsson P, Magnúsdóttir S, et al (2016) Fracture systems of the Northern Volcanic Rift Zone, Iceland: an onshore part of the Mid-Atlantic plate boundary. Geol Soc Lond Spec Publ 420:297–314

Jónasson K, Bessason B, Helgadóttir Á, et al (2021) A harmonised instrumental earthquake catalogue for Iceland and the northern Mid-Atlantic Ridge. Nat Hazards Earth Syst Sci 21:2197–2214. https://doi.org/10.5194/nhess-21-2197-2021
Kowsari M, Halldorsson B, Eftekhari N, et al (2019) Sensitivity Analysis of Seismicity Parameters and Ground Motion Models used in PSHA to its Input Assumptions: A Case Study of Húsavík, North Iceland. In: Proceedings of the Northquake 2019 workshop (Ed. S. Jónsson et al.). Húsavík Academic Centre, Husavik, Iceland, 21-24 May
Kowsari M, Sonnemann T, Halldorsson B, et al (2020) Bayesian Inference of Empirical Ground Motion Models to Pseudo-Spectral Accelerations of South Iceland Seismic Zone Earthquakes based on Informative Priors. Soil Dyn Earthq Eng 132:106075. https://doi.org/10.1016/j.soildyn.2020.106075
Maccaferri F, Rivalta E, Passarelli L, Jónsson S (2013) The stress shadow induced by the 1975–1984 Krafla rifting episode. J Geophys Res Solid Earth 118:1109–1121. https://doi.org/10.1002/jgrb.50134
Magnúsdóttir S, Brandsdóttir B (2011) Tectonics of the Þeistareykir fissure swarm. Jökull 61:65–79
Metzger S, Jónsson S (2014) Plate boundary deformation in North Iceland during 1992–2009 revealed by InSAR time-series analysis and GPS. Tectonophysics 634:127–138
Metzger S, Jónsson S, Danielsen G, et al (2013) Present kinematics of the Tjörnes Fracture Zone, North Iceland, from campaign and continuous GPS measurements. Geophys J Int 192:441–455
Metzger S, Jónsson S, Geirsson H (2011) Locking depth and slip-rate of the Húsavík Flatey fault, North Iceland, derived from continuous GPS data 2006-2010. Geophys J Int 187:564–576
Olivera CI, Halldorsson B, Ólafsson S, et al (2013) Site Effects Estimation Using Ambient Noise Data in Husavik, North Iceland. In: Earthquakes in North Iceland. Collection of lectures from a workshop in Husavik, North Iceland 6 – 8 June 2013. Húsavík Academic Centre, Húsavík, Iceland, p 4
Rahpeyma S, Halldorsson B, Hrafnkelsson B, Darzi A (2022) Frequency-dependent Site Amplification Functions for key Geological Units in Iceland from a Bayesian Hierarchical Model for Earthquake Strong-motions. Soil Dyn Earthq Eng (in review)
Riedel C, Tryggvason A, Brandsdottír B, et al (2006) First results from the North Iceland experiment. Mar Geophys Res 27:267–281. https://doi.org/10.1007/s11001-006-9007-0
Rögnvaldsson ST, Guðmundsson Á, Slunga R (1998) Seismotectonic analysis of the Tjörnes Fracture Zone, an active transform fault in north Iceland. J Geophys Res Solid Earth 1978–2012 103:30117–30129
Sæmundsson K (1974) Evolution of the axial rifting zone in northern Iceland and the Tjornes fracture zone. Bull Geol Soc Am 85:495
Sæmundsson K, Karson JA (2006) Stratigraphy and Tectonics of the Húsavík–Western Tjörnes Area. ÍSOR, Reykjavík
Sonnemann T, Halldorsson B, Hrafnkelsson B, et al (2019) Earthquake Source Modeling and Ground Motion Simulation in North Iceland. In: Proceedings of the Northquake 2019 workshop (Ed. S. Jónsson et al.). Húsavík Academic Centre, Husavik, Iceland, 21-24 May
Stefansson R, Gudmundsson GB, Halldorsson P (2008) Tjörnes fracture zone. New and old seismic evidences for the link between the North Iceland rift zone and the Mid-Atlantic ridge. Tectonophysics 447:117–126
Steigerwald L, Einarsson P, Hjartardóttir ÁR (2020) Fault kinematics at the Hengill Triple Junction, SW-Iceland, derived from surface fracture pattern. J Volcanol Geotherm Res 391:106439. https://doi.org/10.1016/j.jvolgeores.2018.08.017
Thordarson T, Hoskuldsson A (2002) Iceland: Classic Geology in Europe. Terra, United Kingdom
Thorgeirsson O (2012) Sögulegir jarðskjálftar á Norðurlandi. Husavik Academic Centre, Husavik, Iceland
Waltl P, Halldorsson B, Pétursson HG, et al (2013) Geomorphological and Geological Aspects of Húsavík for Application in Earthquake Hazard and Risk Analyses. In: Earthquakes in North Iceland. Collection of lectures from a workshop in Husavik, North Iceland 6 – 8 June 2013. Húsavík, Iceland, p 4
Waltl P, Halldorsson B, Pétursson HG, Fiebig M (2019) Concise Map-based Representation of the Tectonics, Geology, Geomorphology and Building Stock of Húsavík, North Iceland. In: Proceedings of the Northquake 2019 workshop (Ed. S. Jónsson et al.). Húsavík Academic Centre, Husavik, Iceland, 21-24 May

NorthQuake 2022 - The 4th International Workshop on Earthquakes in North Iceland
Húsavík, North Iceland, 18-20 October 2022

On the exploration of seismic ground motion amplitudes in North Iceland from dynamic rupture modeling of Húsavík-Flatey Fault Zone earthquake scenarios

Bo Li[1,2], Alice-Agnes Gabriel[1,3], Thomas Ulrich[1], Claudia Abril[4], Benedikt Halldorsson[4,5], Lukas Krenz[6], Michael Bader[6]

[1]*Ludwig-Maximilians Universität München (LMU), Germany (bo.li@geophysik.uni-muenchen.de)*
[2]*King Abdullah University of Science and Technology (KAUST), Saudi Arabia*
[3]*Scripps Institution of Oceanography, University of California (UCSD), USA*
[4]*Icelandic Meteorological Office (IMO), Iceland*
[5]*University of Iceland (UI), Iceland*
[6]*Technical University of Munich (TUM), Germany*

The Húsavík–Flatey fault Zone (HFFZ), with fault segments aligned with the tectonic deformation, is one of the seismically most active zones in Iceland. It is able to host earthquakes with M>6 and poses a high seismic risk to Húsavík town and nearby coastal communities in Northern Iceland. Húsavík is the second largest town in the area and an important touristic site, located directly on the top of the eastern segment of the HFFZ. The seismic hazard assessment of the HFFZ attracts the interests of many seismologists, but the research is challenging due to limited data and mostly offshore fault segments.

In this study, we use the open source **SeisSol** (https://github.com/SeisSol/SeisSol) wave propagation solver (e.g., Käser & Dumbser, Uphoff et al., 2017) to perform 3-D spontaneous dynamic rupture simulations of the HFFZ and investigate physics-based ground motion synthetics in Northern Iceland. We integrate data from high-resolution bathymetry interpretation, offshore seismic reflection campaigns in Northern Iceland (Brandsdóttir et al., 2005; Magnúsdóttir et al., 2015; Hjartardóttir et al., 2016) and relocated seismicity (Aribil et al., 2018) to construct geometric fault models of varying complexity (Figure 1), representing alternative views of the fault system geometry based on the available data. The complex model (Model-A) is a high segmentation model of the HFFZ, consisting of 55 partially intersecting, non-planar vertical faults, each intersecting with the complex free surface. Model-B corresponds to a simplified and less segmented fault mode by smoothing out small-scale complexities, such as sharp features and merging multiple segments. This reduces the HFFZ to four fault segments, with a ~4 km wide open gap separating the central and eastern segments. Model C closes the gap and reduces the HFFZ to only three segments. Motivated by the depth distribution of the relocated seismicity, we limit slip at depth by smoothly tapering deviatoric stresses from 9 km to 11 km at depth. We also implement the topography and bathymetry from GeoMapApp, a 3D velocity structure (Abril et al., 2021) in our model, and account for the the possibility of off-fault energy dissipation, by assuming a non-associated Drucker-Prager elasto-viscoplasticity rheology (Wollherr et al., 2018) and the attenuation following the empirical relation in Olsen et al. (2009). In addition, we also explore the fault roughness effect on rupture dynamics and the ground motions. We load all three models with a laterally homogeneous regional stress field from seismo-tectonic observations (Angelier et al., 2004; Ziegler et al., 2016) combined with physical assumptions on fault fluid pressurization and the Mohr-Coulomb theory of frictional failure, following Ulrich et al., 2019. The dynamic model parameters used for the varying geometry scenarios are summarized in Table 1.

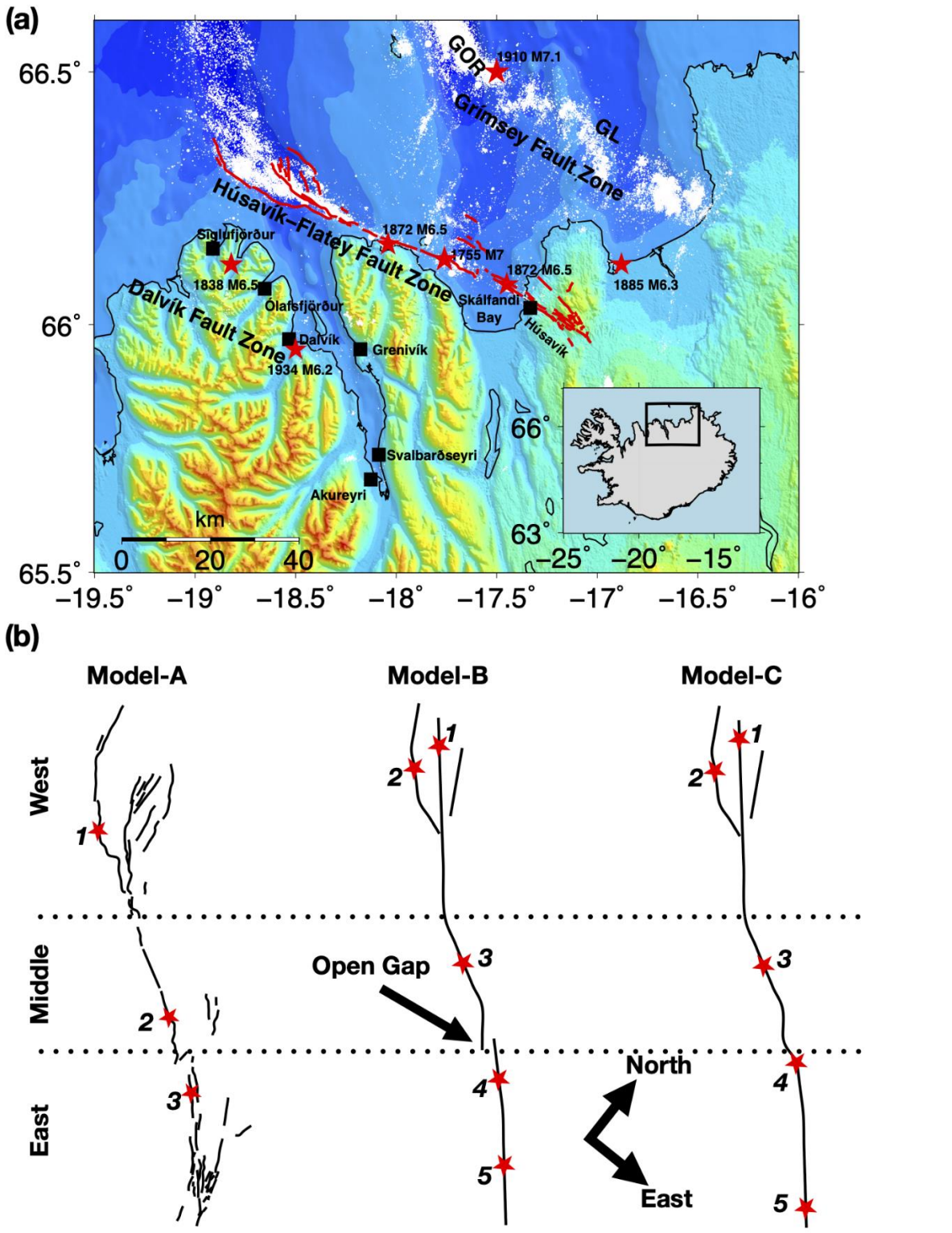

Figure 1. (a) Map of the Tjörnes Fracture Zone. White dots show relocated earthquakes from 1993 to 2019 (Abril et al., 2018) and red stars mark the locations of historic large earthquakes (Stefansson et al., 2008). The red lines show the complex segmented fault traces of the HFFZ (Halldórsson, 2019). The black squares mark the locations of major towns. The inset shows a map of Iceland, with the black box indicating the zoomed-in study region. (b) Fault geometry models used in dynamic rupture simulations. The black solid lines are the fault traces. Stars show the varied epicenter locations, with the index numbers identifying each rupture scenario. The dashed lines divide the HFFZ into the western, central, and eastern sections. The complex Model A is traced in (a).

Table 1. Dynamic model parameters for Model A, B and C. Fault network geometry specific differences are highlighted in bold.

Parameter	**Model A**	**Models B & C**
Static friction coefficient (μ_s)	0.55	0.55
Dynamic friction coefficient (μ_d)	0.1	0.1
Critical slip distance (D_c) within nucleation area (m)	**0.4**	**0.2**
Critical slip distance (D_c) ouside nucleation area (m)	**0.4**	**0.5**
SH_{max}	155	155
Seismogenic depth (km)	10	10
Maximum pre-stress ratio (R_0)	**0.85**	**0.55**
Pore fluid ratio (γ)	**0.75**	**0.6**
Stress shape ratio ($s2_{ratio}$)	0.5	0.5
Nucleation patch radius (km)	1	1.5

With different fault models and varying the hypocenter locations, we explore the rupture dynamics of different scenarios and the associated ground motions. By constraining the regional stress using available stress inversion studies, we are able to generate rupture scenarios that match historic magnitude 6.5 and 7 events (Figure 2a,b). Our results show that the fault geometry has a strong effect on multi-fault rupture dynamics across the HFF. Rupture scenarios based on a more complex geometry (Model A) are characterized by complicated rupture evolution, including distant dynamic and static triggering, backward rupture of fault branches, and episodes of slip at sub-Rayleigh and supershear rupture velocities (Figure 2c,d). On the other hand, rupture scenarios on simpler fault geometries generally propagate more smoothly, at sub-Rayleigh rupture velocity and break a larger portion of the fault system, leading to larger magnitude scenarios. The complex Model-A does not favor rupture scenarios that result in earthquakes larger than Mw7. In contrast, the smooth and connected faults of Model-B and Model-C can be easily ruptured and generate Mw7+ rupture scenarios, with magnitude reaching ~Mw7.3 for a through-going rupture across model-C breaking the whole main fault.

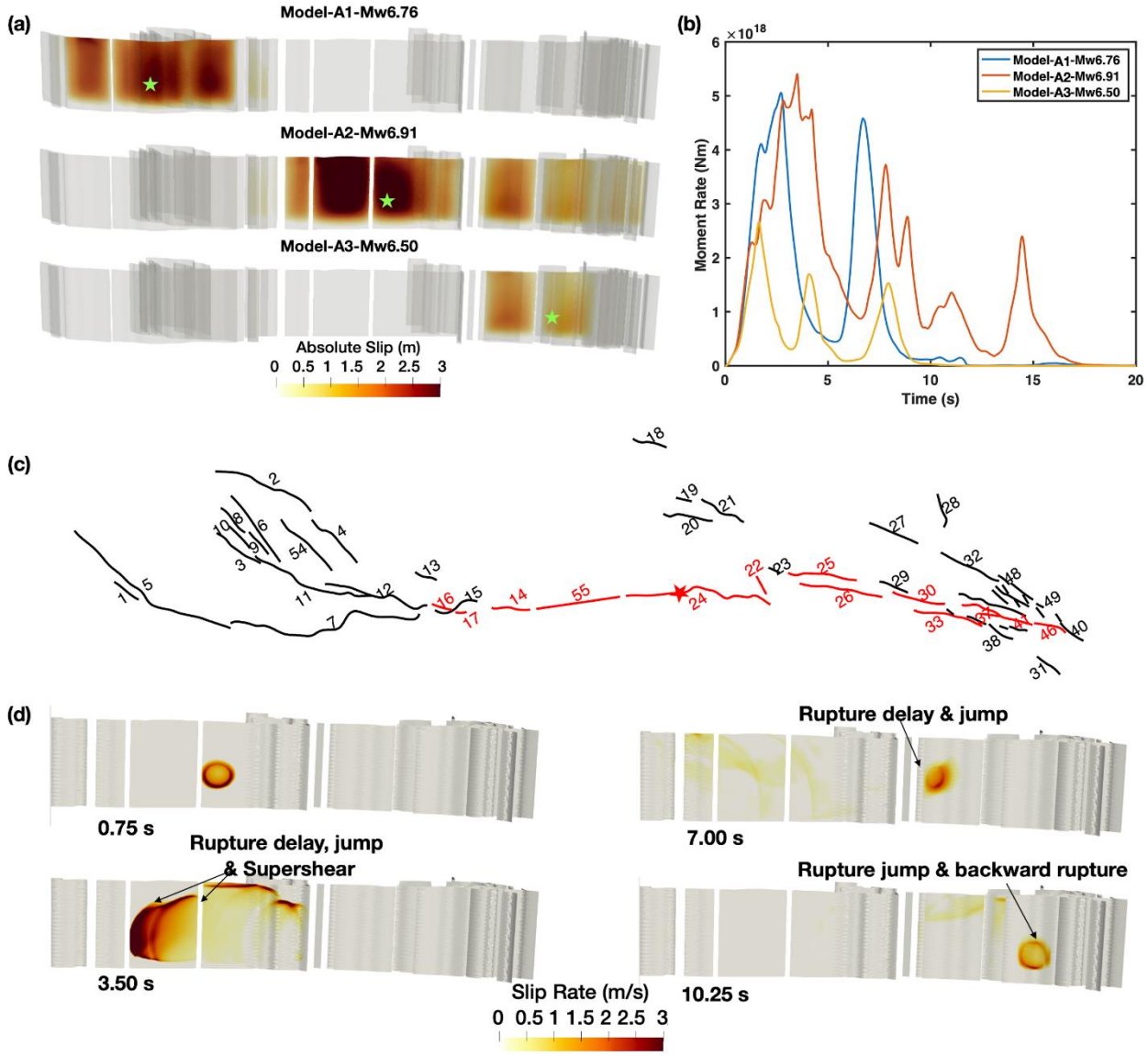

Figure 2. (a) Accumulated fault slip distribution for the three rupture scenarios across Model-A with varying hypocenters. (b) Moment rate evolution for three Model-A scenarios. (c) Map view of the fault traces for Model-A2, with numbers denoting the fault index and red color denoting the ruptured fault segments. (d) Snapshots of the absolute slip rate at selected rupture time for rupture Model-A2.

All simulated scenarios yield heterogeneous ground shaking distributions. We observe ground shaking amplification from rupture directivity, from localized geometric complexities, such as fault gaps and kinks, and both amplification and shielding from topography (Figure 3a,b). The attenuation of the physics-based ground motion with distance from the faults shows magnitude consistent attenuation relationship, especially in the near-fault region, and overall good agreement with empirical ground motion models (GMMs) specific to the Southern Iceland Seismic Zone (Kowasari et al., 2020) (Figure 3c,d). The ground motion variability changes with distance to the fault and has higher values for unilateral than bilateral rupture scenarios.

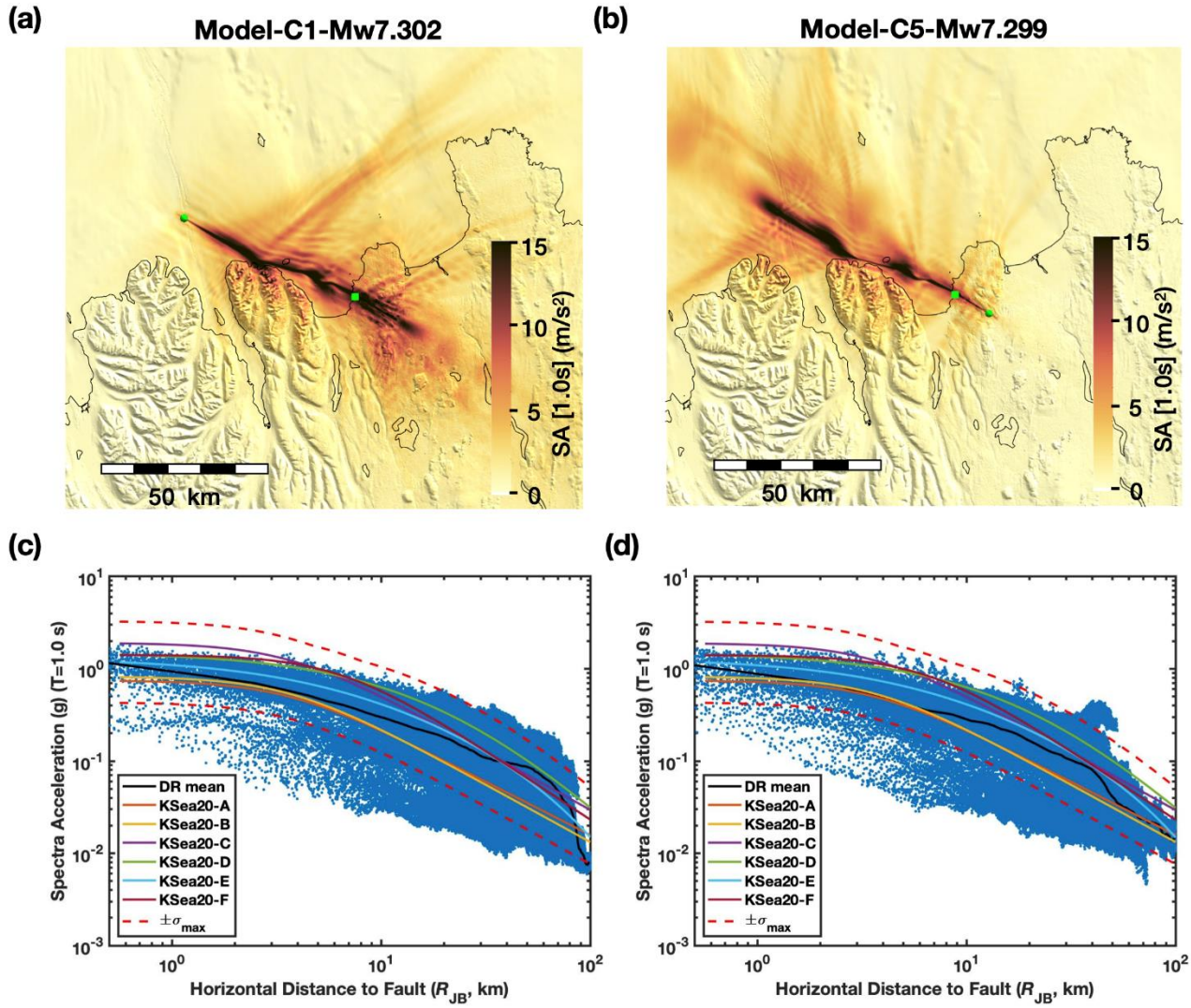

Figure 3. (a) and (b) show the ground motion (spectral acceleration SA[1.0 s] in m/s^2 for two rupture scenarios across Model C. (c) and (d) are the comparison between the synthetic ground motion and empirical GMMs.

Table 2 summaries the peak ground motion (SA[1.0 s]) at selected towns showing in Figure 1a. It shows Húsavík, which sits on the eastern segment of the HFFZ, experiences the strongest ground shakings in most scenarios. The strongest SA[1.0 s] of up to ~1.55 g is in the Mw7.3 scenario C3. We note that at Húsavík, Mw7.3 scenarios C4 and C5 and Mw6.9 scenarios B4 and B5 generate similar levels of ground shaking, despite their differing magnitudes. This suggests that for such large earthquakes, a small portion of the ruptured faults can dominate locally the near field ground shaking.

In addition, we use another open-source code **SHERIFS** (Chartier et al., 2019, https://github.com/tomchartier/SHERIFS) to estimate annual seismic rates on each fault segment and the whole HFFZ. The simulation results show good agreement with the available catalog data. We are continuing building up the dynamic rupture scenarios database consisting of hundreds to thousands mechanically plausible scenarios in HFFZ. These will enable us to perform a fully physics-based probabilistic seismic hazard assessment in our study region.

Table 2. Simulated peak ground shaking (SA[1.0 s], g) at selected towns in Northern Iceland for varying earthquake scenarios. The model with -R representing scenarios with fault roughness.

MODEL	Mw	Húsavík	Akureyri	Dalvík	Ólafsf.	Sigluf.	Grenivík
A1	6.76	0.06	0.05	0.08	0.11	0.17	0.10
A2	6.91	0.36	0.08	0.15	0.13	0.06	0.21
A3	6.50	0.32	0.04	0.05	0.03	0.02	0.06
B1	7.145	0.60	0.04	0.05	0.04	0.04	0.08
B2	6.786	0.03	0.01	0.03	0.03	0.07	0.03
B3	7.155	0.52	0.02	0.03	0.07	0.14	0.04
B4	6.945	0.66	0.02	0.02	0.02	0.01	0.04
B5	6.944	0.79	0.02	0.04	0.03	0.03	0.05
C1	7.302	1.41	0.06	0.08	0.05	0.07	0.09
C1-R	7.250	0.79	0.05	0.09	0.05	0.05	0.09
C3	7.294	1.55	0.02	0.06	0.09	0.20	0.03
C3-R	7.031	0.03	0.01	0.03	0.05	0.15	0.02
C4	7.294	0.63	0.02	0.08	0.09	0.22	0.05
C4-R	6.869	0.46	0.02	0.01	0.01	0.01	0.01
C5	7.299	0.80	0.04	0.10	0.10	0.21	0.06
C5-R	7.245	0.72	0.05	0.08	0.09	0.21	0.08

References

Abril, C., O. Gudmundsson, & SIL seismological group, Relocating earthquakes with empirical traveltimes. *Geophysical Journal International*, **214(3)**, 2098-2114, 2018.

Abril, C., A. Tryggvason, Ó. Gudmundsson, & R. Steffen, Local Earthquake Tomography in the Tjörnes Fracture Zone (North Iceland). *Journal of Geophysical Research: Solid Earth*, *126*(6), e2020JB020212, 2021.

Angelier, J., R. Slunga, F. Bergerat, R. Stefansson, & C. Homberg, Perturbation of stress and oceanic rift extension across transform faults shown by earthquake focal mechanisms in Iceland. *Earth and Planetary Science Letters*, **219**(3-4), 271-284, 2004.

Brandsdóttir, B., C. Riedel, B. Richter, G. Helgadóttir, E. Kjartansson, R. Detrick,... & N. Driscoll. Multibeam bathymetric maps of the Kolbeinsey Ridge and Tjörnes Fracture Zone, N-Iceland. *EGU General Assembly*, 2005.

Chartier, T., O. Scotti, & H. Lyon-Caen, SHERIFS: Open-source code for computing earthquake rates in fault systems and constructing hazard models. *Seismological Research Letters*, **90**(4), 1678-1688, 2019.

Hjartardóttir, Á. R., P. Einarsson, S. Magnúsdóttir, Þ. Björnsdóttir, & B. Brandsdóttir, Fracture systems of the Northern Volcanic Rift Zone, Iceland: an onshore part of the Mid-Atlantic plate boundary. *Geological Society, London, Special Publications*, **420(1)**, 297-314, 2016.

Halldórsson, B. Towards improved seismic monitoring, earthquake modeling and ground motion simulation for early warning and hazard estimates in north iceland. *In proceedings of the northquake 2019 workshop*, edited by Sigurjón Jónsson, Benedikt Halldórsson, Kristín Jónsdóttir, Páll Einarsson, Ragnar Stefánsson, Helena Eydís Ingólfsdóttir and Heiða Elín Aðalsteinsdóttir (p. 124-127), 2019.

Käser, M., & M. Dumbser, An arbitrary high-order discontinuous Galerkin method for elastic waves on unstructured meshes—I. The two-dimensional isotropic case with external source terms. *Geophysical Journal International*, ***166***(2), 855-877, 2006.

Kowsari, M., T. Sonnemann, B. Halldorsson, B. Hrafnkelsson, J.Þ. Snæbjörnsson & S. Jonsson, Bayesian inference of empirical ground motion models to pseudo-spectral accelerations of south Iceland seismic zone earthquakes based on informative priors. *Soil Dynamics and Earthquake Engineering*, **132**, 106075, 2020.

Magnúsdóttir, S., B. Brandsdóttir, N., Driscoll, & R. Detrick, Postglacial tectonic activity within the Skjálfandadjúp Basin, Tjörnes Fracture Zone, offshore Northern Iceland, based on high resolution seismic stratigraphy. *Marine Geology*, *367*, 159-170, 2015.

Olsen, K. B., S. M. Day, L. A. Dalguer., J. Mayhew, Y. Cui, J. Zhu, ... & A. Chourasia, ShakeOut-D: Ground motion estimates using an ensemble of large earthquakes on the southern San Andreas fault with spontaneous rupture propagation. *Geophysical Research Letters*, *36*(4), 2009.

Stefansson, R., G.B. Gudmundsson, & P. Halldorsson, Tjörnes fracture zone. New and old seismic evidences for the

link between the North Iceland rift zone and the Mid-Atlantic ridge. *Tectonophysics*, **447**(1-4), 117-126, 2008.
Ulrich, T., A. A. Gabriel, J. P. Ampuero, & W. Xu, Dynamic viability of the 2016 Mw 7.8 Kaikōura earthquake cascade on weak crustal faults. *Nature communications*, **10(1)**, 1213, 2019.
Uphoff, C., S. Rettenberger, M. Bader, E. H. Madden, T. Ulrich, S. Wollherr & A. A. Gabriel, Extreme scale multi-physics simulations of the tsunamigenic 2004 sumatra megathrust earthquake. In *Proceedings of the international conference for high performance computing, networking, storage and analysis* (pp. 1-16), 2017.
Wollherr, S., Gabriel, A. A., & Uphoff, C. (2018). Off-fault plasticity in three-dimensional dynamic rupture simulations using a modal Discontinuous Galerkin method on unstructured meshes: implementation, verification and application. *Geophysical Journal International*, **214**(3), 1556-1584.
Ziegler, M., M. Rajabi, O. Heidbach, G. P. Hersir, K. Ágústsson, S. Árnadóttir & A. Zang, The stress pattern of Iceland. *Tectonophysics*, **674**, 101-113, 2016.

NorthQuake 2022 - The 4th International Workshop on Earthquakes in North Iceland
Húsavík, North Iceland, 18-20 October 2022

Modeling potential earthquake-tsunami scenarios from earthquake rupture simulations on the Húsavík-Flatey Fault Zone, North Iceland

Fabian Kutschera[1], Alice-Agnes Gabriel[2,1], Sara A. Wirp[1], Bo Li[3,1], Thomas Ulrich[1], Claudia Abril[4], and Benedikt Halldórsson[5,6]

[1]*Institute of Geophysics, Department of Earth and Environmental Sciences, Ludwig-Maximilians-University, Munich, Germany (fabian.kutschera@geophysik.uni-muenchen.de, sara.wirp@geophysik.uni-muenchen.de, bo.li@geophysik.uni-muenchen.de, thomas.ulrich@geophysik.uni-muenchen.de)*
[2]*Institute of Geophysics and Planetary Physics, Scripps Institution of Oceanography, UC San Diego, United States (algabriel@ucsd.edu)*
[3]*King Abdullah University of Science and Technology (KAUST), Thuwal, Saudi Arabia*
[4]*Department of Earth Sciences, Uppsala University, Sweden (claudia.abril@geo.uu.se)*
[5]*Division of Processing and Research, Icelandic Meteorological Office, Reykjavík, Iceland*
[6]*Faculty of Civil and Environmental Engineering, University of Iceland, Reykjavík, Iceland (skykkur@hi.is)*

Joint earthquake and tsunami hazard assessment plays an important role to mitigate the economical and societal impact of future tsunamigenic events. Crustal earthquakes associated with unexpected tsunamis such as the 2018 Mw 7.5 strike-slip Sulawesi or 2020 Mw 7.0 normal-faulting Samos event emphasize the necessity to intensify studies of the tsunami potential posed by active submarine faults. We investigate physics-based 3D dynamic earthquake rupture scenarios and tsunami generation for the ~100km long Húsavík Flatey Fault Zone (HFFZ) in North Iceland using one-way linking (Madden et al., 2020; Wirp et al., 2021) and novel fully-coupled earthquake-tsunami modeling techniques (Krenz et al., 2021). The one-way linked workflow uses the simulated time-dependent seafloor displacement as forcing term for a non-linear shallow water solver. The fully-coupled method captures in a unique 3D model earthquake rupture, seismic and acoustic wave propagation in the Earth and the ocean, as well as tsunami wave generation and propagation (Abrahams et al., 2022).

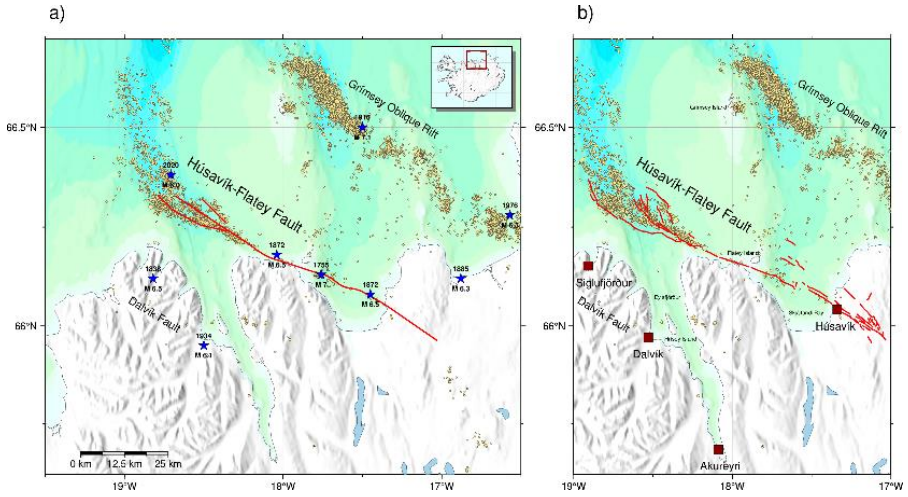

Figure 1. Overview of the Tjörnes Fracture Zone with yellow circles representing relocated seismicity from 1993 to 2019 (Abril et al., 2018, 2019). a) Simple fault geometry shown by red lines and (historic) large earthquakes with $M \geq 6$ indicated by blue stars (Ambraseys and Sigbjörnsson, 2000; Stefansson et al., 2008; Þorgeirsson, 2011; Jónsson, 2019). b) Complex fault geometry of the HFFZ with 55 fault segments in red (Brandsdóttir et al., 2005; Magnúsdóttir and Brandsdóttir, 2011; Magnúsdóttir et al., 2015; Hjartardóttir et al., 2016; Abril et al., 2021; Li et al., 2022)

together with major towns in the region of Norðurland eystra.

The HFFZ belongs to the Tjörnes Fracture Zone (TFZ) and is situated in-between the Grímsey Oblique Rift (GOR) and the Dalvík Fault (DF). The TFZ is part of the Mid-Atlantic Ridge (MAR) connecting the Kolbeinsey Ridge (KR) with fault segments traversing Iceland onshore. The Eurasian Plate diverges eastwards with an average plate spreading velocity of ~18mm/yr relative to the North American Plate (Demets et al., 2010). Metzger and Jónsson (2014) estimated that 1/3 of the full transform motion is taken up by the HFFZ, which corresponds to a slip rate of 6–9 mm/yr. The locked HFFZ may host potential Mw 6.8±0.1 earthquakes (Metzger et al., 2011, 2013), posing a significant threat to coastline communities such as the city of Húsavík, which is located directly above the Húsavík Flatey Fault Zone at the eastern side of Skjálfandi Bay. The region of Norðurland eystra has experienced several stronger earthquakes in the past. Two magnitude 6 earthquakes occurred in 1872 (Jónsson, 2019) and a recent Mw 6 earthquake struck on the western end of the HFFZ in 2020 (Fig. 1). The strongest historically recorded Mw 7 event in 1755 caused extensive damage and may have generated a series of waves hitting the coastline (Þorgeirsson, 2011; Ruiz-Angulo et al., 2019).

We first present physics-based 3D dynamic rupture models with varying hypocenter locations simulated with SeisSol (https:// github.com/SeisSol). SeisSol enables us to explore newly inferred simpler and complex fault geometries (Fig. 1) that have been compiled and proposed in the ChEESE project (https://cheese-coe.eu) by using unstructured tetrahedral meshes together with high-order accuracy in space and time based on the ADER-DG method. Next, for the one-way linking to tsunami simulations, we use the time-dependent seafloor displacement output from SeisSol to initialise sea surface perturbations within sam(oa)^2-flash. The dynamically adaptive, parallel software sam(oa)^2-flash solves the hydrostatic non-linear shallow water equations (Meister et al., 2016). Here we consider the contribution of the horizontal ground deformation of realistic bathymetry to the vertical displacement following Tanioka and Satake (1996). In distinction, the fully-coupled approach combines earthquake rupture and tsunami generation into one single simulation to account for 3D elastic, acoustic and gravity (i.e., tsunami) wave excitation and propagation simultaneously (Krenz et al., 2021).

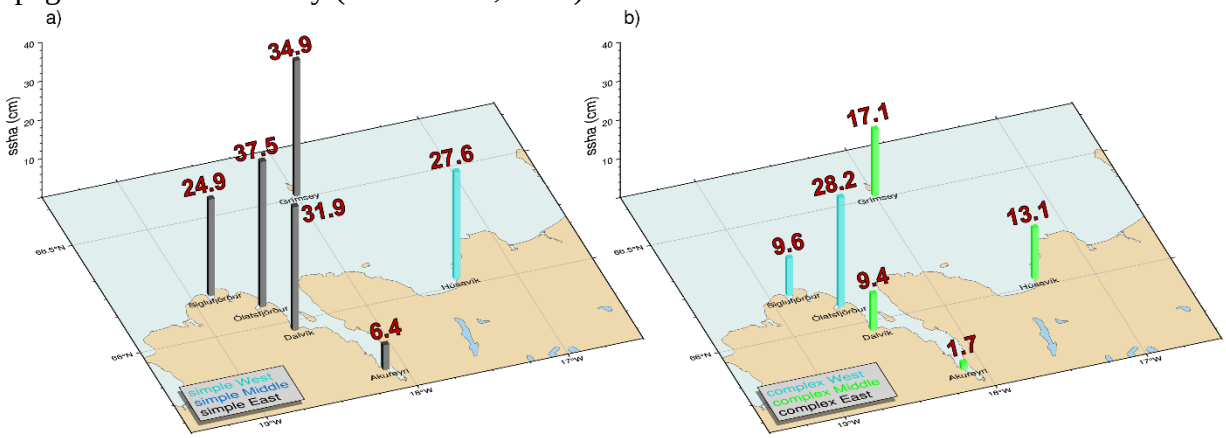

Figure 2. Maximum sea surface height anomaly (ssha [cm]) recorded at synthetic tide gauge stations nearby local communities in North Iceland for the one-way linked scenarios based on the simpler fault geometry (a) and the complex fault geometry (b). The figure aggregates the maximum ssha across the explored hypocenter locations.

Our dynamic rupture scenarios can generate up to ~1m of vertical coseismic displacement with magnitude ranges between Mw 6.7 to 7.3. All simulations are controlled by spontaneous fault

interaction in terms of dynamic and static stress transfer and rupture jumping across the complex fault network. The initial conditions are constrained by seismic and geodetic data, including a 3D velocity model (Abril and Gudmundsson, 2018; Abril et al., 2021), the locking depth (Metzger and Jónsson, 2014), estimates of the maximum horizontal stress (Angelier et al., 2004; Ziegler et al., 2016) together with Andersonian theory of faulting (Anderson, 1905). The models reveal dynamic rake rotation of ±20◦ near the surface, indicating the presence of dip-slip components, which has recently been observed for surface breaking earthquakes using slickenlines (Kearse et al., 2019; Kearse and Kaneko, 2020). The locally high amplitudes of shallow fault slip of up to 8m and distributed off-fault plastic yielding contributing 2.87% to the total seismic moment further add to the tsunami genesis. The sea surface height anomaly (ssha), which is defined as the deviation from the ocean at rest and measured at synthetic tide gauge stations along the coastline, provides an estimate about the impact of the tsunami. Our physically informed "worst-case" tsunami simulation caused by dynamic earthquake rupture of Mw 7.3 on the simpler fault geometry with the hypocenter in the East results in a total amplitude (maximum crest to valley difference) of ∼1m with nearly 40cm positive wave height observed at synthetic tide gauge stations in the vicinity of coastal towns (Fig. 2).

The comparison of the one-way linked and fully-coupled results reveal comparable maximum simulated wave heights. Acoustic waves and normal dispersion of the tsunami, which are neglected in the one-way linked scenarios, are present in the fully-coupled simulations (Fig. 3). Space-time plots of the sea surface vertical velocity (ssvv) provide valuable insight into the complex superposition of different wave types within the shallow bathymetry in North Iceland. A better understanding of these realistic scenarios may enhance future tsunami early warning (Yamamoto, 1982; Stiassnie, 2010; Gomez and Kadri, 2021).

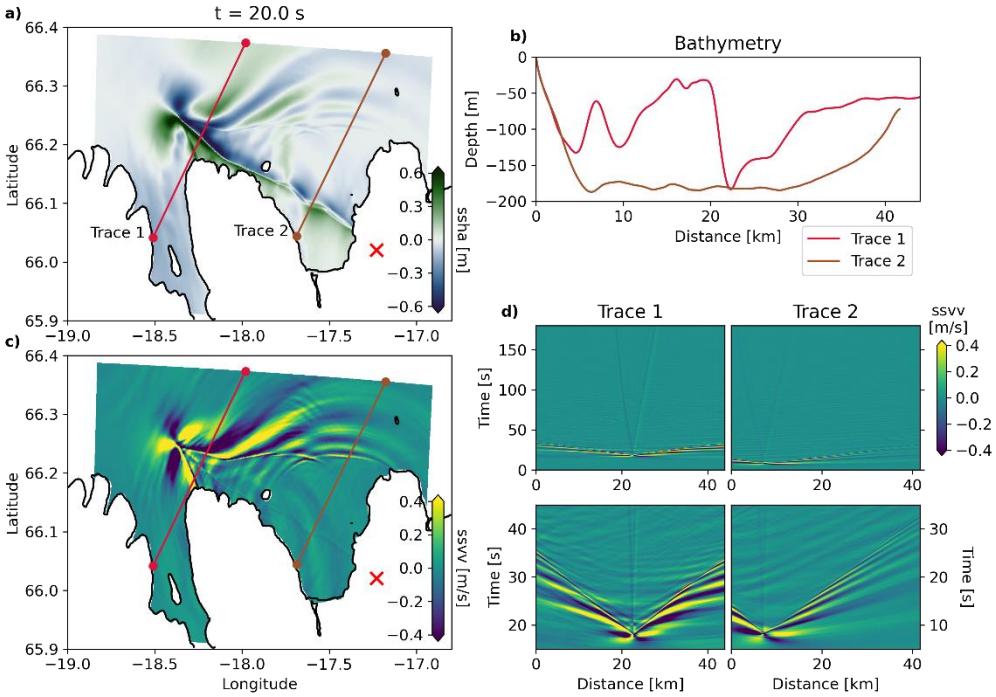

Figure 3. Fully-coupled scenario (cf. Krenz et al. (2021)) with dynamic earthquake rupture on the simpler fault geometry and hypocenter in the East (red cross). Snapshots at t = 20s of a) the sea surface height anomalies (ssha) and c) sea surface vertical velocity (ssvv). b) Corresponding bathymetry profiles along the two selected traces stretching from the shoreline (0km) towards the open ocean. d) Space-time plots of ssvv along the two traces for the full simulation (upper row, focusing on the tsunami waves) and initial tsunami generation (lower row, focusing on the acoustic waves).

References

Abrahams, L. S., L. Krenz, E. M. Dunham, A. A. Gabriel, and T. Saito, Comparison of methods for coupled earthquake and tsunami modeling, Geophysical Journal International, https://eartharxiv.org/repository/view/3453, 2022.

Abril, C., O. Gudmundsson and the SIL seismological group: Relocating earthquakes with empirical traveltimes, *Geophysical Journal International*, **214**, 2098–2114, https://doi.org/10.1093/GJI/GGY246, 2018.

Abril, C., O. Gudmundsson, and A. Tryggvason, Earthquake Relocation in the Tjörnes Fracture Zone, in: *Proceedings of the Northquake 2019 workshop*, edited by Jónsson, S., Halldórsson, B., Jónsdóttir, K., Einarsson, P., Stefánsson, R., Ingólfsdóttir, H. E., and Aðalsteinsdóttir, H. E., pp. 37–40, Þekkingarnet Þingeyinga / Husavik Academic Centre, https://hac.is/wp-content/uploads/Northquake2019.pdf, 2019.

Abril, C., A. Tryggvason, O. Gudmundsson, and R. Steffen: Local Earthquake Tomography in the Tjörnes Fracture Zone (North Iceland), Journal of Geophysical Research: Solid Earth, **126**, e2020JB020 212, https://doi.org/10.1029/2020JB020212, 2021.

Ambraseys, N., and R. Sigbjörnsson, Re-appraisal of the seismicity of Iceland, Polytechnica – Engineering Seismology, 3, 183, 2000.

Anderson, E. M., The dynamics of faulting, *Transactions of the Edinburgh Geological Society*, **8**, 387–402, https://doi.org/10.1144/TRANSED.8.3.387, 1905.

Angelier, J., R. Slunga, F. Bergerat, R. Stefansson, and C. Homberg, Perturbation of stress and oceanic rift extension across transform faults shown by earthquake focal mechanisms in Iceland, *Earth and Planetary Science Letters*, **219**, 271–284, https://doi.org/10.1016/S0012821X(03)00704-0, 2004.

Brandsdóttir, B., C. Riedel, B. Richter, G. Helgadóttir, E. Kjartansson, R. Detrick, T. Dahm, L. Mayer, B. Calder, and N. Driscoll, Multibeam bathymetric maps of the Kolbeinsey Ridgeand Tjörnes Fracture Zone, N-Iceland, European Geosciences Union, https://meetings.copernicus.org/www.cosis.net/abstracts/EGU05/07219/EGU05-J-07219.pdf, 2005.

Demets, C., R. Gordon, and D. Argus, Geological current plate motions, Geophysical Journal International, 181, 1–80, https://doi.org/10.1111/j.1365-246X.2009.04491.x, 2010.

Gomez, B. and U. Kadri, Near real-time calculation of submarine fault properties using an inverse model of acoustic signals, *Applied Ocean Research*, **109**, 102 557, https://doi.org/10.1016/J.APOR.2021.102557, 2021.

Hjartardóttir, A. R., P. Einarsson, S. Magnúsdóttir, T. Björnsdóttir, and B.Brandsdóttir, Fracture systems of the Northern Volcanic Rift Zone, Iceland: An onshore part of the Mid-Atlantic plate boundary, *Geological Society Special Publication*, **420**, 297–314,75, https://doi.org/10.1144/SP420.1, 2016.

Jónsson, S., Do large Earthquakes in North Iceland usually occur in Winter?, in: *Proceedings of the Northquake 2019 workshop*, edited by Jónsson, S., pp. 45–48, Húsavík Academic Centre, https://hac.is/wp-content/uploads/Northquake2019.pdf, 2019.

Kearse, J. and Y. Kaneko, On-Fault Geological Fingerprint of Earthquake Rupture Direction, *Journal of Geophysical Research: Solid Earth*, **125**, e2020JB019 863, https://doi.org/10.1029/2020JB019863, 2020.

Kearse, J., Y. Kaneko, T. Little, and R. Van Dissen, Curved slickenlines preserve direction of rupture propagation, *Geology*, **47**, 838–842, https://doi.org/10.1130/G46563.1, 2019.

Krenz, L., C. Uphoff, T. Ulrich, A. A. Gabriel, L. S. Abrahams, E. M. Dunham, and M. Bader, M., 3D Acoustic-Elastic Coupling with Gravity: The Dynamics of the 2018 Palu, Sulawesi Earthquake and Tsunami, International Conference for High Performance Computing, Networking, Storage and Analysis, SC, https://doi.org/10.1145/3458817.3476173, 2021.

Li, B., A. A. Gabriel, T. Ulrich, C. Abril, and B. Halldórsson, Physics-based dynamic rupture models, fault interaction and ground motion simulations for the segmented Húsavík-Flatey Fault Zone, Northern Iceland, *Journal of Geophysical Research: Solid Earth*, 2022.

Madden, E. H., M. Bader, J. Behrens, Y. Van Dinther, A. A. Gabriel, L. Rannabauer, T. Ulrich, C. Uphoff, S. Vater, and I. Van Zelst, Linked 3-D modelling of megathrust earthquake-tsunami events: from subduction to tsunami run up, *Geophysical Journal International*, **224**, 487–516, https://doi.org/10.1093/GJI/GGAA484, 2020

Magnúsdóttir, S. and B. Brandsdóttir, Tectonics of the Þeistareykir fissure swarm, *Jökull*, pp. 65–79, 2011.

Magnúsdóttir, S., B. Brandsdóttir, N. Driscoll, R. and Detrick, Postglacial tectonic activity within the Skjálfandadjúp Basin, Tjörnes Fracture Zone, offshore Northern Iceland, based on high resolution seismic stratigraphy, *Marine Geology*, **367**, 159–170, https://doi.org/10.1016/J.MARGEO.2015.06.004, 2015.

Meister, O., K. Rahnema, and M. Bader, Parallel Memory-Efficient Adaptive Mesh Refinement on Structured Triangular Meshes with Billions of Grid Cells, ACM Transactions on Mathematical Software (TOMS), 43, https://doi.org/10.1145/2947668, 2016.

Metzger, S. and S. Jónsson, Plate boundary deformation in North Iceland during 1992–2009 revealed by InSAR time-series analysis and GPS, *Tectonophysics*, **634**, 127–138, https://doi.org/https://doi.org/10.1016/j.tecto.2014.07.027, 2014.

Metzger, S., S. Jónsson, and H. Geirsson, Locking depth and slip-rate of the Húsavík Flatey fault, North Iceland, derived from continuous GPS data 2006-2010, *Geophysical Journal International*, **187**, 564–576, https://doi.org/10.1111/j.1365-246X.2011.05176.x, 2011.

Metzger, S., S. Jónsson, G. Danielsen, S. Hreinsdottir, F. Jouanne, D. Giardini, and T. Villemin, Present kinematics of the Tjörnes Fracture Zone, North Iceland, from campaign and continuous GPS measurements, *Geophysical Journal International*, **192**, 441–455, https://doi.org/10.1093/gji/ggs032, 2013.

Ruiz-Angulo, A., K. Jónsdóttir, R. H. Þrastarson, B. Halldórsson, V. Drouin, H. Grímsdóttir and S. Jónsson, Preliminary Simulations for Tsunami Hazard in Connection with a major Earthquake on the Húsavík-Flatey Fault, in: *Proceedings of the Northquake 2019 workshop*, edited by Jónsson, S., pp. 54–60, Husavik Academic Centre, https://hac.is/wp-content/uploads/Northquake2019.pdf, 2019.

Stefansson, R., G. B. Gudmundsson and P. Halldorsson, Tjörnes fracture zone. New and old seismic evidences for the link between the North Iceland rift zone and the Mid-Atlantic ridge, *Tectonophysics*, **447**, 117–126, https://doi.org/10.1016/J.TECTO.2006.09.019, 2008.

Stiassnie, M.: Tsunamis and acoustic-gravity waves from underwater earthquakes, *Journal of Engineering Mathematics 2009* **67**:1, 67, 23–32, https://doi.org/10.1007/S10665-009-9323-X, 2010.

Tanioka, Y. and Satake, K.: Tsunami generation by horizontal displacement of ocean bottom, Geophysical Research Letters, 23, 861–864, https://doi.org/https://doi.org/10.1029/96GL00736, 1996.

Wirp, A. S., A. A. Gabriel, M. H. Schmeller, E. Madden, I. van Zelst, L. Krenz, Y. van Dinther and L. Rannabauer, 3D Linked Subduction, Dynamic Rupture, Tsunami, and Inundation Modeling: Dynamic Effects of Supershear and Tsunami Earthquakes, Hypocenter Location, and Shallow Fault Slip, *Frontiers in Earth Science*, **9**, 177, https://doi.org/10.3389/feart.2021.626844, 2021.

Yamamoto, T.: Gravity waves and acoustic waves generated by submarine earthquakes, *International Journal of Soil Dynamics and Earthquake Engineering*, **1**, 75–82, https://doi.org/10.1016/0261-7277(82)90016-X, 1982.

Ziegler, M., M. Rajabi, O. Heidbach, G. P. Hersir, K. Ágústsson, S. Árnadóttir, and A. Zang, The stress pattern of Iceland, *Tectonophysics*, **674**, 101–113, https://doi.org/10.1016/J.TECTO.2016.02.008, 2016.

Þorgeirsson, O.: Sögulegir jarðskjálftar á Norðurlandi (Historic earthquakes in Northern Iceland), in: *Proceedings of a workshop in Husavik, North Iceland*, Þekkingarnet Þingeyinga, https://hac.is/sogulegir-jardskjalftar-a-nordurlandi, 2011.

NorthQuake 2022 - The 4th International Workshop on Earthquakes in North Iceland
Húsavík, North Iceland, 18-20 October 2022

A new physics-based fault system model for the Southwest Iceland bookshelf zone

Farnaz Bayat [1], Milad Kowsari[1], and Benedikt Halldorsson[1,2]

[1]*Faculty of Civil and Environmental Engineering, School of Engineering and Natural Sciences, University of Iceland, Reykjavik, Iceland (fab14@hi.is; milad@hi.is; skykkur@hi.is)*
[2]*Geoscience Research Group, Division of Processing and Research, Icelandic Meteorological Office, Reykjavik, Iceland*

Reykjavík, the capital of Iceland, is located in the vicinity of the South Iceland seismic zone and the Reykjanes peninsula oblique rift (SISZ-RPOR) where the largest earthquakes have repeatedly taken place throughout history and caused damage. Reykjavík is home to about 2/3 of the island's population, with the additional considerations of the smaller towns surrounding the area that make the region critical to Iceland's economy (e.g., infrastructure and lifelines of our modern society, such as pipelines, bridges, roads, electric transmission lines etc.) (Einarsson 1991). The SISZ-RPOR is aligned East-West and separates the North American (moving West) and Eurasian (moving East) tectonic plates. But, rather than a single long sinistral transform fault, along the plate margin, the plate motion is released by "bookshelf faulting" on an array of short dextral and parallel North-South strike-slip faults located side by side along the entire zone (Steigerwald et al. 2020, and references therein). As such, the seismic risk is highest in Southwest Iceland (Einarsson 1991, 2008, 2014) and would require an extensive plan to prepare or recover quickly after a strong earthquake. A probabilistic seismic hazard assessment (PSHA) is the best way to reduce the risk following an earthquake (Petersen et al. 2007; Baker et al. 2021). Though the standard PSHA has been updated over the years, it could be refined even more. A reliable PSHA, requires the state-of-the-art specification of three key elements: first, the identification of seismic sources, then its seismic activity rates via a magnitude frequency distribution (MFD), and lastly creation of ground motion models (GMMs) that describe the ground shaking at any given location (McGuire 1995; Kramer 1996; Baker et al. 2021). Issues with past PSHAs in Iceland (e.g., Tryggvason et al. 1958; Solnes et al. 1994; Sigbjörnsson et al. 2008; Delavaud et al. 2012; Sólnes 2016) included that they were based on statistical analyses of various earthquakes catalogues that are subject to varying types and degrees of uncertainties, simplistic seismic source descriptions which ignored the bookshelf faulting mechanism and its extension beyond the SISZ into the RPOR (Kowsari et al. 2017; Bayat et al. 2022a, b). In this study, therefore, we present results that constitute improvements to the first two key PSHA elements, developed from first principles, that combine seamlessly and lay the foundation for physics-based approaches to PSHA in Southwest Iceland. (1) New 3D finite-fault system models of the entire Southwest Iceland bookshelf transform zone. In this model each fault is completely specified in terms of its maximum expected magnitude, dimensions (i.e., length and width) via multiple fault system realizations as revealed through our comprehensive literature research, along with their resulting long-term slip and moment rates. The model accounts for the systematic changes in how large the earthquakes can become along the zone by subdividing the SISZ-RPOR into six distinct zones, with the largest earthquakes ($\sim M_{\mathrm{w}}7$) taking place in the Eastern SISZ and the smallest ($\sim M_{\mathrm{w}}5.5$) in the Western RPOR, respectively as indicated in Figure 5. In addition, the seismogenic depth of earthquakes in the western RPOR and their gradual increase to the east in the easternmost SISZ were employed in our decision-making (Stefansson et al. 1993; Panzera et al. 2016). This zonation shown in Figure 5 will provide the salient characteristics of, and model differences between the zones in sufficient detail in what follows

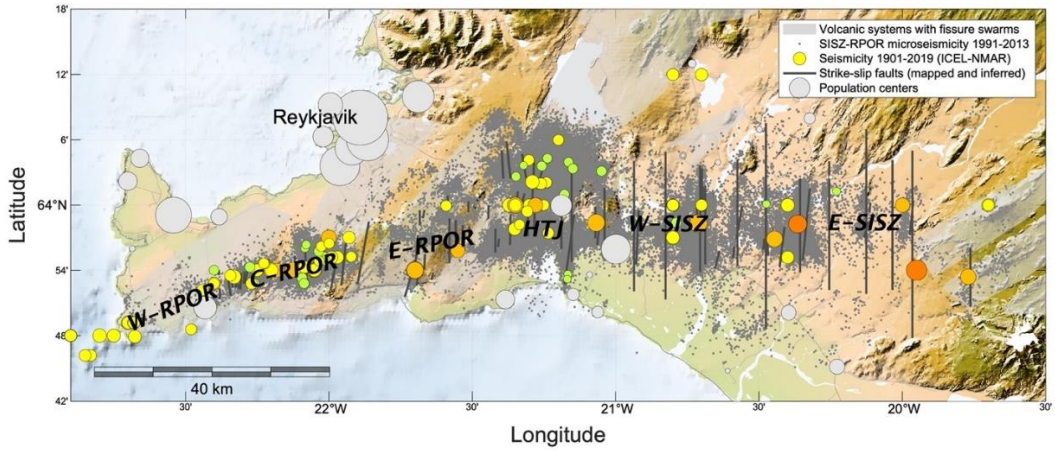

Figure 5. The seismicity along the East-West fracture zone of the SISZ-RPOR. The circles denote the revised historical earthquake catalogue of significant events from 1901-2019 (ICEL-NMAR) (Jónasson et al. 2021) and the grey dots denote the complete revised catalogue of instrumented microearthquakes from 1991-2013 (Panzera et al. 2016). The grey solid North-South lines in the SISZ denote the likely locations and fault plane extents of historical earthquakes and shorter grey lines in the RPOR indicate mapped surface traces of North-South strike-slip earthquakes.

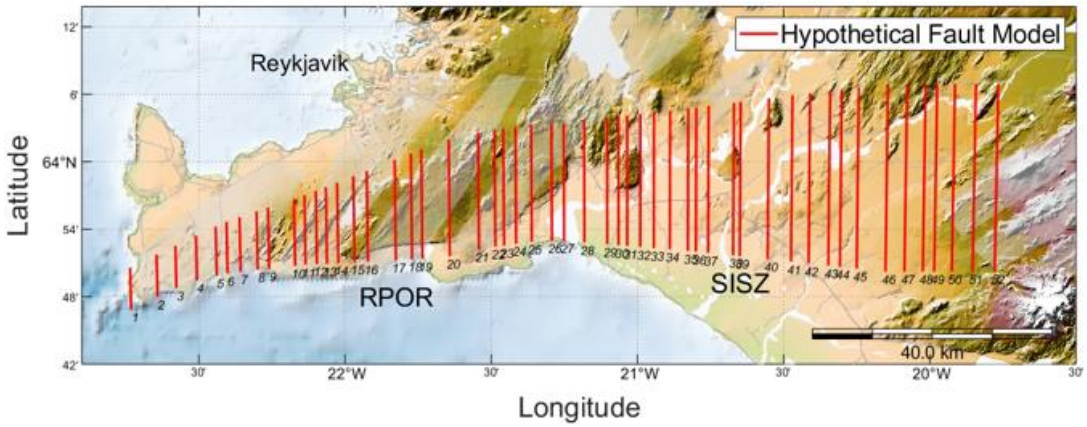

*Figure 6. One example realization of the bookshelf fault system model with North-South red lines indicating the surface fault projections of the maximum-size fault planes of near-vertical dextral strike-slip faults with the assumption of the random (**d**=1-5 km) inter-fault distance along the entire SISZ-RPOR.*

The model is then calibrated to the steady-state relative plate velocity of transcurrent tectonic motions across the zone and constrained by the geometry and the spatially variable seismogenic potential, allowing for both deterministic and random fault locations along the whole zone. In order to simulate the long-term fault slip rates for each fault, we extend the Sigmundsson et al. (1995) method by allowing variable seismogenic potential along the entire zone and assuming that the accumulation of shear strain causes the crustal blocks on each side of a N-S dextral strike-slip fault to rotate counter-clockwise, accommodating the plate motion across the zone. We then test the reliability of the model through sensitivity analyses of its all-key parameters and the total seismic moment rates produced by the fault system are completely consistent with those reported in the literature. Figure 6 shows one example of fault system realizations where we model smooth transition between zones with the systematic reduction in fault lengths from East-to-West modeling the decreasing seismogenic potential. Thigh spatial resolution in our model allows us to infer the key parameters of zone-specific MFDs i.e., the *a*-and *b*-values of the Gutenberg-Richter relationship for each zone, that results in a zone-median fault slip rate equivalent to that of the

median slip rate of our whole realizations. The new long-term Gutenberg-Richter relationships have been proposed by converting the slip rates to the corresponding seismic activity rate along with its uncertainty for each of the zones, something that was practically impossible due to the paucity of data in the historical earthquake catalogue, especially for the RPOR, and its reliability has been tested by comparing it to the historical earthquake catalogue in Southwest Iceland. The result is shown in Figure 7 where the zone-specific MFDs are shown as dotted lines, and their total MFD as the black solid line, with the grey shaded region representing the minimum extent of the uncertainty resulting from the 16-84 percentile range of slip rate distribution of all the realizations. We see in this figure that the seismicity that the physics-based model predicts effectively explains the earthquake catalogues for the transform zone of Southwest Iceland (Bayat et al. 2022a, b). The new proposed fault system model has multiple practical applications with important implications. Most notably it lays the foundation for physics-based approaches to time-independent PSHA and better mitigation of the destructive impact of the largest earthquakes in Southwest Iceland e.g., using advanced modeling methods for finite-fault earthquake rupture and seismic ground motion simulations. In addition, through the simplified but equivalent seismic source zonation and their corresponding MFDs along with the new empirical Bayesian GMMs recently proposed for Iceland (Kowsari et al. 2020), the engineering approach to PSHA can also be employed and compared to physics-based PSHA as both can now be based on the same physical model.

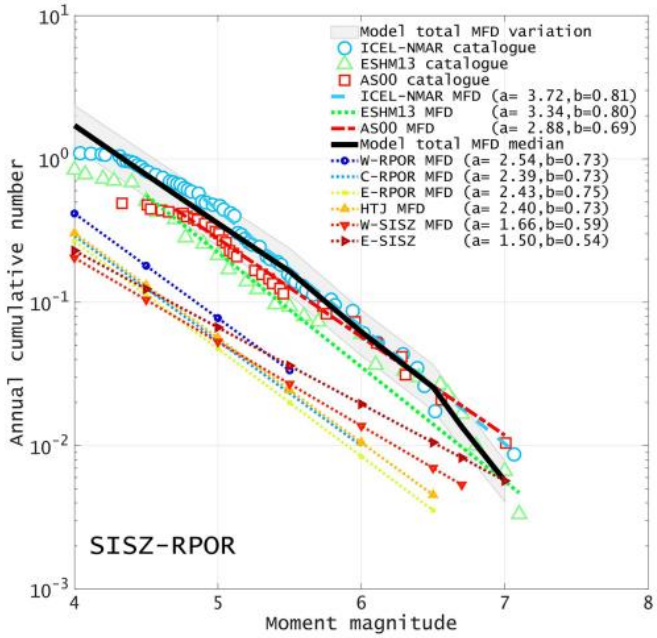

Figure 7. The Gutenberg-Richter relationship, GRs (i.e., a- and b-values) of the six subzones shown by dotted lines along with their total MFD (solid black line) for the entire zone, with the shaded region representing its uncertainty. For comparison the GRs based on various earthquake catalogues are shown as colored circles: Ambraseys and Sigbjörnsson (2000), the European Seismic Hazard Model (ESHM13, Woessner et al. (2015)) and the latest revision ICEL-NMAR (Jónasson et al. 2021).

References

Ambraseys N. N., R. Sigbjörnsson, Re-appraisal of the seismicity of Iceland. Acta Polytechnica Scandinavica 2000–003:1–184m, 2002.

Baker J., B. Bradley and P. Stafford, Seismic hazard and risk analysis. Cambridge University Press, 2021.

Bayat F., B. Halldorsson, M. Kowsari, On the Calibration of a New Finite-fault Bookshelf Fault System Model for Southwest Iceland. In: Proceedings of the 3rd European Conference on Earthquake and Engineering Seismology (3ECEES). Bucharest, Romania, p 8 (Paper No. 4353), 2022a.

Bayat F., M. Kowsari, B. Halldorsson, A new 3-D finite-fault model of the Southwest Iceland bookshelf transform zone. Geophysical Journal International 231:1618–1633. https://doi.org/10.1093/gji/ggac272, 2022b.

Delavaud E., F. Cotton, S. Akkar et al., Toward a ground-motion logic tree for probabilistic seismic hazard assessment in Europe. Journal of Seismology 16:451–473, 2012.

Einarsson P., Mechanisms of Earthquakes in Iceland. In: Beer M, Kougioumtzoglou IA, Patelli E, Au IS-K (eds) Encyclopedia of Earthquake Engineering. Springer Berlin Heidelberg, Berlin, Heidelberg, pp 1–15, 2014.

Einarsson P., Earthquakes and present-day tectonism in Iceland. *Tectonophysics* **189**:261–279, 2009.

Einarsson P., Plate boundaries, rifts and transforms in Iceland. *Jökull* **58**:35–58, 2008.

Jónasson K., B. Bessason, A. Helgadóttir, et al., A Harmonized Instrumental Earthquake Catalogue for Iceland and the Northern Mid-Atlantic Ridge. *Natural Hazards and Earth System Sciences* **21**:2197–2214. https://doi.org/10.5194/nhess-21-2197-2021, 2021.

Kowsari M., B. Halldorsson, J. Þ. Snæbjörnsson, On the Probabilistic Seismic Hazard Estimate for Húsavík, North Iceland on the basis of Monte Carlo Methods. In: *16th World Conference on Earthquake Engineering* (16WCEE). Santiago, Chile, p Paper no. 2823, 2017..

Kowsari M., T. Sonnemann, B. Halldorsson, et al., Bayesian Inference of Empirical Ground Motion Models to Pseudo-Spectral Accelerations of South Iceland Seismic Zone Earthquakes based on Informative Priors. *Soil Dynamics and Earthquake Engineering* **132**:106075. https://doi.org/10.1016/j.soildyn.2020.106075, 2020.

Kramer S. L., Geotechnical earthquake engineering. Prentice Hall, USA: New Jersey, 1996.

McGuire R. K., Probabilistic seismic hazard analysis and design earthquakes: closing the loop. *Bulletin of the Seismological Society of America* **85**:1275–1284, 1995.

Panzera F., J. D. Zechar, K. S. Vogfjörd, D. A. J. Eberhard, A Revised Earthquake Catalogue for South Iceland. *Pure Appl Geophys* **173**:97–116. https://doi.org/10.1007/s00024-015-1115-9, 2016.

Petersen M. D., T. Cao, K. W. Campbell, A. D. Frankel, Time-independent and time-dependent seismic hazard assessment for the State of California: Uniform California Earthquake Rupture Forecast Model 1.0. *Seismological Research Letters* **78**:99–109, 2007.

Sigbjörnsson R., J. Th. Snæbjörnsson, S. M. Higgins et al., Probabilistic hazard assessment of fault displacements. In: *14th World Conference on Earthquake Engineering* (14WCEE). Beijing, China, p Paper No. 07-0096, 2008.

Sigmundsson F., P. Einarsson, R. Bilham, E. Sturkell, Rift-transform kinematics in south Iceland: Deformation from Global Positioning System measurements, 1986 to 1992. Journal of Geophysical Research: Solid Earth 100:6235–6248. https://doi.org/10.1029/95JB00155, 1995.

Sólnes J., Assessment of earthquake hazard and seismic risk in Iceland. In: *International Workshop on Earthquakes in North Iceland. Húsavík, Iceland,31 May - 3 June 2016*, 2016.

Solnes J., R. Sigbjörnsson, B. Halldorsson, Assessment of Seismic Risk and Earthquake Hazard Based on Simulated and Upgraded Earthquake Catalogues. In: *Proceedings of the 9th International Seminar on Earthquake Prognostics*, San José, Costa Rica, 1994.

Stefansson R., R. Bodvarsson R. Slunga et al., Earthquake prediction research in the South Iceland seismic zone and the SIL project. *Bulletin of the Seismological Society of America* **83**:696–716, 1993.

Steigerwald L., P. Einarsson, Á. R. Hjartardóttir Fault kinematics at the Hengill Triple Junction, SW-Iceland, derived from surface fracture pattern. *Journal of Volcanology and Geothermal Research* **391**:106439. https://doi.org/10.1016/j.jvolgeores.2018.08.017, 2020.

Tryggvason E., S. Thoroddsen, S. Thorarinsson, Report on earthquake risk in Iceland. *Timarit Verkfraedingafelags Islands* **43**:81–97, 1958.

Woessner J., D. Laurentiu, D. Giardini et al., The 2013 European seismic hazard model: key components and results. *Bulletin of Earthquake Engineering* **13**:3553–3596, 2015.

NorthQuake 2022 - The 4th International Workshop on Earthquakes in North Iceland
Húsavík, North Iceland, 18-20 October 2022

Simulation of finite-fault earthquake catalogues for Monte Carlo hazard assessment

Milad Kowsari[1], Benedikt Halldorsson[1,2], and Farnaz Bayat[1]

[1]*Faculty of Civil and Environmental Engineering, School of Engineering and Natural Sciences, University of Iceland, Reykjavik, Iceland (milad@hi.is; skykkur@hi.is; fab14@hi.is)*
[2]*Geoscience Research Group, Division of Processing and Research, Icelandic Meteorological Office, Reykjavik, Iceland*

In Iceland, destructive earthquakes have repeatedly taken place throughout history in two large transform zones, the Tjörnes fracture zone in the North, and the South Iceland seismic zone (SISZ) and Reykjanes Peninsula oblique rift (RPOR) in the Southwest Iceland. In Southwest Iceland, the entire capital region along with multiple small towns are either in close proximity or on top of the fault system in the SISZ-RPOR. Therefore, the earthquake hazard is highest in these regions and performing a probabilistic seismic hazard assessment (PSHA) is vital for seismic risk mitigation and management. For the purpose of a reliable PSHA, the state-of-the-art specification of its three key elements is required: (1) seismic source models, (2) seismic activity rates denoted by a magnitude frequency distribution (MFD e.g., the Gutenberg-Richter relationship), and (3) the ground motion models (GMMs) that describe the ground-shaking parameter as a set of predictive variables such as magnitude, distance, and site effects. However, previous PSHA in Iceland have been based on simplistic statistical analyses of historical earthquake catalogues, that are subject to varying types and degrees of uncertainties. Moreover, they relied on either simplistic or plain incorrect source descriptions. Furthermore, previous PSHA in Iceland relied on either a single theoretical or empirical GMM using local data from the SISZ, regional European empirical GMMs, or several GMMs recommended for use in oceanic crustal regions. However, these GMMs did not capture the characteristics of Icelandic seismic motions, handled the uncertainties in a very limited way, did not account for the complex near-fault effects, and finally, did not account for important differences in local geology (i.e., rock, soft soil, lava-rock) (Kowsari et al. 2019, 2020).

In this study, therefore, we present a preliminary result for physics-based PSHA in Southwest Iceland using the improvements of its key elements that are: (1) a new 3D finite-fault model of the entire Southwest Iceland bookshelf transform zone, calibrated based on the rate of the tectonic plate motions across the zone and constrained by the salient features of fault geometries and seismicity characteristics, as revealed through our comprehensive literature research (Bayat et al. 2022). The model accounts for the systematic changes in how large the earthquakes can become along the zone by subdividing the SISZ-RPOR into six distinct zones, with the largest maximum earthquakes ($\sim M_{\mathrm{w}}7$) taking place in the Eastern SISZ and the smallest ($\sim M_{\mathrm{w}}5.5$) in the Western RPOR, respectively. The fault system model allows both for deterministic and random fault locations, and each fault is completely specified in terms of its maximum expected magnitude, its maximum dimensions, and its long-term seismic activity. (2) the new model allows the derivation of simple but self-consistent MFDs. This high spatial resolution allows the modelling of the seismic activity of each of the subzones, despite nearly non-existent historical data of larger magnitude

earthquakes in about half of the zone. Importantly, the long-term total MFD of the entire zone effectively explains our historical earthquake catalogue of Southwest Iceland (Fig. 1, left). Then, we extend the modelling and apply the MFDs in the generation of a synthetic catalogue of magnitude occurrences in each zone for a given catalogue length in years, something that was severely hampered due to the scarcity of data in the historical catalogue, in particular for the RPOR catalogues (Kowsari et al. 2022). In the synthetic catalogue, each earthquake magnitude is allowed to take location randomly within each zone around the center line from West to East of the historic and instrumental seismicity and constrained to the North and South by the seismicity and extent of mapped faults in the region and within the North-South extent of maximum fault lengths in the zones (Fig. 1, right).

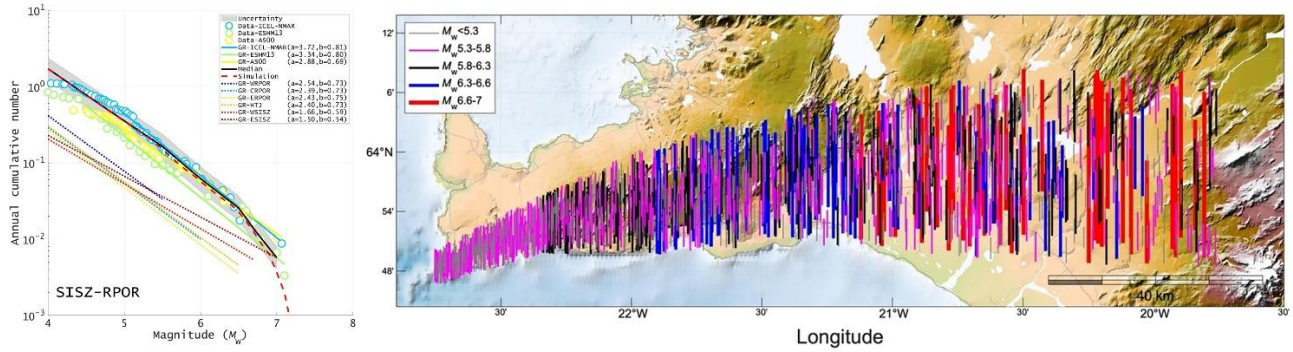

Figure 1. Left: the magnitude-frequency relationship of the six subzones shown by dotted lines along with their cumulative relationship (solid black line) and simulated finite-fault catalogue (dashed red line) with the shaded region representing its uncertainty for the SISZ-RPOR. Right: One realization of a hypothetical 3D fault system model for each zone consistent in activity with the MRD of the zone, as derived from the 3D fault system model realizations.

(3) a new set of empirical Bayesian GMMs for PGA and PSA that were calibrated to the Icelandic strong motions based on the informative priors for the physics-based saturation of near-fault peak motions at larger magnitudes (Kowsari et al. 2019, 2020). The new Bayesian GMMs thus fully capture the salient characteristics of the Icelandic ground motions, except for the complex near-fault effects.

We showed the Monte Carlo simulated finite-fault earthquake catalogues for the SISZ-RPOR are compatible with both the earthquake faulting and the long-term seismicity in the region. Therefore, these developments in the three key elements of PSHA i.e., the 3D fault system model, the finite-fault earthquake catalogues and the Icelandic Bayesian GMMs now enable the first comprehensive physics-based revision of PSHA of the SISZ-RPOR. For this purpose, we perform a Monte Carlo PSHA using six Icelandic Bayesian GMMs in a logic tree by assigning equal weights for each GMM. Fig.2 shows the mean hazard map at 10% probability of exceedance in 50 years for PGA. The PSHA are calculated over a dense grid of 145 hypothetical stations in Southwest Iceland (10*10 km) where the horizontal distance to the vertical surface projection of each fault, R_{JB}, is used as the source-to-site distance measure. The results show that the PGA values follow the spatial pattern of the faults and decreases when moving away from them, which is expected since local amplification from site effects is not considered. The highest values of ground motions are seen along the entire lengths of the SISZ-RPOR zone (i.e., PGA> 0.5 g) while it reduces to 0.08-0.14 g in the capital area.

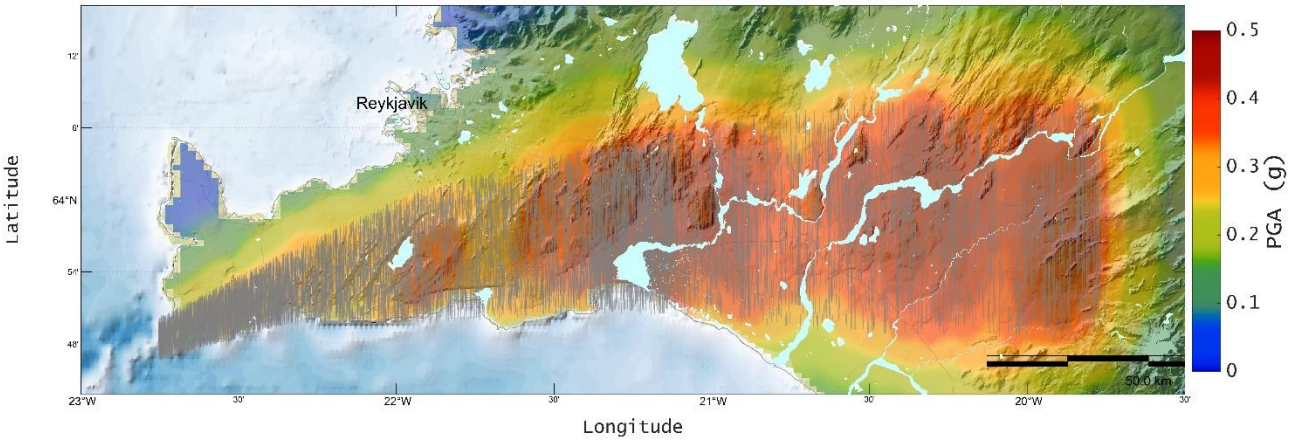

Figure 2. A preliminary PSHA map for the 10% probability in 50 years of peak ground acceleration exceedance, based on the finite-fault catalogue (gray fault lines). The faults are one realization of the 3D finite-fault system and based on the Bayesian ground motion models.

The first look at the revision of PSHA for Southwest Iceland completely avoids the use of limited statistics from observed catalogues and has firm roots in a completely physical finite-fault system of the bookshelf transform zone. The synthetic but physically consistent fault system models therefore allow bridging the gap between physics-based and statistical PSHA. Moreover, it is well known both from observations as well as physics-based modeling of earthquake rupture and near-fault ground motion simulations, that the most damaging part of near-fault seismic motion is the velocity pulse, the large-amplitude and long-period pulse-like ground motions found along the fault and away from the ends of strike-slip faults. However, Fig. 2 does not account for the near-fault effects, but it is our future task to include the near-fault effects into the physics-based PSHA for Iceland.

References

Bayat F., M. Kowsari, B. Halldorsson, A new 3-D finite-fault model of the Southwest Iceland bookshelf transform zone. *Geophysical Journal International* **231**:1618–1633, 2022.

Kowsari M., B. Halldorsson, F. Bayat, Preparation of Finite-fault Earthquake Catalogues Enabling Physics-based PSHA in Southwest Iceland. In: *Proceedings of the 3rd European Conference on Earthquake and Engineering Seismology (3ECEES)*. Bucharest, Romania, p 8 (Paper No. 8441), 2022.

Kowsari M,, B. Halldorsson, B. Hrafnkelsson, et al., Calibration of ground motion models to Icelandic peak ground acceleration data using Bayesian Markov Chain Monte Carlo simulation. *Bulletin of Earthquake Engineering* **17**:2841–2870, 2019.

Kowsari M., T. Sonnemann, B. Halldorsson, et al., Bayesian Inference of Empirical Ground Motion Models to Pseudo-Spectral Accelerations of South Iceland Seismic Zone Earthquakes based on Informative Priors. *Soil Dynamics and Earthquake Engineering* **132**:106075, 2020.

Steigerwald L., P. Einarsson, Á. R. Hjartardóttir, Fault kinematics at the Hengill Triple Junction, SW-Iceland, derived from surface fracture pattern. *Journal of Volcanology and Geothermal Research* **391**:106439, 2020.

NorthQuake 2022 - The 4th International Workshop on Earthquakes in North Iceland
Húsavík, North Iceland, 18-20 October 2022

On the validation of CyberShake in the Southwest Iceland Transform Zone Earthquakes

Otilio Rojas[1], Marisol Monterrubio-Velasco[1], Juan E. Rodríguez[1], Scott Callaghan[2], Claudia Abril[3], Benedikt Halldorsson[4,5], Milad Kowsari[5], Farnaz Bayat[5], Kim Olsen[6], Alice Agnes-Gabriel[7,8], Josep de la Puente[1]

[1]*Barcelona Supercomputing Center (BSC-CNS), Spain (otilio.rojas@bsc.es, marisol.monterrubio@bsc.es, juan.rodriguez@bsc.es, josep.delapuente@bsc.es)*
[2]*University of Southern California, USA (scottcal@usc.edu)*
[3]*Uppsala University, Sweden (claudia.abril@geo.uu.se)*
[4]*Icelandic Meteorological Office, Iceland (benedikt@vedur.is)*
[5]*University of Iceland, Iceland (milad@hi.is, fab14@hi.is)*
[6]*San Diego State University, USA (kbolsen@sdsu.edu)*
[7]*LMU, Munchen, Germany (alice-agnes.gabriel@geophysik.uni-muenchen.de)*
[8]*Scripps Institution of Oceanography, UC San Diego*

CyberShake is a high-performance computing (HPC) platform developed by the Southern California Earthquake Center to facilitate Physics-Based Probabilistic Seismic Hazard Analysis (PB-PSHA) by computing a large set of earthquake synthetic ground motion time histories from kinematic rupture scenarios on three-dimensional finite-faults. A description of the scientific methods and codes supporting CyberShake, as well as its progressive code optimization on HPC facilities can be followed in Graves et al. (2011), Callaghan et al. (2008) and Callaghan et al. (2014). Until now, CyberShake studies have been focused on California, but this work summarizes the status of the migration of the platform to the Southwest Iceland transform zone, consisting of the South Iceland Seismic Zone (SISZ) and the Reykjanes Peninsula Oblique Rift (RPOR) (~63.8° - 64.1°N, ~20°-23°W). This transform zone is one of two such regions in Iceland that are associated with the highest earthquake hazard. The SISZ-RPOR is also associated with the highest seismic risk region in Iceland, due to the proximity of the capital region where 2/3 of the population resides, in addition to several towns and villages either inside or near the zone (see Fig. 1).

In this work, we use a realization of the 3D fault system model of the SISZ-RPOR that has been proposed by Bayat et. al (2022), as constrained by fault estimated maximum extents (from slip inversions and surface mappings) and their systematic magnitude variation across the region. It presents zone-specific magnitude-frequency distribution (MFD, i.e., Gutenberg-Richter) MDFs that are representative of the average cumulative slip-rates on the 3D fault system. Such MDFs are the key input in standard PSHA using traditional engineering approaches. However, we have expanded the modeling that allows simulating a catalogue of earthquake magnitudes for a long time interval with random locations in the region that is completely consistent with the time-independent activitity predicted by the 3D fault system. This synthetic earthquake catalogue however simulates finite-size earthquake fault planes in 3D thus facilitating a PB-PSHA using either dynamic or kinematic earthquake rupture models and the corresponding ground motion simulations in particular for low-frequency and near-fault ground motion simulations. In addition, it also allows for a standard engineering approach to PSHA using empirical ground motion models in particular for the

far-field region and ground motion parameters at higher frequencies. These synthetic but physically consistent fault system models therefore will be the foundation of PB-PSHA for the SISZ-RPOR.

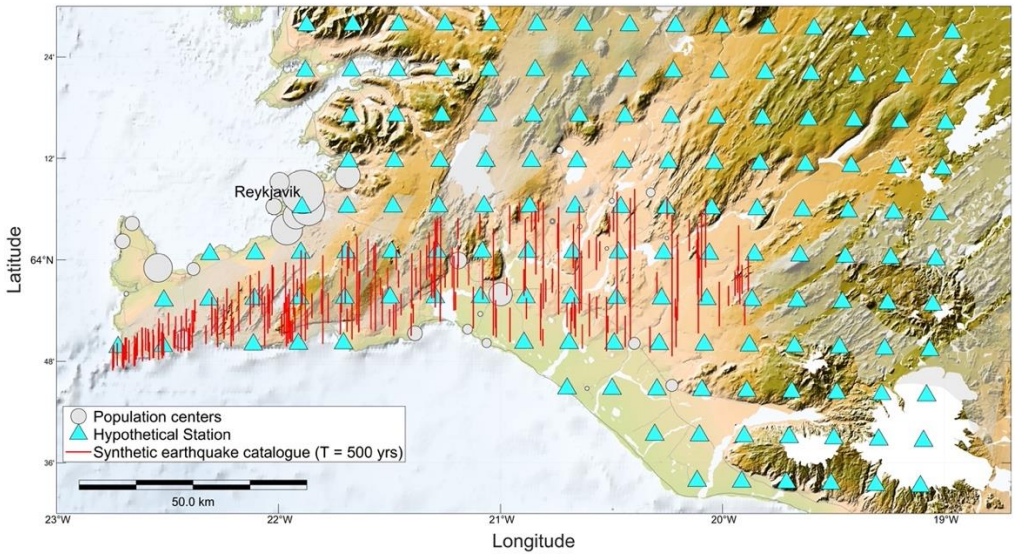

Figure 1. One realization of the synthetic fault system model (red lines) for an earthquake catalogue of 500 years, comprising 223 dextral transform faults in SISZ-RPOR and the hypothetical recording stations with 10 km grid spacing (triangles). The nearby population centers are shown in gray circles, their relative diameters indicating population size differences.

An input earthquake rupture forecast model comprised of a 500 year synthetic finite-fault earthquake catalogue has been generated using a Monte-Carlo approach, and consists of 223 dextral transform faults with magnitudes ranging from Mw5 to 7. In this overview we use an updated 1-D layered velocity model and a hypothetical grid of sites with 10 km spacing (see Fig. 1). The considered velocity model results from coupling two 1-D layered models, each one recently updated for the SISZ and the RPOR regions, based on the original model presented in Dubois et.al (2020). To avoid strong reflections from material interfaces, this model is smoothed out by applying a Gaussian moving average filter in depth.

Graves-Pitarka (GP) kinematic rupture generation starts with a random slip distribution in the wavenumber domain, that is processed by using a Von Karmann (VK) filter to roughly follow a wavenumber-squared falloff. The VK corner parameters along the strike aS and dip ad directions control the physical asperity sizes in the resulting slip model. In California CS applications, aS=2.5 and dip ad=1.5 have been set to the proposed values in Mai and Beroza (2002). Slip inversions of recent earthquakes in South Iceland are characterized by few large asperities that drive strong slip pulses at near fault locations. The GP2016 rupture generation method, with a detailed description in Graves and Pitarka (2016), are applied to produce synthetic slip distributions that are consistent with those observed in SISZ-RPOR earthquakes. Fig. 2 presents an example of a slip distribution realization, and shows that hypocenters take place out of the high-slip asperities which is also statistically consistent to slip inversions as discussed in Mai et al. (2005). The selection of GP2016 over a previous code version was the first step on this migration, with the second step being the regionalization i.e., adjustment of the model parameters for the purpose of simulating strong Icelandic earthquake rupture.

For earthquake modeling, CyberShake exploits seismic reciprocity to scale the number of simulations to the number of hazard sites, usually smaller than the size of earthquake catalogs

required for PSHA. For each hazard location, two simulations are performed using a source delta function polarized along a horizontal direction in each simulation, to compute the response of the strain tensor at each fault surface point (Strain Green Tensors-SGTs). At each fault, several kinematic rupture models are generated by the Graves-Pitarka (GP) methods that have variable hypocentral location. The convolution of these SGT with GP ruptures produce particle-velocity seismograms at each hazard site. These integrations are completely independent and therefore embarrassing parallel. The second step is the development of the UnifiedCSWflow, an open workflow manager that orchestrates the processes involved in computing the database, and largely replaces the original Pegasus- and HTC-condor-based implementation (Rodriguez J.E et al., 2022). UnifiedCSWflow has allow us to sucessfully run CyberShake at MareNostrum4, a supercomputing facility at the Barcelona Supersomputing Center (BSC).

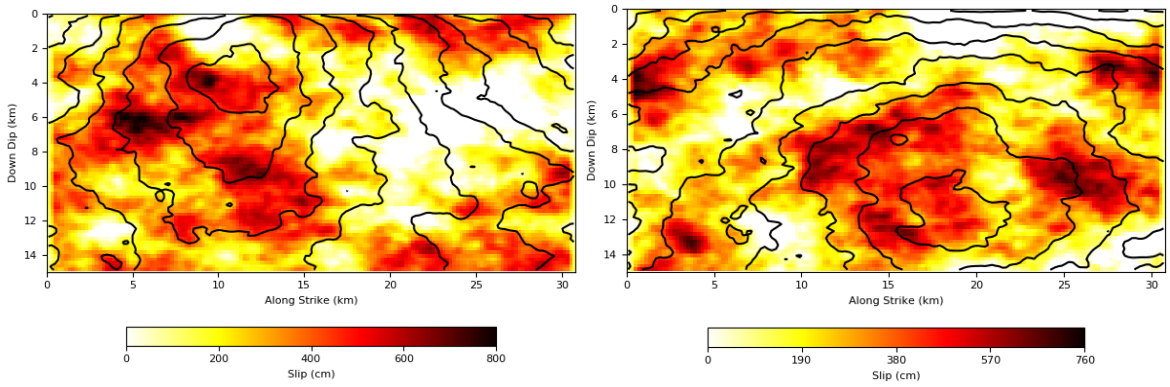

Figure 2. Two examples of slip realizations for a M_w7 event produced by the GP2016 method on a 19 km long and 9 km wide fault with varying hypocentral locations. The contour lines of the propagating rupture front are also shown.

The CyberShake ground motion simulations have been analysed and the pseudo-acceleration spectral response values have been calculated. Fig. 3 shows their comparison to a recently calibrated GMPE models for the region, (Kowsari et. al.2020). The example results are shown for events of *M*w6.0 and 6.5, left and right, respectively. Most of CyberShake results fall into a one standard-deviation band around GMPE average values, which statistically validates its migration and serves as a preliminary step for new applications for larger seismic catalogues. The results shown agree well with reference GMPEs for fault-site distances in the distance range of data availability. These satisfactory results represent an important step in the validation of the CyberShake migration to the SISZ-RPOR, and we move towards a simulation over longer synthetic catalogues on a larger and denser hypothetical station network, and to higher frequencies, to capture all the salient features of large amplitude and long-period near-fault ground motion. That will enable a full-scale PB-PSHA for the Southwest Iceland transform zone, and is an important prerequisite for the planned application of CyberShake in the Tjörnes Fracture Zone in North Iceland.

Acknowledgements
The research leading to these results has received funding from the European Union's Horizon 2020 research and innovation programme under the ChEESE project, grant agreement No. 823844. This project has also received funding from the European Union's Horizon 2020 research and innovation

programme under the Marie Sklodowska-Curie grant agreement No. 777778 MATHROCKS, and the Icelandic Research Fund (No. 196089, 'SENSHAZ'; No. 228782, GeoSitEff2Haz). Additional funding for this work comes from the DT-Geo project funded by Horizon Europe under the grant agreement No 101058129 and Geo-Inquire, grant agreement No 101058518.

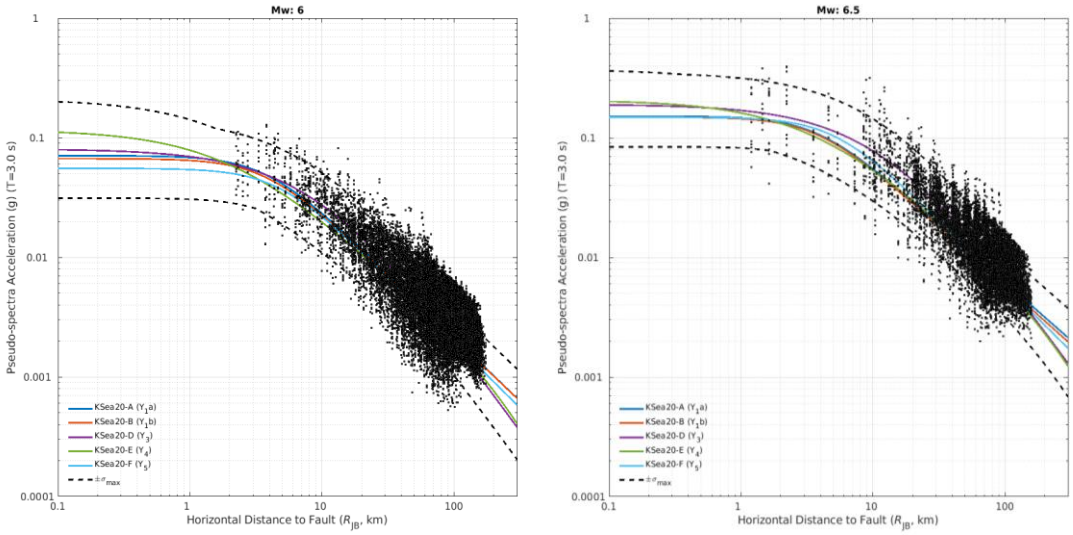

Figure 3. CyberShake PSA at 3s for events of Mw6.0 and 6.5 are compared to a reference GMPE.

References

Graves, R., T. H. Jordan, S. Callaghan, E. Deelman, E. Field, G. Juve, ... & K. Vahi, CyberShake: A physics-based seismic hazard model for Southern California. Pure and Applied Geophysics. **168**, 367-381, 2011.

Callaghan, S., P. Maechling, E. Deelman, K. Vahi, G. Mehta, G. Juve, ... & T. Jordan, Reducing time-to-solution using distributed high-throughput mega-workflows-experiences from SCEC CyberShake. In IEEE Fourth International Conference on Escience, 151-158, 2008.

Callaghan, S., P. J. Maechling, G. Juve, K. Vahi, E. Deelman, & T. H. Jordan, Optimizing CyberShake Seismic Hazard Workflows for Large HPC Resources. In AGU Fall Meeting Abstracts, pp. IN21C-3720, 2014.

Mai, P. M., and G. C. Beroza, A spatial random field model to characterize complexity in earthquake slip. Journal of Geophysical Research: Solid Earth, **107**, ESE 10-1-ESE 10-21.

Mai, P. M., P. Spudich and J. Boatwright, Hypocenter locations in finite-source rupture models. Bulletin of the Seismological Society of America, **95**, 965-980, 2005.

Graves, R., and A. Pitarka, Kinematic ground-motion simulations on rough faults including effects of 3D stochastic velocity perturbations. Bulletin of the Seismological Society of America, **106**, 2016.

Rodriguez, J. E., M. Monterrubio-Velasco, and O. Rojas and J. de la Puente. BSC-SCEC collaborative report, 2021.

Bayat, F., M. Kowsari, and B. Halldorsson, A new 3-D finite-fault model of the Southwest Iceland bookshelf transform zone. Geophysical Journal International, **231**, 1618-1633, 2022.

Kowsari, M., T. Sonnemann, B. Halldorsson, B. Hrafnkelsson, J. Snæbjörnsson, and S. Jonsson, Bayesian inference of empirical ground motion models to pseudo-spectral accelerations of South Iceland Seismic Zone earthquakes based on informative priors. Soil Dynamics and Earthquake Engineering, **132**, 106075, 2020.

Dubois, L., K. L. Feigl, D. Komatitsch, T. Árnadóttir and F. Sigmundsson, Three-dimensional mechanical models for the June 2000 earthquake sequence in the south Iceland seismic zone. Tectonophysics, **457**, 12-29, 2008.

NorthQuake 2022 - The 4th International Workshop on Earthquakes in North Iceland
Húsavík, North Iceland, 18-20 October 2022

New Geology-based Freaquency-dependent Site Amplification Functions for units in Iceland

Sahar Rahpeyma[1], Benedikt Halldorsson[1,2], Birgir Hrafnkelsson[3], and Atefe Darzi[1]

[1]*Faculty of Civil- and Environmental Engineering, School of Engineering and Natural Sciences, University of Iceland (sahar@hi.is; skykkur@hi.is (B.Ha.); atefe@hi.is)*
[2]*Division of Processing and Research, Icelandic Meteorological Office (benedikt@vedur.is)*
[4]*Faculty of Physical Sciences, School of Engineering and Natural Sciences, University of Iceland (birgirhr@hi.is)*

In Iceland, due to the prevalent surface rock condition, whether it is older bedrock or more recent lava-rock, and the relatively thin and thus easily removable topsoil layer, site effects have largely been assumed to be small and insignificant in different engineering applications. The most commonly used empirical earthquake ground motion models (GMMs) and consequently all past seismic hazard studies in Iceland largely ignore site effects. However, recent comprehensive site effect studies using advanced Bayesian statistical methods (*Rahpeyma et al., 2016, 2019, 2022*) have revealed that (i) the site effects can vary significantly, even over relatively short distances; (ii) some rock sites exhibit considerable and frequency-dependent site-effects; and (iii) site effects on variable geology are both much stronger and more variable than for rock.

In general, V_{S30} (i.e., the time-averaged shear-wave velocity in the uppermost 30 m) is known as the most common indicator to quantify site effects and used for site classifications. However, systematic estimation of V_{S30}, mapping the velocity profile with depth, or that of other proxies for the purpose of quantifying site effects has not been carried out in Iceland. To overcome this limitation, we implement a new Bayesian Hierarchical Model (BHM), that enables us to partition the ground motion residuals into various terms associated with the source, propagation path, and station terms (*Rahpeyma et al., 2018*). We use 83 strong motion data from 6 strike-slip Icelandic earthquakes recorded by the Iceland Strong motion Network (ISMN) and the first small-aperture urban array (ICEARRAY I) strong-motion stations in the South Iceland Seismic Zone (SISZ). The data were recorded by 34 strong motion stations (i.e., 25 ISMN and 9 ICEARRAY I stations). The new Bayesian GMM for peak ground acceleration (PGA) and spectral responses of various simple oscillators (PSA at different oscillator periods of T =0.01-3.0 sec) can be developed as:

$$\log Y_{es} = \log \mu_{es} + \delta B_e + \delta S2S_s + \delta WS_{es} + \delta R_{es} \quad \text{for} \quad e = 1, \dots, N \ \& \ s = 1, \dots, Q \tag{1}$$

where $\log \mu_{es}$ is a predictive model (i.e., GMM) that provides median ground motion in terms of independent variables. We use the predictive functional form of the latest GMM developed for SISZ proposed by *Kowsari et al.* (2020) as follows:

$$\log \mu_{es} = \beta_1 + \beta_2 M_e + \beta_3 \log_{10} \sqrt{R_{es}^2 + Z(M_e)^2}$$
$$Z(M_e) = \beta_4 + \beta_5 (M_e - \beta_6)^2 H(M_e - \beta_6) \tag{2}$$

In addition, δB_e presents inter-event residual (i.e., event term) denotes the overall effects, corresponding to an individual earthquake, of the observed ground motions from corresponding median estimates of the ground motion model, $\log \mu_{es}$. The event terms are assumed to be

independent of each other and follow a Gaussian distribution with zero mean and variance of τ^2. $\delta S2S_s$ presents inter-station residuals (i.e., station terms) indicates the average intra-event residual at each station and can be used to scale the ground motion model prediction to a site-specific prediction. The station terms are modelled a priori with a mean zero Gaussian distribution with an exponential covariance function (a sub-class of the Mátern family) with the inter-station variance of ϕ_{S2S}^2. The site- and event-corrected residual, δWS_{es}, captures record-to-record variability, and can be investigated for other repeatable effects. We refer to δWS_{es} as the event-station term and model it as spatially correlated variables from a zero-mean Gaussian field governed by a covariance function from the Mátern family with a marginal variance of ϕ_{SS}^2. Finally, δR_{es} is the remaining variability of the amplification factor from one record to another and it is referred to as the unexplained term. The unexplained terms are assumed to be independent and follow a mean zero Gaussian distribution with a variance of ϕ_R^2 (for more details see Rahpeyma et al. (2018)).

The Markov Chain Monte Carlo (MCMC) simulations provide estimates of the posterior distribution of the model parameters. By using the posterior median of the model parameters, the median predictions of the scaling of PGA and PSA as a function of oscillator period can be estimated. We found that the posterior distributions of $\boldsymbol{\delta S2S}$ show a systematic trend with the frequency that allows us to group them. We classify the ISMN stations into four groups of key geological units in Iceland: hard rock, rock, lava rock, and soil based on available geological information. Fig. 1 presents four groups of $\delta S2S$s classified based on geological units. We then calculate the average frequency-dependent site amplification functions for these four geological units.

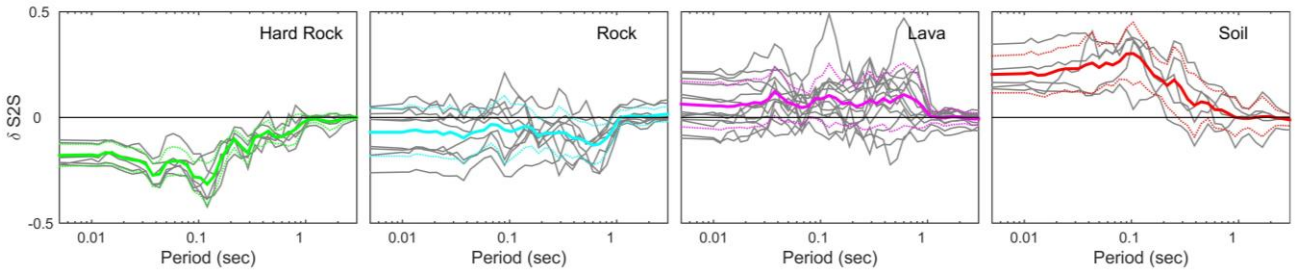

Fig. 1- Posterior median estimates (grey lines) of station terms $\delta S2S_s$, the average frequency-dependent site amplification curves (solid lines), $\overline{\delta S2S}_C \pm 1SD$ (dotted lines) that were assigned to each of the four groups of geological key units (i.e., Hard Rock, Rock, Lava, and Soil) plotted as a function of oscillator period.

By considering the geological condition we define an independent variable with which we can update our GMM. We introduce a new term, $\overline{\delta S2S}_{\mathrm{r}} = \frac{1}{N_r}\sum_i \delta S2S_i$, ($N_r$: no. of reference sites) which is the average station term of the reference stations. The average ground motion predictions at reference sites then become $\log \mu_{\mathrm{r},es} = \log \mu_{es} + \overline{\delta S2S}_{\mathrm{r}}$. Then, we estimate the predictions at other stations relative to the reference sites as $\log \mu_{\mathrm{r},es} + \delta S2S_s^{\mathrm{r}}$ where the new station terms have now been redefined as being relative to the average reference station terms $\overline{\delta S2S_s^{\mathrm{r}}} = \delta S2S_s - \overline{\delta S2S}_{\mathrm{r}}$.

Fig. 2(a) shows the GMM predictions for PSA at $T = 0.2$ sec along with the observed data, the magnitude association of which is illustrated with color-coding. This figure shows that the near-fault, as well as far-field ground motion amplitudes, are well-constrained to the Icelandic data. Furthermore, the ground motion predictions exhibit good stability outside the magnitude range of

the data (M_w>6.5) and up to the largest possible earthquake magnitude in the SISZ (M_w7.2). Fig. 2(b) compares the predictions of the new updated GMM for the hard rock site class (i.e., reference stations) with the original BHM GMM. Fig. 2(c) represents an overview of the site class-specific GMM predictions for PSA at $T = 0.2$ sec that are based on the reliable and quantitative estimates of frequency-dependent site amplification functions for key geological units in Iceland. The predictions are shown for a wide range of magnitudes that have been selected so that each respective ground motion prediction does not overlap with the next. Finally, we show in Fig. 2(d) the PSA amplitudes at $T = 0.2$ s recorded at station IS105 which is characterized as "soil" site from earthquake ground motions from three earthquakes that span a narrow magnitude range M_w6.3-6.5. Here, the reference motion $\log \mu_{r,es}$ is shown as the green dashed curve, being the reference site condition of hard rock. Then, the station term at the specified period is added to the reference motion, thus showing the station-specific prediction $\mu_r + \delta S2S_s^r$ as a black solid line. Then, the prediction for the site class that the station is associated with is shown i.e., $\mu_r + \overline{\delta S2S_C^r}$ as a red curve for station IS105. The comparison with the most recent GMM developed for Iceland (i.e., KSea20 from *Kowsari et al. (2020)*) clearly shows that the station-specific prediction improves predicting the data and the average site class prediction does almost an equally good job in predicting the ground motion amplitudes at station IS105.

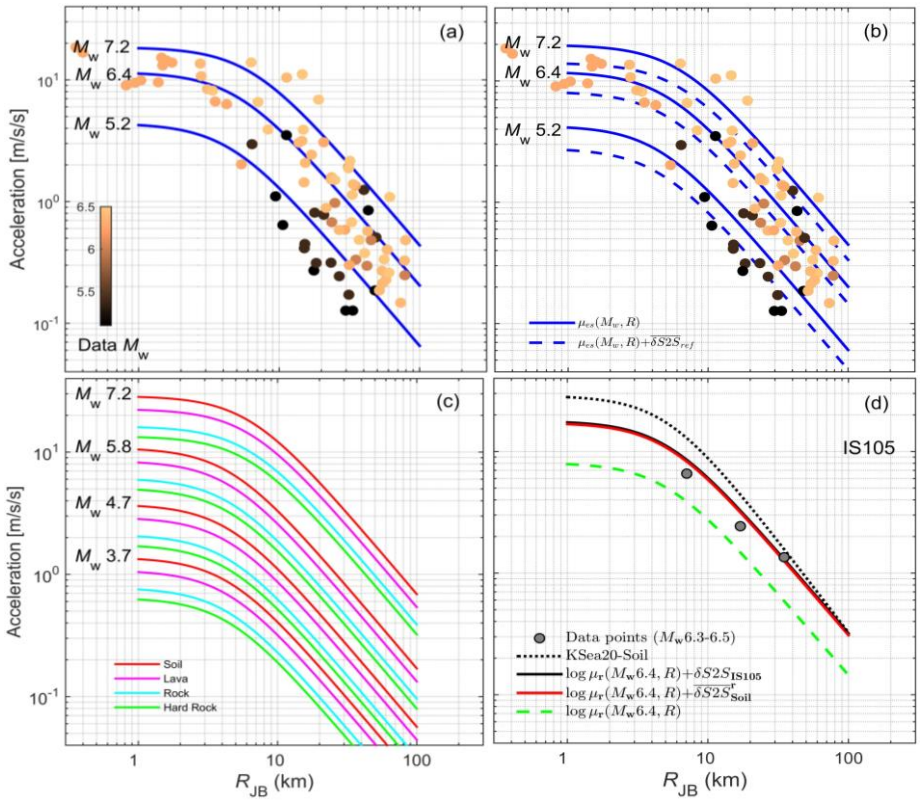

Fig. 2- (a) The attenuation of the BHM-GMM at PSA, T=0.2 sec (blue lines). The models are evaluated at three different magnitudes. The observed data are shown as color-coded circles by magnitude; (b) The GMM predictions of PSA (T=0.2 sec) at three different magnitudes for the hard rock site class (i.e., reference site class, dashed) and the ensemble average prediction model (solid, see (a)); (c) The site class-specific GMM predictions of PSA at T=0.2 sec and at various magnitudes ranging. Hard rock, rock, lava, and soil site predictions are shown by different colors, green, cyan, pink and red; (d) The site class-specific predictions of PSA at T=0.2 sec (solid lines) at station IS105 characterized as soil along with the station-specific prediction using the reference site with the relative station term added for a M_w6.4 earthquake, shown along with station data (dots) from earthquakes of M_w6.3-6.5. The reference site

(hard rock) prediction is also shown as dashed green line. For comparison, the prediction of the latest GMM that primarily provides rock vs. stiff soil predictions (Kowsari et al., 2020) are shown as black dotted lines.

References

Kowsari, M., T. Sonnemann, B. Halldorsson, B. Hrafnkelsson, J. Þ. Snæbjörnsson, and S. Jónsson, Bayesian Inference of Empirical Ground Motion Models to Pseudo-Spectral Accelerations of South Iceland Seismic Zone Earthquakes based on Informative Priors. *Soil Dynamics and Earthquake Engineering*, **132**, 106075. DOI: 10.1016/j.soildyn.2020.106075, 2020.

Rahpeyma, S., B. Halldorsson, B. Hrafnkelsson, R. A. Green and S. Jónsson, Site effect estimation on two Icelandic strong-motion arrays using a Bayesian hierarchical model for the spatial distribution of earthquake peak ground acceleration. *Soil Dynamics and Earthquake Engineering*, **120**, 369–385. DOI: 10.1016/j.soildyn.2019.02.007, 2019.

Rahpeyma, S., B. Halldorsson, B. Hrafnkelsson and S. Jónsson, Bayesian hierarchical model for variations in earthquake peak ground acceleration within small-aperture arrays. *Environmetrics*, **29**(3), e2497. DOI: 10.1002/env.2497, 2018.

Rahpeyma, S., B. Halldorsson, B. Hrafnkelsson and S. Jónsson, Frequency-dependent site factors for the Icelandic strong-motion array from a Bayesian hierarchical model of the spatial distribution of spectral accelerations. *Earthquake Spectra*, **38**(1), 648–676. SAGE Publications Ltd STM. DOI: 10.1177/87552930211036921, 2022.

Rahpeyma, S., B. Halldorsson, C. Olivera, R. A. Green and S. Jónsson, Detailed site effect estimation in the presence of strong velocity reversals within a small-aperture strong-motion array in Iceland. *Soil Dynamics and Earthquake Engineering*, **89**, 136–151. DOI: 10.1016/j.soildyn.2016.07.001, 2016.

NorthQuake 2022 - The 4th International Workshop on Earthquakes in North Iceland
Húsavík, North Iceland, 18-20 October 2022

New ground motion models for the extreme near-fault region of strike-slip earthquakes

Farnaz Bayat [1], Milad Kowsari[1], and Benedikt Halldórsson[1,2]

[1]*Faculty of Civil and Environmental Engineering, School of Engineering and Natural Sciences, University of Iceland, Reykjavik, Iceland (fab14@hi.is; milad@hi.is; skykkur@hi.is (B.H.))*
[2]*Geoscience Research Group, Division of Processing and Research, Icelandic Meteorological Office, Reykjavik, Iceland*

Iceland is the most seismically active region in Northern Europe where the strong earthquakes occur in two large transform zones, the Tjornes fracture zone (TFZ) in the northeast and the South Iceland seismic zone (SISZ) and the Reykjanes Peninsula oblique rift (RPOR) in the southwest. It is well known both from observations as well as physics-based modeling of earthquake rupture and near-fault ground motion simulations, that the most damaging part of near-fault seismic motion is the velocity pulse, the large-amplitude and long-period pulse-like ground motions, found along the fault and away from the ends of strike-slip faults (Somerville 2003; Mavroeidis and Papageorgiou 2003, 2010; Dalguer and Mai 2011; Cork et al. 2016). The velocity pulses are the result of rupture directivity effects and permanent tectonic displacements (i.e., fling steps), respectively (Mavroeidis and Papageorgiou 2002). The term "directivity" as used in the literature is a catch-all term meant to describe all the factors that cause ground motion amplitudes and polarization to vary at a constant distance from an earthquake rupture (Spudich et al. 2013). In general, directivity produces larger amplitude velocity pulses in the ground motion time histories when rupture occurs towards the site of interest and smaller amplitude when rupture propagates away from the site (Somerville et al. 1997).

The PSHA is the international standard practice on which the optimized seismic risk assessment is based and requires the state-of-the-art specification of its three key elements, (1) earthquake fault locations and sizes, their (2) seismic activity, and (3) the ground motion models (GMM). However, the GMM that is a mathematical function that includes source, path and site parameters to estimate the intensity measures (such as peak ground acceleration, PGA and pseudo spectral acceleration, PSA) has the most influential effects on the PSHA results. Recently, a set of empirical GMMs were calibrated to the Icelandic ground motion dataset using Bayesian inference through a Markov Chain Monte Carlo algorithm and informative priors for large magnitude near-fault saturation of peak motions (Kowsari et al. 2019, 2020). However, due to the lack of strong-motion data in Iceland for earthquakes larger than M_{w}6.5, the GMMs are not calibrated to constrain their complex near-fault effects. This is of utmost importance since the response of the structures to near-fault ground motions are different and design spectra that are mostly derived from far-fault records are not appropriate for engineering structures located in the near-fault region. Particularly, for SISZ-RPOR that is collocated with infrastructures and lifelines of a modern society, and the near-fault effect has been observed for the last well-recorded three strong earthquakes (M_{w} 6.3-6.5) in southwest Iceland (Halldórsson et al. 2007; Sigbjörnsson et al. 2009).

Recently, a new 3D physics-based fault system model of the bookshelf strike-slip faults in

the SISZ-RPOR has been developed that not only quantifies the location of the earthquake fault system but captures the long-term seismic activity of the region, thus effectively explaining the historical earthquake catalogue (Kowsari et al. 2022b, a; Bayat et al. 2022a, b). This model has been formally incorporated into CyberShake, the physics-based earthquake rupture modeling and ground motion simulator developed by Southern California Earthquake Center and the foundation of physics-based PSHA (PB-PSHA) for California (Graves et al. 2011; Rojas et al. 2021). As a result, the simulator captures all salient features of near-fault velocity pulses from strong Icelandic earthquakes (Halldórsson et al. 2007). On the other hand, a synthetic finite-fault catalogue of 223 earthquakes larger than M_w5 consistent with the new 3D fault system model has been generated, equivalent to a duration of 500 years seismic activity in the SISZ-RPOR (Figure 1, stars) (Kowsari et al. 2022b). Then, CyberShake has been applied in the simulation of multiple earthquake rupture scenarios for each event capturing the variability in the hypocentral locations, and the corresponding three-component synthetic ground motion time histories simulated at every station of a dense grid of 145 hypothetical stations in Southwest Iceland (Figure 8, triangles). As a result, the largest synthetic dataset of physically realistic seismic ground motion time histories has been produced for the SISZ-RPOR that consists of ~350.000 event-station pairs i.e., sets of three-component synthetic ground motion time histories.

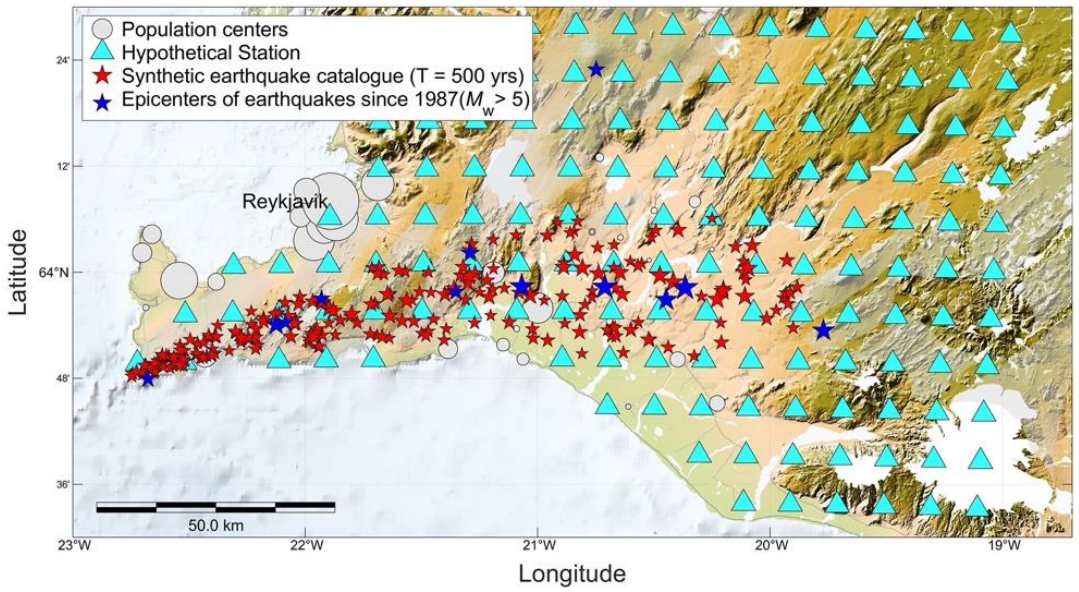

Figure 8. The region of Southwest Iceland along a 10x10 km grid of hypothetical stations for which the ground motions are simulated for each hypothetical earthquake in the 500 year-long finite-fault synthetic earthquake catalogue (red stars indicating the epicenter). The gray circles schematically indicate the locations and relative population differences of the main population centers in the region.

For comparison, the entire dataset of strong-motion time histories from tectonic earthquakes in Southwest Iceland that have been recorded on the relatively sparse Icelandic strong-motion network in the region are merely 83 event-station pairs. The actual dataset only has $M_w6.5$ as the maximum recorded earthquake magnitude with the Easternmost SISZ believed to be capable of producing M_w7-7.2 earthquake (Einarsson 2014; Jónasson et al. 2021). The first and preliminary look at the parametrization of the synthetic ground motions (in terms of horizontal pseudo spectral acceleration at 1 s period of oscillation) is presented in Figure 9 as black dots, each representing one event-station pair. In contrast, the red dots represent actual data. Both are plotted relative to the new

suite of Bayesian GMMs that importantly, confirms the validity of the synthetic dataset where we have data, and highlights the need for revised calibration at the largest magnitudes where no real data exists.

This synthetic ground motion dataset now enables us to develop a near-fault GMM by combining the prior information from synthetic dataset with the likelihood function from observed dataset in the context of Bayesian statistics. For this purpose, the advanced Bayesian Hierarchical Model (BHM) can be used that offers a flexible probabilistic framework for multilevel modeling of ground motion parameters, in which a collection of random variables can be decomposed into a series of conditional models. It also describes the relative contribution of source, path, and site effects to the overall GMM uncertainty, through its event, event-site, and site-terms, respectively, along with their associated uncertainties (Rahpeyma et al. 2021). This feature has made it beneficial for the development of GMMs in Iceland, where due to both the limited number of strong-motion recordings and their narrow earthquake magnitude ranges, all regression coefficients for a given functional form cannot be properly constrained by data alone (Kowsari et al. 2019). In this study, therefore, we augment the far-field GMMs with a physics-based near-fault directivity term (Spudich et al. 2013) and recalibrate the regression coefficients of the GMM to the synthetic and observed dataset of Iceland using a BHM. The new GMMs of this study will describes adequately the nature of the near-fault ground motions in Southwest Iceland and can be used with confidence along with the first two key elements proposed in Bayat et al. (2022), for a full-based physics-based PSHA in this region.

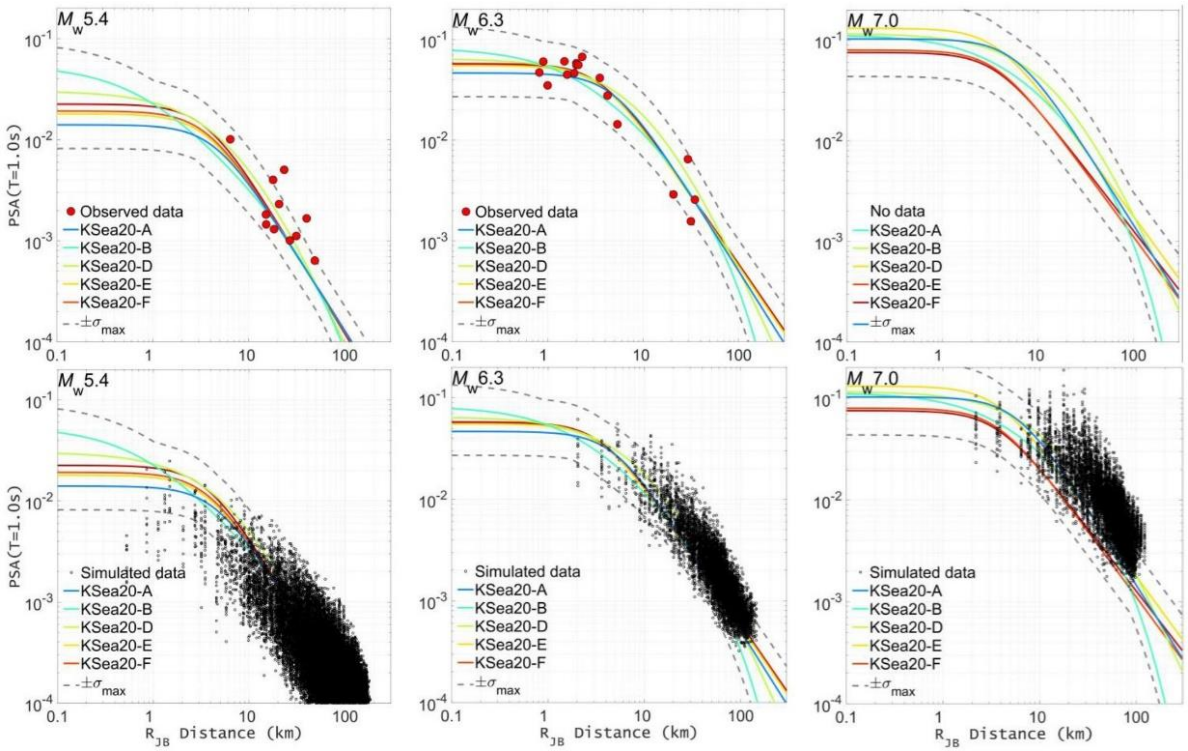

Figure 9. The attenuation with distance of pseudo spectral acceleration (PSA) at 1 s period (on rock site condition) as predicted by the new suite of Icelandic Bayesian ground motion models (solid lines) along with the envelope of their standard deviations (dashed lines), for three different magnitudes (left to right): $\boldsymbol{M_w}$5.4, 6.3 and 7.0. At top, the red circles show the extent of the actual data from earthquake mainshocks of those magnitudes that were recorded in Southwest Iceland from 1987-2008. Note that no data exists for magnitude 7. At bottom, the corresponding parametrization of the synthetic dataset is shown as a black dot, representing each event-station pair of given rupture scenario for each star and each hypothetical station in shown Figure 1.

References

Bayat F., B. Halldorsson, M. Kowsari, On the Calibration of a New Finite-fault Bookshelf Fault System Model for Southwest Iceland. In: *Proceedings of the 3rd European Conference on Earthquake and Engineering Seismology* (3ECEES). Bucharest, Romania, p 8 (Paper No. 4353), 2022a.

Bayat F., M. Kowsari, B. Halldorsson, A new 3-D finite-fault model of the Southwest Iceland bookshelf transform zone. *Geophysical Journal International* **231**,1618–1633. https://doi.org/10.1093/gji/ggac272, 2022b.

Cork T. G., J. H. Kim, G. P. Mavroeidis, et al., Effects of Tectonic Regime and Soil Conditions on the Pulse Period of Near-Fault Ground Motions. *Bulletin of Earthquake Engineering* **80**,102–118, 2016.

Dalguer L. A., P. M. Mai, Near-Source Ground Motion Variability from M∼ 6.5 Dynamic Rupture Simulations. In: 4th IASPEI/IAEE International Symposium: Effects of Surface Geology on Seismic Motion. IASPEI and IAEE, 2011.

Einarsson P., Mechanisms of Earthquakes in Iceland. In: Beer M, Kougioumtzoglou IA, Patelli E, Au IS-K (eds) Encyclopedia of Earthquake Engineering. Springer Berlin Heidelberg, Berlin, Heidelberg, pp 1–15, 2014

Graves R., T. H. Jordan, S. Callaghan et al., CyberShake: A physics-based seismic hazard model for southern California. *Pure and Applied Geophysics* **168**,367–381, 2011.

Halldórsson B., S. Ólafsson, R. Sigbjörnsson, A fast and efficient simulation of the far-fault and near-fault earthquake ground motions associated with the June 17 and 21, 2000, earthquakes in South Iceland. *Journal of Earthquake Engineering* **11**,343–370, 2007.

Jónasson K., B. Bessason, Á. Helgadóttir et al., A Harmonised Instrumental Earthquake Catalogue for Iceland and the Northern Mid-Atlantic Ridge. *Natural Hazards and Earth System Sciences* **21,**2197–2214. https://doi.org/10.5194/nhess-21-2197-2021, 2021.

Kowsari M., S. Ghasemi, F. Bayat, B. Halldorsson, A backbone seismic ground motion model for strike-slip earthquakes in Southwest Iceland and its implications for near-and far-field PSHA. *Bulletin of Earthquake Engineering* 1–24. https://doi.org/10.1007/s10518-022-01556-z, 2022a.

Kowsari M., B. Halldorsson, F. Bayat, Preparation of Finite-fault Earthquake Catalogues Enabling Physics-based PSHA in Southwest Iceland. In: *Proceedings of the 3rd European Conference on Earthquake and Engineering Seismology* (3ECEES). Bucharest, Romania, p 8 (Paper No. 8441), 2022b.

Kowsari M., B. Halldorsson, B. Hrafnkelsson et al., Calibration of ground motion models to Icelandic peak ground acceleration data using Bayesian Markov Chain Monte Carlo simulation. *Bulletin of Earthquake Engineering* **17,**2841–2870. https://doi.org/10.1007/s10518-019-00569-5, 2019.

Kowsari M., T. Sonnemann, B. Halldorsson et al., Bayesian Inference of Empirical Ground Motion Models to Pseudo-Spectral Accelerations of South Iceland Seismic Zone Earthquakes based on Informative Priors. *Soil Dynamics and Earthquake Engineering* **132**,106075. https://doi.org/10.1016/j.soildyn.2020.106075, 2020.

Mavroeidis G. P., A. S. Papageorgiou, A Mathematical Representation of Near-Fault Ground Motions. *Bulletin of the Seismological Society of America* **93**,1099–1131. https://doi.org/10.1785/0120020100, 2003.

Mavroeidis G. P., A. S. Papageorgiou, Effect of Fault Rupture Characteristics on Near-Fault Strong Ground Motions. *Bulletin of the Seismological Society of America* **100,**37–58. https://doi.org/10.1785/0120090018, 2010.

Mavroeidis G. P., A. S. Papageorgiou, Near-source strong ground motion: characteristics and design issues. In: *Proc. of the Seventh US National Conf. on Earthquake Engineering* (7NCEE). Boston, MA, USA, p 25, 2002.

Rahpeyma S., B. Halldorsson, B. Hrafnkelsson, S. Jónsson, Frequency dependent site factors for the Icelandic strong-motion array from a Bayesian hierarchical model of the spatial distribution of spectral accelerations. *Earthquake Spectra*. https://doi.org/10.1177/87552930211036921, 2021.

Rojas O. J., J. E. Rodriguez, M. Monterrubio-Velasco et al., Insights on Physics-based Probabilistic Seismic Hazard Analysis in South Iceland using CyberShake. In: AGU Fall Meeting 2021. AGU, 2021.

Sigbjörnsson R., J. T. Snæbjörnsson, S. M. Higgins, et al., A note on the M w 6.3 earthquake in Iceland on 29 May 2008 at 15: 45 UTC. *Bulletin of Earthquake Engineering* **7,**113–126, 2009.

Somerville P. G., Magnitude scaling of the near fault rupture directivity pulse. *Physics of the earth and planetary interiors* **137**,201–212, 2003.

Somerville P. G., N. F. Smith, R. W. Graves, N. A. Abrahamson, Modification of empirical strong ground motion attenuation relations to include the amplitude and duration effects of rupture directivity. *Seismological Research Letters* **68**,199–222, 1997.

Spudich P., J. R. Bayless, J. W. Baker, et al., Final Report of the NGA-West2 Directivity Working Group, 2013.

NorthQuake 2022 - The 4th International Workshop on Earthquakes in North Iceland
Húsavík, North Iceland, 18-20 October 2022

The implications of the new European Seismic Hazard Model 2020 for Iceland

Benedikt Halldorsson[1,2], Milad Kowsari[1], Farnaz Bayat[1], Claudia Abril[3], Atefe Darzi[1], Bjarni Bessason[1] and Jónas Þór Snæbjörnsson[4]

[1]*Faculty of Civil and Environmental Engineering, School of Engineering and Natural Sciences, University of Iceland (skykkur@hi.is (B.H.), milad@hi.is, fab14@hi.is, atefe@hi.is, bb@hi.is)*
[2]*Division of Processing and Research, Icelandic Meteorological Office, Iceland (benedikt@vedur.is)*
[3]*Uppsala University, Sweden (claudia.abril@geo.uu.se)*
[4]*Reykjavik University, Iceland (jonasthor@ru.is)*

Probabilistic seismic hazard assessment (PSHA) is the international standard practice for seismic risk management worldwide and is used as the foundation for evaluating the basis peak ground motion parameters used by structural building codes for earthquake resistant design (e.g., Eurocode 8) (see e.g., McGuire 2004; Baker et al. 2021, and references therein). The PSHA results for any given location in a seismic region are generally presented in the form of hazard curves that specify the annual recurrence rate of exceeding a given level of horizontal peak ground acceleration (PGA). For multiple sites, the PSHA results are presented in the form of a map that shows the spatial distribution of PGA levels for a given annual recurrence rate. An example of such a hazard map is shown in Figure 1 for Iceland which is the in-force Icelandic National Annex to the Eurocode 8 building code for earthquake resistant design of structures (Standards Council of Iceland / Staðlaráð Íslands (SI) and Halldorsson 2010). The Icelandic seismic hazard map was originally published in 2002, and updated in 2010. The update effectively involved increasing the maximum PGA values from 40%g to 50%g, with g being the acceleration of gravity. In 2013, the results of a harmonized effort in PSHA for the whole of Europe were published (Woessner et al. 2015). Interestingly, no Icelandic participants had been included in this European research and innovation project and upon detailed scrutiny of the supporting documents of the ESHM13, it became clear that very limited information had been sought by the European consortium from Icelandic seismologists or engineers during the project. In the end, the ESHM13 results pertaining to Iceland in the form of a seismic hazard map (see Figure 2, for the 10% in 50 years probability of exceedance of PGA) showed incredible inconsistency with the Icelandic National Annex. In particular, the hazard values for large areas of the country, most notably the capital city of Reykjavik where 2/3 of the population reside, were effectively seen to increase from ~10%g or less to ~50%g. Such an increase in values is considered completely unrealistic and while the ESHM13 hazard map did not affect the earthquake resistant design of structures in Iceland, it did influence the insurance rates of re-insurance for the Icelandic Natural Catastrophe Insurance company.

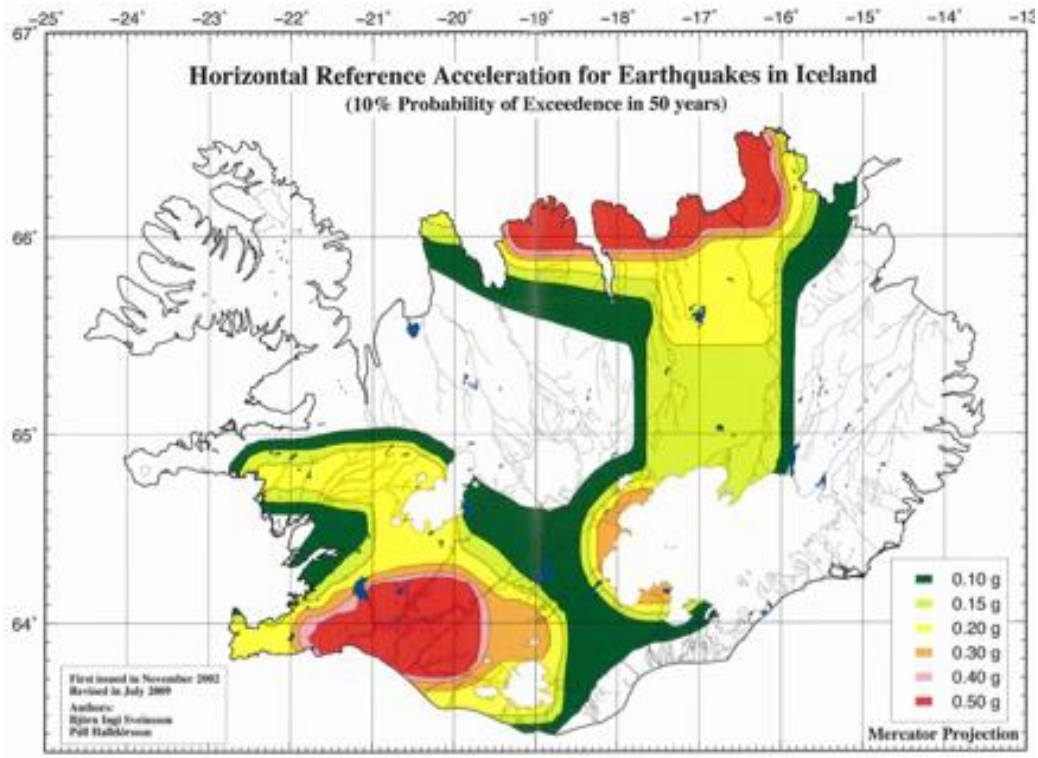

Figure 10. The Icelandic National Annex to Eurocode 8 showing the 10% in 50 years probability of exceedance of peak

Intense efforts have been undertaken in hazard research in Iceland since the update of the Icelandic National Annex and the publication of the ESHM13 results (see e.g., Rahpeyma et al. 2016, 2018, 2019, 2022; Kowsari et al. 2019a, b, 2020, 2021, 2022b, a; Sonnemann et al. 2020). They have been systematically focused on addressing all the fundamental elements required for a reliable PSHA, namely the specification of (1) earthquake fault locations and sizes, their (2) seismic activity, and (3) the ground motion models (GMMs) that describe the scaling of earthquake ground shaking with magnitude, distance, site effects etc., with special focus on uncertainty handling and sensitivity analyses. Most notably, a new physics-based 3D fault system model has been produced for the unique bookshelf fault system in the South Iceland Seismic Zone (SISZ) and Reykjanes Peninsula Oblique Rift (RPOR) in Southwest Iceland (Bayat et al. 2022a, b). It is calibrated to the rate of tectonic plate motions across the transform zone, subdivides the zone based on the systematic spatial variation in maximum expected magnitudes, and simulates bookshelf fault locations across the zone along with their maximum expected dimensions and fault slip rates, effectively addressing the fundamental element No. 1 above. Importantly, the seismicity rates predicted by the model along the SISZ-RPOR zone effectively explain the historical earthquake catalogue for the region, effectively the fundamental element No. 2 above. The fault system model furthermore enables the generation of synthetic finite-fault earthquake catalogues that are consistent both with the model and the historical seismicity (Kowsari et al. 2022b). That lays the foundation for physics-based seismological approaches to time-independent PSHA based on complex kinematic and dynamic rupture models of finite-fault earthquake rupture. Moreover, the flexibility of the model also allows for the conventional engineering approach to PSHA, with the results from both approaches being consistent as both are based on the same physics-based fault system model. The conventional engineering approach to PSHA then requires the third fundamental element, the

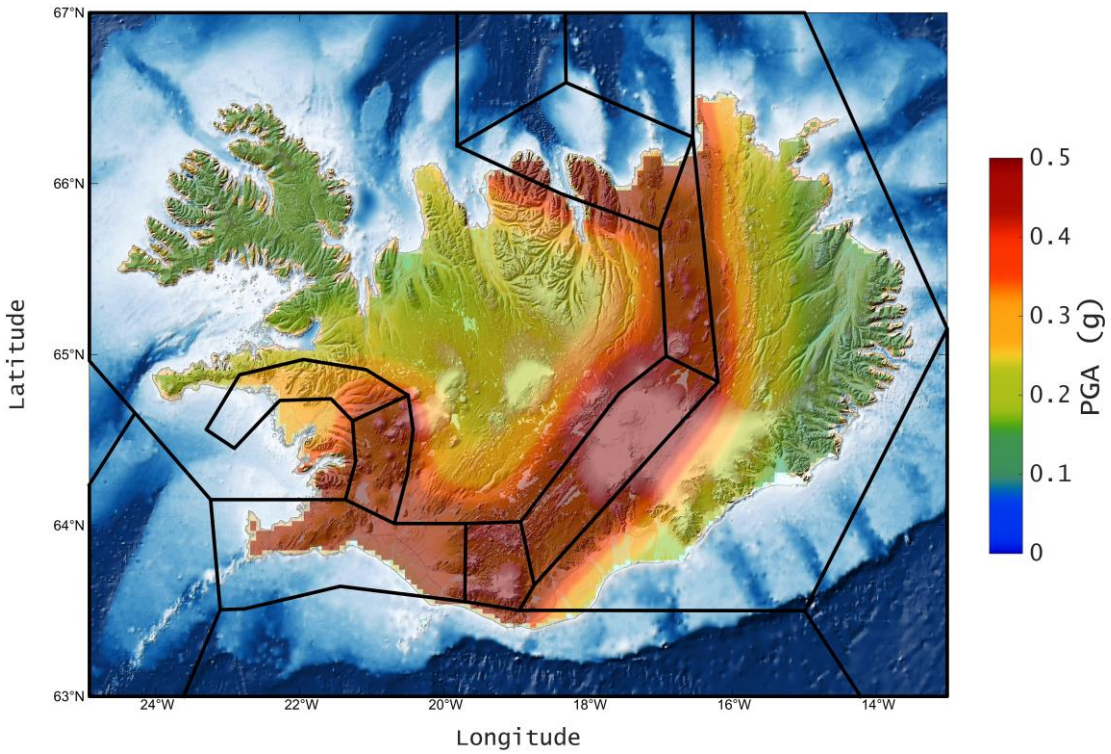

Figure 11. Map of the topography and bathymetry of Iceland region superimposed by the seismic hazard map of the SHARE/ESHM13 project for the 10% in 50 years probability of exceedance of peak ground acceleration (PGA).

GMMs. Those that were used in previous PSHA studies for Iceland were somewhat inconsistent with the character of seismic ground motion attenuation in Iceland or/and did not satisfy the criteria for the functional form of GMMs for use in PSHA (see in Kowsari et al. 2019a, b, 2020). Therefore, a suite of new hybrid empirical Bayesian GMMs have been proposed that are devoid of such limitations and allow for a physically-consistent prediction of ground motion peak amplitudes over the entire range of frequencies of engineering interest (Kowsari et al. 2020). Moreover, the Bayesian Hierarchical Modelling approach has been used to inspect the GMM model residuals classified into source, path and site residuals over the frequency range considered (Rahpeyma et al. 2018, 2019, 2022). The results have confirmed the relative consistency of seismic ground motions of strong earthquakes in the SISZ (Kowsari et al. 2020; Sonnemann et al. 2020) and the unique site response observed and modelled on Holocene lava rock (Bessason and Kaynia 2002; Rahpeyma et al. 2016). Moreover, the results have quantified the systematic variation of site effects associated with four different key geological units in Iceland (Rahpeyma et al. 2022), that will allow geology specific prediction of ground motions and their inclusion in PSHA. Finally, a new harmonized and long-term earthquake catalogue for Iceland has been published that combines local estimates of earthquake epicentral locations with moment magnitude estimates from international seismic monitoring agencies (the ICEL-NMAR catalogue, Jónasson et al. 2021). The catalogue of instrumented significant earthquakes in Iceland from 1901-2019 is particularly useful for the specification of seismicity rates, i.e., the fundamental element No. 2 above. In addition, the ICEL-NMAR also confirms the systematic spatial variation of earthquake epicenters, particularly in the southwest transform zone, the SISZ-RPOR and the Tjörnes Fracture Zone (TFZ) in the northeast, when compared with available short-term microseismic catalogues (Panzera et al. 2016; Abril 2018).

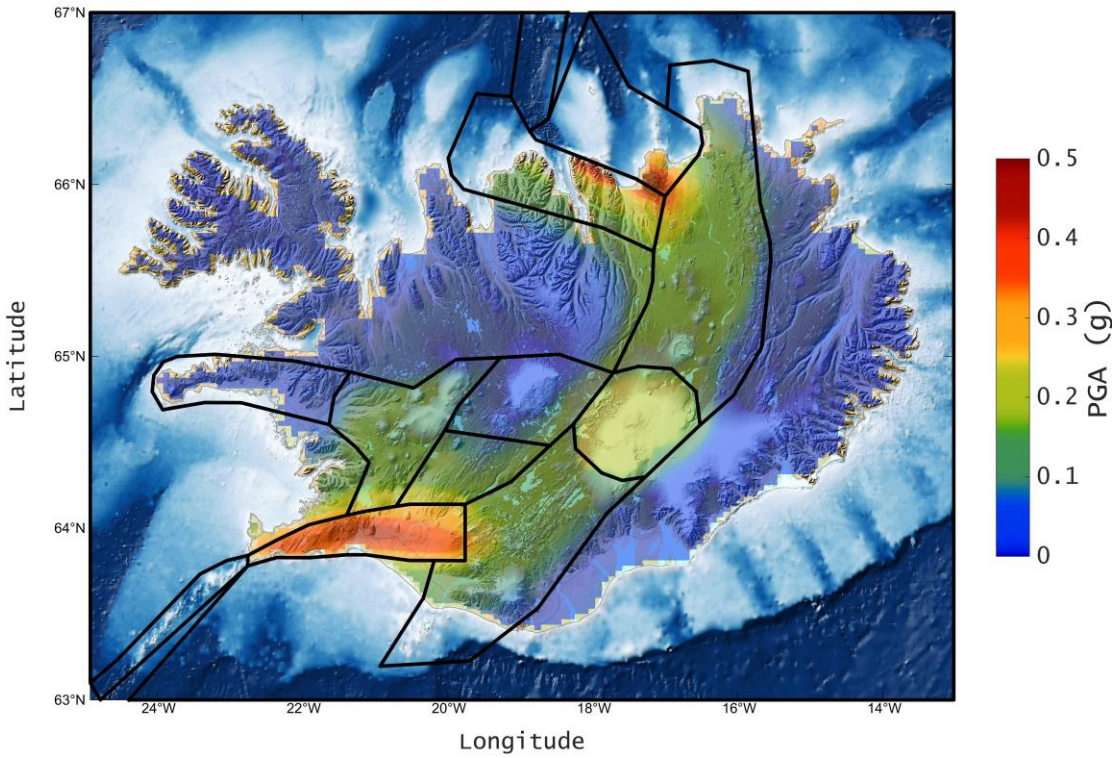

Figure 12. Map of the topography and bathymetry of Iceland region superimposed by the seismic hazard map of the ESHM20 project for the 10% in 50 years probability of exceedance of peak ground acceleration (PGA).

A new European research project on European Seismic Hazard Model (ESHM20) started in 2017 with the purpose of updating the ESHM13. Again, the project was without any Icelandic participants and therefore there was a real chance that the results for Iceland would not improve. However, we actively took an initiative to seek out our European colleagues for the purpose of informing and infusing the ESHM20 development local state-of-the-art knowledge and selected research results from the above mentioned efforts so that the ESHM20 might provide more realistic hazard values, in particular with respect to the spatial pattern of seismicity and maximum earthquake magnitudes (Halldorsson et al. 2022). In summary, we simplified our results and proposed a new area source zonation for the country, along with a and b values and maximum magnitudes for each zone. For the SISZ-RPOR the zonation was detailed and based on the new finite-fault system model, while only a basic zonation was provided for the TFZ as the finite-fault system model for that transform zone has not been completed. For the volcanic/extensional zones in Iceland we based the zonation on the main features of the spatial extent of volcanic systems and their fissure swarms, and their activity based on the ICEL-NMAR. There are several limitations to the proposed zonation, but as the ESHM20 project was without direct Icelandic participation, our influence in the end was limited by time and other constraints (see Halldorsson et al. 2022). In the end, the results of the ESHM20 are shown in Figure 3, in a form comparable to that of Figure 1 but particularly Figure 2.

The ESHM20 seismic hazard map is drastically different from ESHM13, showing more realistic hazard values that are spatially much more similar to those in the Icelandic National Annex. We note however that the final incorporation of the ESHM20 of our provided input was unexpectedly somewhat inconsistent with what we provided (see Halldorsson et al. 2022). Most notably the subzonation of the southwest Iceland transform zone that specified varying maximum

magnitudes and different activity rates appears not to have been used. Also, while the hazard pattern in the TFZ appears to highlight the Húsavík-Flatey Fault Zone, a new physics-based fault system model is required to capture the much more complex spatial pattern of fault locations and activities in the TFZ.

The earthquake hazard research so far have been supported by Rannís and the European Commission. Considerable work still needs to be funded to complete and enable a consistent and comprehensive revision of PSHA in Iceland. In particular this work involves: (a) Finalizing the earthquake source model for the TFZ in a similar way as has been done for the SISZ-RPOR, using physics-based approaches to ground motion simulations to improve the near-fault GMMs and enable physics-based PSHA, (b) Incorporate quantitative site effects in the PSHA along with other proxies, (c) Systematically revise the area zonation for all volcanic systems.

References

Abril C., Seismicity and crustal structure in Iceland. Ph.D. Dissertation, Acta Universitatis Upsaliensis, Uppsala, Sweden, 2018.

Baker J., B. Bradley, P. Stafford, Seismic Hazard and Risk Analysis. Cambridge University Press, Cambridge, 2021.

Bayat F., B. Halldorsson, M. Kowsari, On the Calibration of a New Finite-fault Bookshelf Fault System Model for Southwest Iceland. In: *Proceedings of the 3rd European Conference on Earthquake and Engineering Seismology (3ECEES)*. Bucharest, Romania, p 8 (Paper No. 4353), 2022a.

Bayat F., M. Kowsari, B. Halldorsson, A new 3-D finite-fault model of the Southwest Iceland bookshelf transform zone. *Geophys J Int* **231**:1618–1633. https://doi.org/10.1093/gji/ggac272, 2022b

Bessason B., A. M. Kaynia, Site amplification in lava rock on soft sediments. Soil Dyn Earthq Eng 22:525–540. https://doi.org/10.1016/S0267-7261(02)00035-0, 2002.

Danciu L., S. Nandan, C. Reyes, et al., The 2020 update of the European Seismic Hazard Model - ESHM20: Model Overview. In: *EFEHR Technical Report* 001, v1.0.0. DOI: 10.12686/a15, 2021.

Halldorsson B., C. Abril, F. Bayat, M. Kowsari, On the Establishment of Physics-based Finite-fault Earthquake Source Models of the Transform Zones of Iceland. In: *Proceedings of the 3rd European Conference on Earthquake and Engineering Seismology (3ECEES)*. Bucharest, Romania, p 10 (Paper No. 7077), 2022.

Jónasson K., B. Bessason, Á. Helgadóttir et al., A Harmonised Instrumental Earthquake Catalogue for Iceland and the Northern Mid-Atlantic Ridge. *Nat Hazards Earth Syst Sci* **21**:2197–2214. https://doi.org/10.5194/nhess-21-2197-2021 2021.

Kowsari M., S. Ghasemi, F. Bayat, B. Halldorsson, A backbone seismic ground motion model for strike-slip earthquakes in Southwest Iceland and its implications for near-and far-field PSHA. *Bull Earthq Eng* 1–24. https://doi.org/10.1007/s10518-022-01556-z, 2022a.

Kowsari M., B. Halldorsson, F. Bayat, Preparation of Finite-fault Earthquake Catalogues Enabling Physics-based PSHA in Southwest Iceland. In: *Proceedings of the 3rd European Conference on Earthquake and Engineering Seismology (3ECEES)*. Bucharest, Romania, p 8 (Paper No. 8441), 2022b.

Kowsari M., B. Halldorsson, B.Hrafnkelsson et al., Calibration of ground motion models to Icelandic peak ground acceleration data using Bayesian Markov Chain Monte Carlo simulation. *Bull Earthq Eng* **17**:2841–2870. https://doi.org/10.1007/s10518-019-00569-5, 2019a.

Kowsari M., B. Halldorsson, B. Hrafnkelsson, S. Jonsson, Selection of earthquake ground motion models using the deviance information criterion. *Soil Dyn Earthq Eng* **117**:288–299. https://doi.org/10.1016/j.soildyn.2018.11.014 2019b.

Kowsari M., B. Halldorsson, J. Þ. Snæbjörnsson, S. Jónsson, Effects of different empirical ground motion models on seismic hazard maps for North Iceland. *Soil Dyn Earthq Eng* **148**:106513, https://doi.org/10.1016/j.soildyn.2020.106513, 2021.

Kowsari M., T. Sonnemann, B. Halldorsson et al., Bayesian Inference of Empirical Ground Motion Models to Pseudo-Spectral Accelerations of South Iceland Seismic Zone Earthquakes based on Informative Priors. *Soil Dyn Earthq Eng* **132**:106075. https://doi.org/10.1016/j.soildyn.2020.106075, 2020.

McGuire R. K., Seismic hazard and risk analysis. Earthquake engineering research institute, 2004.

Panzera F., J. D. Zechar, K. S. Vogfjörd, D. A. J. Eberhard, *A Revised Earthquake Catalogue for South Iceland. Pure Appl Geophys* **173**:97–116. https://doi.org/10.1007/s00024-015-1115-9, 2016.

Rahpeyma S., B. Halldorsson, B. Hrafnkelsson et al., Site effect estimation on two Icelandic strong-motion arrays using a Bayesian hierarchical model for the spatial distribution of earthquake peak ground acceleration. *Soil Dyn Earthq Eng* **120**:369–385. https://doi.org/10.1016/j.soildyn.2019.02.007, 2019.

Rahpeyma S., B. Halldorsson, B. Hrafnkelsson, S. Jónsson Bayesian hierarchical model for variations in earthquake peak ground acceleration within small-aperture arrays. *Environmetrics* **29**:e2497. https://doi.org/10.1002/env.2497, 2018.

Rahpeyma S., B. Halldorsson, B. Hrafnkelsson, S. Jónsson, Frequency-dependent site factors for the Icelandic strong-motion array from a Bayesian hierarchical model of the spatial distribution of spectral accelerations. *Earthq Spectra* **38**:648–676. https://doi.org/10.1177/87552930211036921, 2022.

Rahpeyma S., B. Halldorsson, C. Olivera et al., Detailed site effect estimation in the presence of strong velocity reversals within a small-aperture strong-motion array in Iceland. *Soil Dyn Earthq Eng* **89**:136–151. https://doi.org/10.1016/j.soildyn.2016.07.001, 2016.

Sonnemann T., B. Halldorsson, B. Hrafnkelsson, S. Jónsson, Bayesian Inference of a Physical Seismological Model to Earthquake Strong-motion in South Iceland. *Soil Dyn Earthq Eng* **138**:106219. https://doi.org/10.1016/j.soildyn.2020.106219, 2020.

Standards Council of Iceland / Staðlaráð Íslands (SI), P. Halldorsson, Icelandic National Annexes to EUROCODES. Staðlaráð Íslands, Reykjavík, Iceland, 2010.

Woessner J., D. Laurentiu, D. Giardini et al., The 2013 European seismic hazard model: key components and results. *Bull Earthq Eng* **13**:3553–3596, 2015.

NorthQuake 2022 - The 4th International Workshop on Earthquakes in North Iceland
Húsavík, North Iceland, 18-20 October 2022

Foundation types of buildings in Húsavík in the context of seismic hazard

Brynjar Örn Arnarson[1],Benedikt Halldórsson[1,2]

[1]*University of Iceland (boa17@hi.is, skykkur@hi.is)*
[2]*Icelandic Meteorological Office*

The seismic potential in Iceland is the highest in the two transform zones, in the South Iceland Seismic Zone (SISZ), and in the Tjörnes Fracture Zone (TFZ) in the North, due to an Eastwards offset of the Mid Atlantic Ridge on land in Iceland. The seismic activity in the zones is a constant threat to inhabitants. The Húsavík-Flatey Fault (HFF) in the TFZ is the largest transform fault in Iceland. Recent studies on the HFF show that it currently has the potential for a single 6.8-7.0 magnitude earthquake. A major earthquake like this must be considered hazardous or catastrophic. Buildings in Iceland are known to handle earthquakes relatively well, given past experiences in earthquakes in the South Iceland Seismic Zone in the magnitude 6 earthquake in 1987, 6.4 and 6.5 earthquakes in 2000, and 6.3 in 2008. Before that, repeated such moderate-to-strong earthquakes, around magnitude 6-6.5 occurred in 1896, and a magnitude 7 earthquake in 1912. In that context, the requirements of the earthquake-resistant design of structures have been increasing in the last few decades, particularly since 1976 and 2002 in formal building codes, and in the South, the majority of buildings were built before 1976 and all have been tested by earthquake strong shaking. This is in stark contrast to the building stock of Húsavík that has not been tested by a large earthquake as the oldest standing house in the town is built in 1883 but the last large nearby earthquake occurred 11 years before that in 1872. Thus, the oldest category of houses in Húsavík (since 1883) is more vulnerable to seismic shaking than younger buildings. There is however a large contrast in the availability of information on the age and material of houses in the Icelandic registry compared to that of building foundations, which is relatively nonexistent. As the seismic waves need to travel through the building's foundation before the building is subjected to earthquake loading, the foundation is a critical element that affects its level of seismic vulnerability. The foundation of old buildings varies greatly, but most are built on short concrete wall foundations with some on gravel foundations. Then, others are on very thin or nonexistent foundations, and some are on mortar wall foundations. This is in contrast with modern-day foundations, compacted gravel cushions, or steel-reinforced concrete wall foundations that are resilient to earthquake shaking. Another element that contributes to the seismic hazard in Húsavík is geology. Most buildings are built on firm ground as the topsoil is easily removable with easy access to a relatively hard geological material below. The geology of the ground varies within Húsavík and recent research efforts have mapped the variability of the associated seismic hazard. The information compiled in this study, of the types of building foundations along with their distribution within Húsavík is expected to increase the knowledge levels and awareness related to the compromised resilience of older buildings against earthquake strong shaking, relative to newer buildings, with special attention to the role that weak foundations may play in terms of the level of the potential damage of such houses.

Detailed research on the earthquake hazard must be done in the area of Húsavík for

sustainable risk management. In this study, which is a part of the ongoing ICEARRAY II project in Húsavík, information was collected on the foundations and geology beneath the oldest, and therefore most vulnerable buildings in Húsavík with respect to seismic ground motion. Considerable information exists on the building superstructure's age and materials i.e., their seismic resistance capability, while little information exists for the building's foundations. Namely, the seismic ground motion must first go through the building's foundation before the superstructure itself sustains the earthquake loading. Therefore, the foundations are an integral part of the seismic resiliency of any building. This thesis contributes to the ongoing seismic hazard research in Húsavík by collecting information on the foundations of buildings in Húsavík with a focus on the oldest buildings. The oldest buildings in Húsavík were most found to have concrete foundations. Some buildings are built on compacted foundations, and in some cases, little or no foundations were the basis for the building's superstructure. A few buildings are built on mortar wall foundations, which are suspected to have a very low resistance to horizontal seismic ground shaking. This study concludes that the information on the building stock in seismic regions in Iceland is incomplete and must be augmented with information on the types of building foundations in order for a complete seismic vulnerability assessment can be made, and therefore more accurate risk assessment. A database has been constructed that hopefully enables earthquake engineers and the municipality to estimate better the seismic vulnerability of buildings in Húsavík from their foundation type. Due to privacy concerns, the database is not public and only used for research purposes without the possibility of identification of individuals

Fig 1. The typical foundation beneath an old building built around 1900. The rocks can be seen from the outside and the concrete grouting in between, often called a mortar wall.

Fig 2. Concrete foundation, the foundation is most commonly hidden and can't be seen. Typical for building built after 1930.

Fig 3. Example of a house, sitting on no foundation. The house sits on top of the soil. Difficult to identify.

References

Boore, David M. and William B. Joyner, Site amplifications for generic rock sites. In: *Bulletin of the Seismological Society of America* **87**.2, pp. 327–341, http://www.bssaonline.org/content/87/2/327.short, 1997.

Einarsson, P., Plate boundaries, rifts and transforms in Iceland, *Jökull*, **58**,35–58, http://earthice.hi.is/sites/earthice.hi.is/files/Pdf_skjol/Jokull58_pdf/jokull58-einarsson.pdf (visited on 03/15/2022), 2008.

Einarsson, P., B. Brandsdóttir, and Á. R. Hjartardóttir, Seismicity, faults, and bathymetry of the Tjörnes Fracture Zone. Ed. by Sigurjón Jónsson et al. In: *Proceedings of the Northquake 2019 workshop. Húsavík Academic Center*. 12-15. https://hac.is/wp-content/uploads/ Northquake2019.pdf (visited on 03/17/2022), 2019.

Halldorsson, B. and R. Sigbjörnsson, The M_W6.3 Ölfus earthquake at 15:45 UTC on 29 May 2008 in South Iceland: ICEARRAY strong-motion recordings. In*: Soil Dynamics and Earthquake Engineering* **29**,6, pp. 1073– 1083. doi:

10.1016/j.soildyn.2008.12.006, https: //linkinghub.elsevier.com/retrieve/pii/S0267726108002480 (visited on 11/25/2020), 2009.
Halldórsson, B., et al., ICEARRAY II: A multidisciplinary array of geodetic and strong-motion instruments in Húsavík, North Iceland. Ed. by Gréta Bergrún Jóhannesdóttir et al., *International Workshop on Earth- quakes in North Iceland. Húsavík Academic Center*. 119-123. https://hac. is/wp-content/uploads/Northquake2013.pdf (visited on 04/05/2022), 2013.
Jónsson, S. et al., An update of GPS measurements in North Iceland. Ed. by Sigurjón Jónsson et al. In: *Proceedings of the Northquake 2019 workshop. Húsavík Academic Center*, 107-110, https://hac.is/wp-content/uploads/Northquake2019.pdf (visited on 03/18/2022), 2019.
Magnúsdóttir, S. et al., Tectonic framework of the Skjálfandi and Skjálfandadjúp basins. Ed. by Gréta Jóhannesdóttir et al., *Earth- quakes in North Iceland.* Húsavík Academic Center. 34-38. url: https://hac. is/wp-content/uploads/Northquake2013.pdf, 2013.
Ólafsson, G. P., Perlur: í náttúru Íslands. Edition 6. Mál og Menning, 2013.
Sigbjörnsson, R. et al., A note on the M_W6.3 earthquake in Iceland on 29 May 2008 at 15:45 UTC". In: *Bulletin of Earthquake Engineering* **7**.1, pp. 113– 126. doi: 10.1007/s10518-008-9087-0. http://www. springerlink.com/index/10.1007/s10518-008-9087-0, 2009.
Waltl, P., F. Markus et al., Geomorphology and Building Stock of Húsavík, North Iceland. PhD thesis, 2013.
Waltl, P., B. Halldórsson et al., Concise map-based representation of the tectonics, geology, gemorphology and building stock of Húsavík, North Iceland. *Proceedings of the Northquake 2019 workshop*. Húsavík Academic Center. 74-84, https://hac.is/wp-content/uploads/Northquake2019. pdf (visited on 04/28/2022), 2022.

NorthQuake 2022 - The 4th International Workshop on Earthquakes in North Iceland
Húsavík, North Iceland, 18-20 October 2022

Statistical empirical vulnearbility model for low-rise Icelandic buildings

Bjarni Bessason[1], Rajesh Rupakhety[2], Jón Örvar Bjarnason[3]

[1]*Faculty of Civil and Environmental Engineering, University of Iceland (bb@hi.is)*
[2]*Faculty of Civil and Environmental Engineering, University of Iceland (rajesh@hi.is)*
[3]*Natural Catastrophe Insurance of Iceland (jon@nti.is)*

On 17 and 21 of June 2000, two earthquakes of similar size, Mw6.52 and Mw6.44 (*Jónasson et al. 2021*), struck in the eastern part of the South Iceland Seismic Zone (SISZ) and affected nearly 5000 low-rise residential buildings. Eight years later, on 29 May 2008, a Mw6.31 earthquake struck further west in the zone (*Halldórsson et al, 2009; Jónasson et al. 2021*), and again nearly 5000 buildings were affected. Despite, substantial damage, no residential building collapsed and there were no fatalities. Mandated by law, all properties in Iceland are insured against natural hazards at the Natural Catastrophe Insurance of Iceland (2022). Therefore, after the two 2000 earthquakes and again after the 2008 event, repair cost was assessed for each damaged building to address insurance claims. Registers Iceland (2022) maintains a detailed property database for all building units in Iceland, including, GPS-locations, year of construction, building material, usage, replacement value, etc... Combination of the loss data and the property database were used to build two loss datasets hereafter referred to as the *2000 dataset* and the *2008 dataset*, respectively. The two datasets include loss estimates for every building exposed to estimated PGA of 0.05g or more. The losses for each building has been normalised with replacement value and a so-called damage factor, DF, computed:

$$DF = \frac{Repair\ cost}{Replacement\ value}$$

Having access to two high quality loss datasets from different size earthquakes, affecting the same building typologies in the same region, is rare to find in the literature, and gives opportunity to utilize advanced statistical models to describe the loss data, and then use such models to study building performance and different aspects of seismic vulnerability.

In both the June 2000 earthquakes and the May 2008 earthquake high proportion of the buildings suffered no losses (DF=0). Total losses (DF=1) were on the other hand very rare. Since the loss data includes both “zero” values and “one” values and is bounded in the range [0,1], it is preferable to use a mixed continuous-discrete regression to model the data. That is, discrete models to cover the “zeros” and “ones”, and then continuous regression for data in the range (0,1). In our case where the data includes high fraction of zero loss incidents but negligible number of total losses, a zero-inflated beta regression model (ZIBRM) is well-suited (*Ospina et al.* 2012). The discrete modelling of the total loss buildings (DF=1) is then omitted, but instead the DF for these buildings is assigned a approximation value less than one. A two-step regression process was used to construct a statistical vulnerability model. This approach is explained schematically in Fig.1 where Peak Ground Acceleration (PGA) is used as intensity measure. More details, and

mathematical formulations, are available in *Ioannou et al*. (2018); *Bessason et al*. (2020); *Bessason et al* (2022).

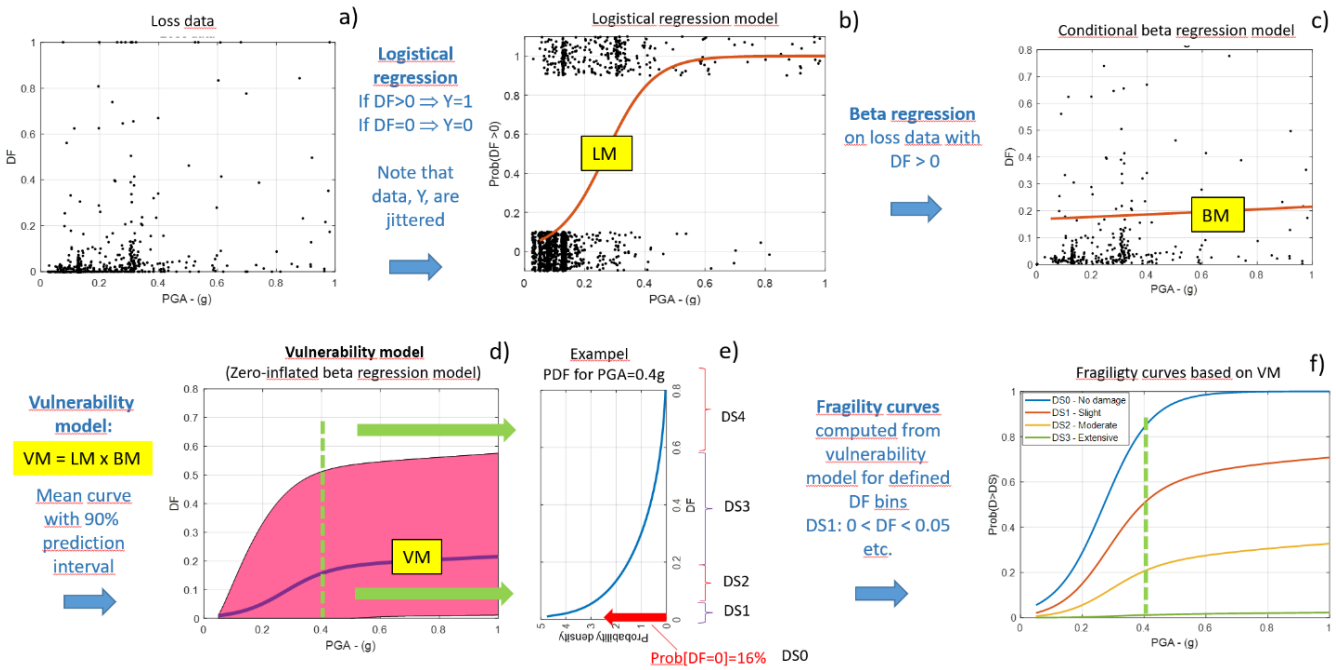

Figure 1. Flowchart that explains the main steps in the zero-inflated beta regression model. Loss data form the June 2000 earthquakes for RC buildings built before 1976 are used as example (Fig 1a). The logistical regression in (Fig. 1b) and the conditional beta regression in (Fig. 1c) are combined to create the vulnerability model given in (Fig. 1d). Then (Fig 1e) shows as an example the vulnerability model for PGA=0.4g. The following definition of damage states: DS0 – No damage; DS1 – 0-5%; DS2 – 5-20%; DS3 – 20-60%; DS4 - >60% are used to compute the fragility curves in (Fig 1f).

In vulnerability studies, affected buildings are commonly classified in number of building typologies to consider that unlike structures are expected to behave differently for given seismic intensity. For instance, low-rise building behave differently from high-rise building, performance of timber building is different from performance of buildings etc. In *Bessason et al* (2022) the so-called Global Earthquake Model (GEM) taxonomy was used to define the building typologies (*Brzev et al. 2013*). Furthermore, the effect of status of seismic codes was also considered. Four code levels where considered, that is: No-code buildings constructed before 1958; Low-code buildings for the period 1958-1976; Moderate-code for the period 1976-2002; and High-code for buildings constructed after 2002. More details can be found in *Crowley et al. (2021*). Table 1 shows classification of the 2000 and 2008 dataset. In this study the No-code and Low-code buildings are combined, and Moderate-code and High-code are combined. All the buildings are low-rise (70% one-story, 20% two-storeys and 10% three- to four-storeys). The lateral force resisting system are structural walls and infills of bricks or hollow blocks, commonly found in South European buildings, do not exist in Iceland.

The Zero-Inflated beta regression model described show in Fig.1 was used to fit the five building typologies shown in Table 1 independently for both the 2000 and the 2008 dataset. The mean vulnerability curves for RC buildings are shown as an example in Figure 2. The scatter in the loss data is quite wide although only data points in the DF range 0 to 0.4 are show.

Table 1. Classification of residential buildings affected by the June 2000 and May 2008 earthquakes.

	Building material	Status of codes	2000 dataset		2008 dataset	
			Number	(%)	Number	(%)
1	Reinforce concrete	No-code & Low-code	1665	35.0	1112	23.4
2	Reinforce concrete	Moderate- & High-code	907	19.1	1003	21.1
3	Timber	No-code & Low-code	692	14.6	649	13.7
4	Timber	Moderate- & High-code	1047	22.0	1623	34.2
5	Masonry	No-code & Low-code	443	9.3	359	7.6
		Total sum:	**4754**	100	**4746**	100

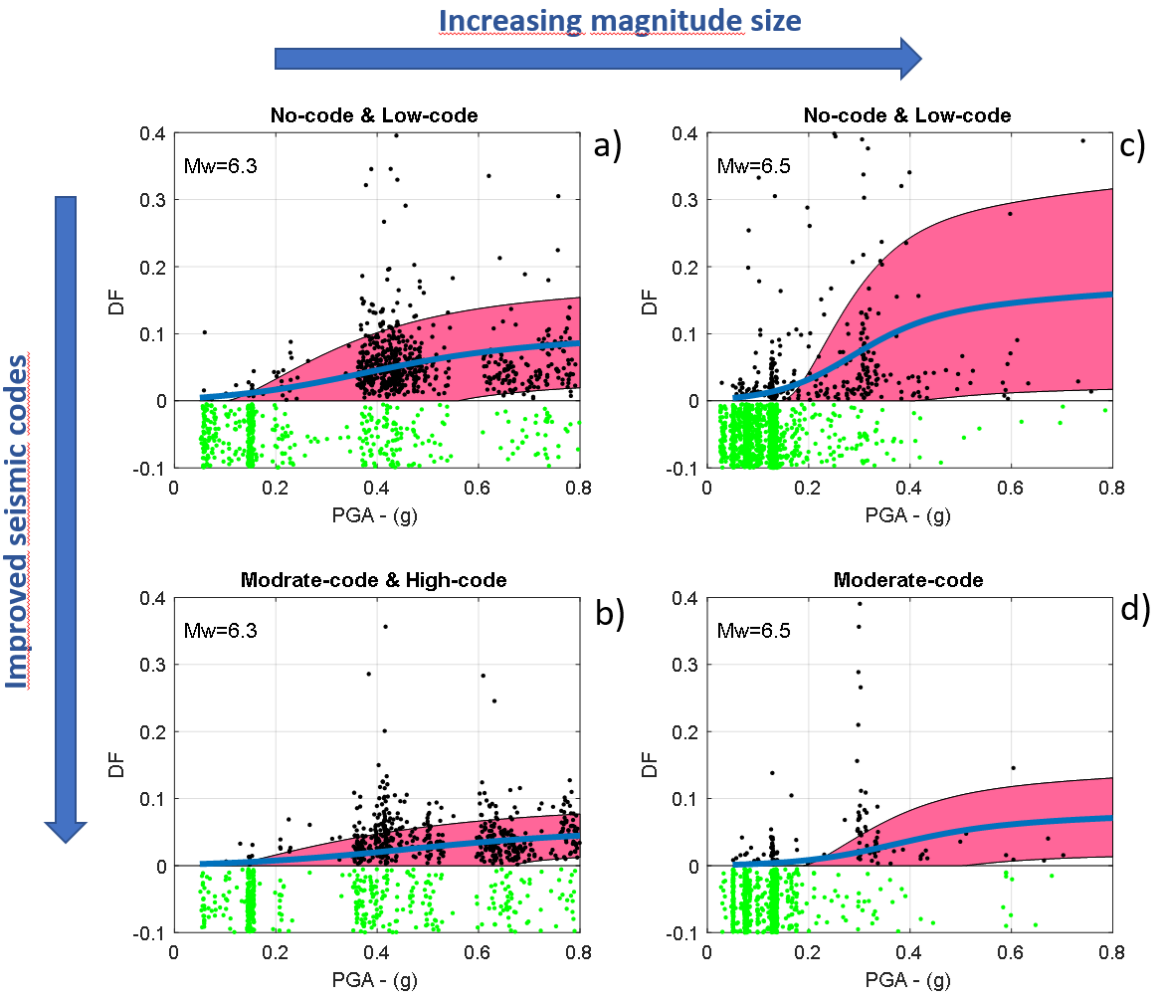

Figure 2. Vulnerability model for RC buildings. Mean loss (blue curve) with 16% and 84% prediction limits (pink area). Black dots show loss data with DF>0 and green dots show no-loss data (DF=0) jittered: a) 2008 dataset and CDN & CDL buildings, b) 2008 dataset and CDM & CDH buildings c) 2000 dataset and CDN & CDL buildings, d) 2000 dataset and CDM buildings.

To better show the high proportion of buildings with no damage (DF=0) these data points are randomly jittered and plotted in the range -0.1 to 1 (green dots). The horizontal blue arrow in Fig.2 underlines the effect of increased magnitude size between the May 2008 event (Mw6.3) and the June 2000 events (~Mw6.5). The mean vulnerability curve is considerably higher for the loss data from the 2000 dataset than the 2008 dataset for alle the building typologies in Table 1. Furthermore, the vertical blue arrow in the Fig.2 shows the effect of improved seismic codes. In all cases Moderate-code & High-code (CDM,CDH) buildings (grouped together) perform better than No-code & Low-code buildings (CDN,CDL). The vulnerability model, calibrated for each building typology, consists of five parameters which are given in Bessason et al. (2022) along with all

formulas needed to construct the curves in Fig. 2.

One of the main findings of the study is that the loss patterns of buildings affected by the June 2000 (Mw~6.5) and the May 2008 events (Mw6.3) are different. The losses caused by the 2000 events (larger magnitude) are substantially higher. The results show that two earthquakes that produce similar PGA at a given site can have very different impact on structures. The study demonstrates the limitation of PGA as a ground motion intensity measure and highlights the pitfalls of combining loss data from different-sized earthquakes in vulnerability modelling with simple intensity measures such as PGA. This all points towards a need for better ground motion intensity measures that can capture the event size effect better.

The calibrated vulnerability models also showed consistently that Moderate-code & High-code buildings showed better performance than No-code & Low-code buildings, which was expected, but important to report.

Owing to the differences in the two models, the conclusion so far is that in seismic risk calculations model parameters calibrated by the 2000 dataset should be used for earthquake scenarios with Mw in the range 6.4-6.6, and model parameters based on the 2008 dataset should be used for earthquake scenarios with Mw in the range 6.2-6.4. Caution is needed when extrapolating empirical vulnerability models calibrated from given destructive earthquake to other magnitude sizes.

Acknowledgements

This work is a part of the SERICE project which is funded by a Grant of Excellence from the Icelandic Centre for Research (RANNIS), Grant Number: 218149-051. We also acknowledge support from the University of Iceland Research Fund. Finally, the authors thank the Natural Catastrophe Insurance of Iceland for placing the earthquake damage database and other relevant information at their disposal.

References

Bessason, B., J.Ö. Bjarnason and R. Rupakhety. Statistical modelling of seismic vulnerability of RC, timber and masonry buildings from complete empirical loss data, *Engineering Structures*, **209** 109969, https://doi.org/10.1016/j.engstruct.2019.109969, 2020.

Bessason, B., R. Rupakhety and J.Ö. Bjarnason. Comparison and modelling of building losses in South Iceland caused by different size earthquakes, *Journal of Building Engineering*, **46** 13806, https://doi.org/10.1016/j.jobe.2021.103806, 2022.

Brzev, S., C. Scawthorn, A.W. Charleson, L. Allen, M. Greene, K. Jaiswal and V. Silva, *GEM Building Taxonomy*, Version 2.0. GEM Technical Report 2013-02, 2013.

Crowley, H., V. Despotaki, V. Silva, J. Dabbeek, X. Romão, N. Pereira, J.M. Castro, J. Daniell, E. Veliu, H. Bilgin, C. Adam, M. Deyanova, N. Ademovic, J. Atalic, A. Karatzetzou, B. Bessason, V. Shendova, A. Tiganescu, D. Toma-Danial, Z. Zugic, S. Akkar and U. Hancilar. Model of seismic design lateral force levels for the existing reinforced concrete European building stock. *Bulletin Earthquake Engineering*, **19** 2839–2865, https://doi.org/10.1007/s10518-021-01083-3, 2022

Halldórsson, B., R. Sigbjörnsson. The Mw6.3 Ölfus earthquake at 15:45 UTC on 29 May 2008 in South Iceland: ICEARRAY strong-motion recordings. *Soil Dynamics and Earthquake Engineering*, **29** 1073–83, https://doi.org/10.1016/j.soildyn.2008.12.006, 2009.

Ioannou, I., B. Bessason, I. Kosmidis, J. Ö. Bjarnason, T. Rossetto. Empirical seismic vulnerability assessment of Icelandic buildings affected by the 2000 sequence of earthquakes, *Bulletin of Earthquake Engineering*, **16** (12) 5875–903, https://doi.org/10.1007/s10518-018-0413-x, 2018

Jónasson, K., B. Bessason, Á. Helgadóttir Á, P. Einarsson, G.B. Gudmundsson, B. Brandsdóttir, K.S. Vogfjörd and K. Jónsdóttir. A harmonised instrumental earthquake catalogue for Iceland and the northern Mid-Atlantic Ridge, *Natural Hazards and Earth System Sciences* **21** 2197–2214, https://doi.org/10.5194/nhess-21-2197-2021, 2021

Natural Catastrophe Insurance of Iceland. http://www.nti.is/en/ (accessed 25 September 2022).

Ospina, R., S. L. P. Ferrari. A general class of zero-or-one inflated beta regression models, *Computational Statistics and Data Analysis*, **56** 1609–23, https://doi.org/10.1016/j.csda.2011.10.005, 2012.
Registers Iceland, http://www.skra.is/english. (accessed 25 September 2022), 2021.

NorthQuake 2022 - The 4th International Workshop on Earthquakes in North Iceland
Húsavík, North Iceland, 18-20 October 2022

High spatial resolution loss estimation using new vulnerability models for Iceland

Atefe Darzi[1], Bjarni Bessason[1], Benedikt Halldorsson[1,2], Mojtaba Moosapoor[1]

[1]*Faculty of Civil and Environmental Engineering, University of Iceland, Reykjavik, Iceland (atefe@hi.is)*
[3] *Division of Processing and Research, Icelandic Meteorological Office, Reykjavik, Iceland*

Iceland is the most seismically active country in northern Europe. Hveragerði is one of the small, populated towns located in the Ölfus region in the South Iceland Seismic Zone and one of the country's tourist destinations with many critical infrastructure facilities. The most recent destructive earthquake striking the town was Mw6.3, 29-May-2008 Ölfus earthquake. Despite the Ölfus earthquake being the costliest natural disaster in Iceland to date and causing widespread damage, there were however no collapsed residential buildings and no casualties. To understand the consequences that a strong earthquake can cause in a high seismic region, we perform seismic risk analyses for the Ölfus earthquake scenario across Hveragerði in a high geographical resolution of building-by-building, contrary to the common municipality-based resolution. Having detailed ground-motion data recorded by ICEARRAY I stations give the unique opportunity to explore the impact of intensity measure (IM) variability on the seismic risk metrics. Finally, the risk metrics resultant from the global fragility curves developed as part of the global seismic risk model are compared with the most recent local models.

To the best of the authors knowledge, there are only a few studies on seismic loss estimation risk assessment for Iceland. The Natural Catastrophe Insurance of Iceland (NTI) owns a fully probabilistic bespoke model for Icelandic earthquake risk assessment and a quick response deterministic model that can model scenarios such as major historical earthquakes to compute the insurance risk routinely based on 19 building classes (Bjarnason et al. 2016). However, the models, detail of the required assumptions and information as well as the corresponding results are not shared publicly. Here we use an open flexible risk assessment tool, SELENA, capable of easy modification and reproduction of results which are of great benefit for seismic risk modelers.

To estimate IMs at building locations for high resolution risk assessment, we carry out Empirical Bayesian Kriging (EBK) geostatistical analyses to generate shake maps for PGA and PSA at 0.3 sec along with their corresponding uncertainty maps (Fig. 1). The IMs are calculated from the time histories of the Ölfus earthquake recorded by ICEARRAY I stations. The spatial areas with low standard errors around stations indicate our full confidence in the estimated IMs. In Fig 1, we observe a consistent spatial pattern with persistently lower IM levels in the central Hveragerði due to specific geology, while largest IMs being observed on the E-W outskirts of town. A N-S fault lies under IS611 and IS608 stations, and further south which serves as a conduit for geothermal water (Sæmundsson and Kristinsson 2005), attenuating higher-frequency motions more effectively than the outskirts of town. The spatial differences in geology contribute to the large scatter of high-frequency motions. The variation of PGA is considerable given the small area of the array with minimum of 4.3 m/s^2 in the centre to a maximum of 8.7 m/s^2 in the E-W parts. The shakemap of PSA(T0.3s) shows that the mean values exceed ~1.0g. We note that the vast majority

of the buildings experienced much larger accelerations than the design value (PGA 0.2g) specified for buildings built before 2002 when no design spectrum was implicitly defined (see Darzi et al. 2021, 2022).

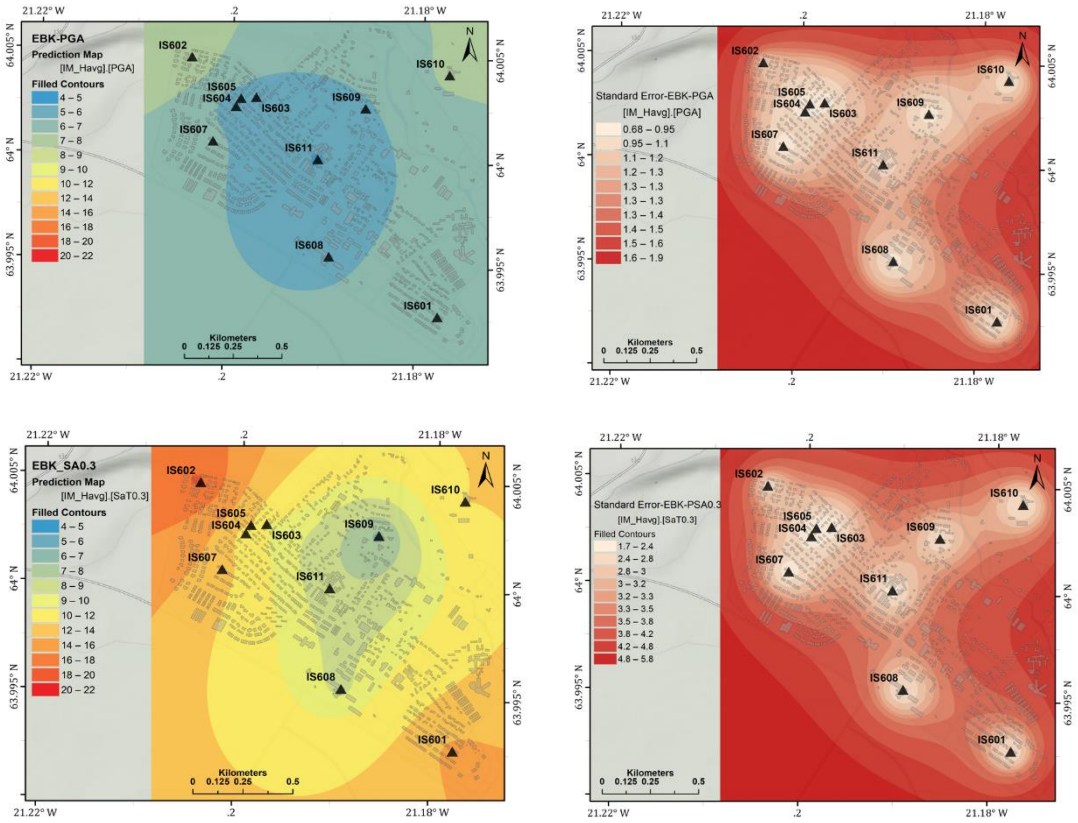

Figure 1. Shake maps of PGA (m/s^2) and PSA (T= 0.3s) (left panels) and their standard error maps (right panels) across Hveragerði. Buildings are indicated by light grey polygons.

The residential building database for Hveragerdi comprised of 56% reinforced concrete (CR), 38% timber (W), and 6% unreinforced masonry (MUR). Table 1 and 2 show the model building typologies for Hveragerði identified as per available local, Bea22 (Bessason et al. 2022), and global fragility functions, MS20 (Martins and Silva 2020). Buildings are classified based on their ductility level as follows: CDN (construction year <1958), CDL (1958 – 1976), CDM (1976-2002), and CDH (construction year >2002). Considering the low-rise buildings in Hveragerði, the local and global fragility models attributed to either PGA or PSA(*T*0.3s). The IM variation as a major uncertainty source is accounted by a logic tree framework.

Fig. 2 - MDR estimates corresponding to a) global and b) local fragility models associated with both high resolution and classical spatial resolution (grey bars) for three IM levels.

Table 1: Building typologies in accordance with local fragility curves (Bea22)

Typology	CR+CIP - CDN+CDL	CR+CIP - CDM+CDH	W+WLI- CDN+CDL	W+WLI- CDM+CDH	MR+CBH+MOC- CDN+CDL
Label	CNL	CMH	WNL	WMH	MNL
No. buildings	176	245	126	162	48

Table 2: Building typologies according to the global fragility functions (MS20)

Typology	CR_LWAL -DUL H1	CR_LWAL -DUL H2	CR_LWAL -DUM H1	CR_LWAL -DUM H2	W_LFM-DUM H1	W_LFM-DUM H2	MUR-CB99 LWAL-DNO H1	MUR-CB99 LWAL-DNO H2
Label	CL1	CL2	CM1	CM2	W1	W2	M1	M2
No. buildings	127	30	240	24	268	20	34	14

Fig. 2 shows the MDR (ratio of repair cost to new construction cost) predictions corresponding to 8 and 5 building typologies as per global and local fragility models, respectively. In Fig. 2a, the MDR estimates obtained from MS20 models are plotted for both the classical municipality level (grey bars) and high-resolution of building-by-building level (see Darzi et al. 2022 for detailed information). The discrepancy between MDRs from high- and classical-resolution risk analysis is insignificant, except for CL2, W2, M1, and M2 typologies where municipality level MDRs are greatly larger. Fig. 2b shows the results of Bea22 models performed at a municipality level. Both models indicate that the most vulnerable building typologies are masonry which are no longer constructed in Iceland mitigating the risk of future earthquakes. For Bea22, the least vulnerable buildings are those made of timber (WMH) with CDM and CDH design period in force and for MS20, the least vulnerable buildings belong to one-storey buildings RC buildings with medium and low ductile (CM1 and CL1). We display the impact of IM variability by obtaining the MDR values for three IM levels. Such impact is more highlighted in MS20 than the Bea22 results. Considering the large difference between risk metrics obtained from global and empirical local fragility models, we stress the necessity of reliable local fragility and vulnerability models that apply to the wide range of damaging earthquakes.

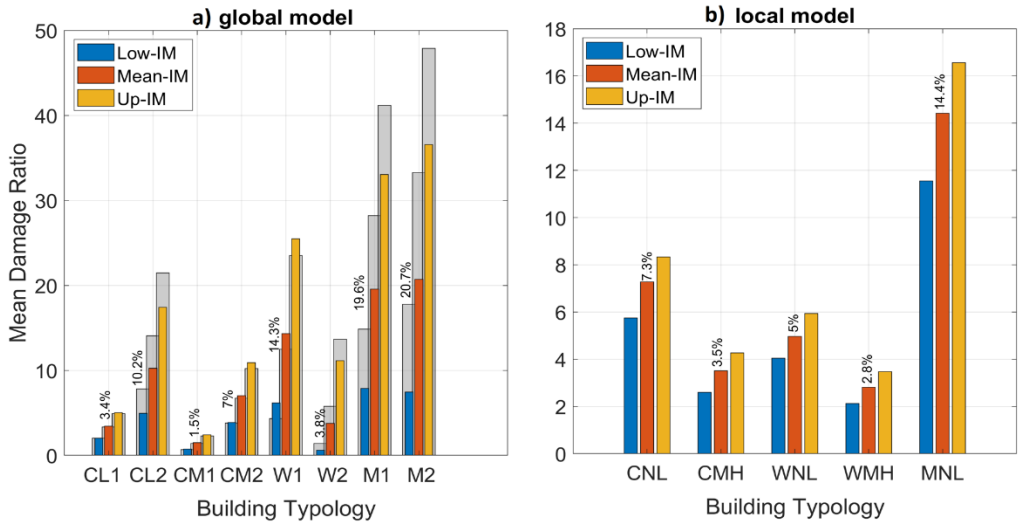

Figure 2. MDR estimates corresponding to a) global and b) local fragility models associated with both high resolution and classical spatial resolution (grey bars) for three IM levels.

This study was funded by the H2020 TURNkey project (#821046) and Postdoctoral grant from Icelandic Research Fund (#218255).

References

Bessason B, R. Rupakhety, J. Ö. Bjarnason, Comparison and modelling of building losses in South Iceland caused by different size earthquakes. *J Build Eng* **46**:103806. https://doi.org/10.1016/j.jobe.2021.103806, 2022.

Bjarnason J.Ö., P. Einarsson, B. Bessason, Iceland Catastrophe Insurance and Earthquake Risk Assessment. In: *International Workshop on Earthquakes in North Iceland. Húsavík, North Iceland*, 2016.

Darzi A., B. Bessason, B. Halldórsson, Ground Motion Intensity Measures, Variability and Seismic Loss Metrics, a Case Study for Hveragerði, South Iceland. In: *The 17th World Conference on Earthquake Engineering* (17WCEE). Japan Association for Earthquake Engineering, Sendai, Japan, p 1, 2021.

Darzi A., B. Bessason, B. Halldorsson et al., High spatial-resolution loss estimation using dense array strong-motion near-fault records. Case study for Hveragerði and the 6.3 Ölfus earthquake, South Iceland. Revis Rev, 2022.

Martins L., V. Silva, Development of a fragility and vulnerability model for global seismic risk analyses. *Bull Earthq Eng*. https://doi.org/10.1007/s10518-020-00885-1, 2020.

Sæmundsson K., S. Kristinsson, Hveragerði. Hitamælingar í jarðvegi og sprungur (Hveragerði: Soil temperature measurements and faults). Iceland GeoSurvey (ÍSOR), Reykjavík, Iceland, 2005.

NorthQuake 2022 - The 4th International Workshop on Earthquakes in North Iceland
Húsavík, North Iceland, 18-20 October 2022

Numerical modeling of U-shaped reinforced concrete walls

Ching-Yi Tsai[1], Bjarni Bessason[2], and Rajesh Rupakhety[3]

[1]*University of Iceland, Iceland (cytsai@hi.is)*
[2]*University of Iceland, Iceland (bb@hi.is)*
[3]*University of Iceland, Iceland (rajesh@hi.is)*

In both the June 2000 South Iceland earthquakes and the May 2008 Ölfus earthquake, structural failures were observed in reinforced concrete (RC) wall buildings in the most affected regions. Therefore, it is worth to utilize numerical modeling techniques to back-calculate these detected damages, calibrate the models, and then use them to evaluate the seismic vulnerability of RC structures in Iceland and to develop fragility curves. Numerical modeling and non-linear seismic response analysis of RC wall buildings is challenging task. As part of the research project SERICE (Seismic Risk in Iceland) sponsored by a Grant of Excellence from the Icelandic Centre for Research (RANNIS), this study aims to develop the numerical modeling techniques to investigate the seismic behaviors of the RC walls.

Three identical large-scale RC U-shaped walls subjected to different combinations of flexure and torsion ratios were tested at the Université catholique de Louvain (UCLouvain), Belgium, in the technological platform LEMSC (Laboratoire Essais Mécaniques, Structures et Génie Civil) of the Institute of Mechanics, Materials and Civil Engineering (iMMC) in 2022 (*Hoults et al.* 2022). A blind prediction contest funded by UCLouvain invited participants to predict the seismic behavior and performance of the first two wall specimens UW1 and UW2 subjected to pure flexure and pure torsion, respectively. Figure 1 shows details of UW1 and UW2. This paper describes the nonlinear finite element analysis predictions conducted by the SERICE research team at the University of Iceland using the open-source structural analysis software OpenSees developed at UC Berkeley (*McKenna et al.* 2000). The model utilized three-dimensional Multiple-Vertical-Line-Element Model (MVLEM-3D) element developed by *Kolozvari et al. 2021*.

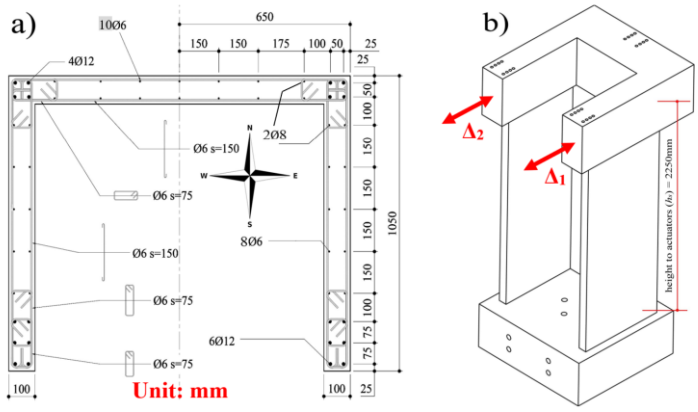

Figure 1. Test specimens UW1 and UW2: (a) cross-section and reinforcement layout, and (b) elevation view with the locations of displacement transducers. (Modified from Hoult et al. 2022).

The U-shaped RC walls UW1 and UW2 are half-scale specimens of the bottom 1.5 stories in a 6-story prototype building. Specimens UW1 and UW2 are identical with a wall thickness of 100 mm, web length of 1300 mm, and flange length of 1050 mm. The U-shaped wall specimen TUB with the same cross-sectional dimensions subjected to flexure was tested by *Beyer et al.* 2008. The wall geometry including reinforcement details is shown in Fig. 1a, and the elevation view of the test specimen with the location of the displacement transducers is given in Fig. 1b. Table 1 lists the key properties of three RC wall specimens including Specimen ID, the effective high of the specimen (H), the thickness of the wall (t_w), the concrete strength (f'_c), the rebar strength (f_y), and the reinforcements for the boundary and the walls.

This study uses the results of the TUB to validate the numerical model, then the same model techniques applied to simulate the responses of the UW1 and UW2. Figure 2 demonstrates the OpenSees modeling details. The MVLEM-3D element as shown in Fig. 2a is a three-dimensional four-node element with 24 DOFs for nonlinear analysis of flexure-controlled non-rectangular RC walls subjected to multidirectional loadings and newly implemented in OpenSees (*Kolozvari et al.* 2021). Figure 2b illustrates the model geometric discretization of the U-shaped wall specimen and for both the flanges and the web 10 MVLEM-3D elements are vertically stacked, in total 30 elements. There are twelve fiber elements in each MVLEM-3D element of the web wall, and there are ten fiber elements in each element of the flange wall (Fig. 2c). Each fiber element contains two uniaxial material models Concrete04 and SteelMPF. The two material behaviors are shown in Figs. 2d and 2e, respectively. All models were pinned at the base.

Table 1. Key properties of RC wall specimens.

Specimen ID	H (mm)	t_w (mm)	f'_c (MPa)	f_y (MPa)	Reinforcement			
					Boundary		Web (@mm)	
TUB	2950	100	54.7	D6: 518 D12: 471	Edge: Corner:	6D12+2D6 4D12+4D6	Vertical: Horizontal:	D6@150 D6@125
UW1	2250	100	38.2	D6: 550 D8: 538	Edge: Corner:	6D12+2D6 4D12+4D8	Vertical:	D6@150
UW2	2250	100	37.1	D12: 580	Edge: Corner:	6D12+2D8 4D12+4D8	Horizontal:	D6@150

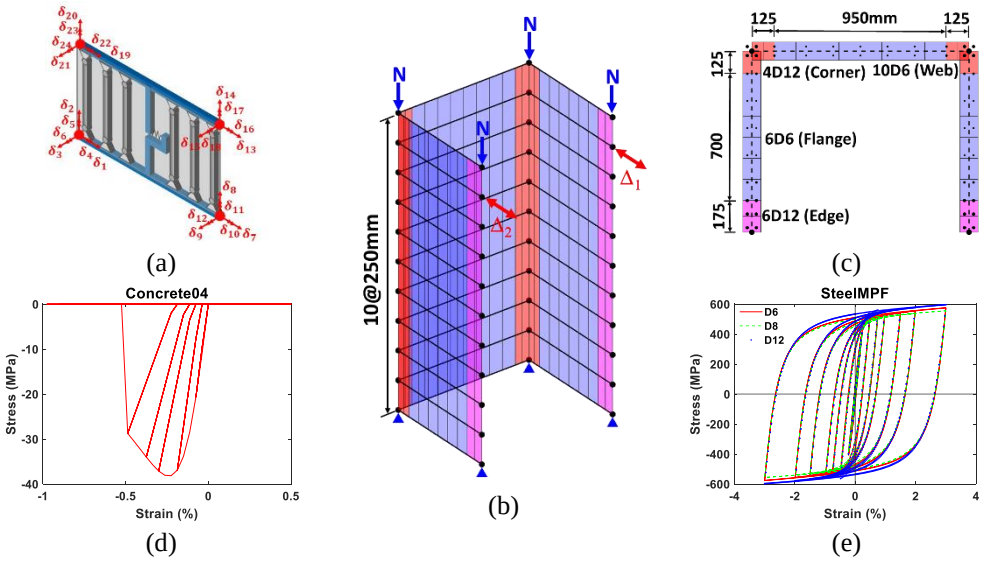

Figure 2. OpenSees Model: (a) MVLEM-3D element (from Kolozvari et al. 2021), (b) discretization and load

application, (c) cross-section discretization, (d) reinforced concrete material Concrete04, and (e) reinforcing steel material SteelMPF.

Figure 3 presents the hysteric responses of both wall specimens and the prediction inputs for the contest are listed in Table 2. The failure mode for UW1 is flexure with buckling of the longitudinal reinforcement followed by concrete failure, and the failure mode for UW2 is flexure with compression failure of concrete without buckling of the longitudinal reinforcement. The peak lateral forces for UW1 are +611kN in north direction and -567.6kN in south direction (see Fig. 1a). The peak torque for UW2 is 782.6kNm. The deformation at first excursion attaining 0.75 peak response is used to compute the initial stiffness for each test. For UW1 prediction, the plastic hinge length for each direction is 750mm (+) and 500mm (-), respectively. In addition, the failure is observed in south direction (Fig. 1a) as shown in Fig. 3a. Failure is here defined when there is a 20% drop in the pushing force or the torque in a load cycle. The results from the Blind Prediction Contest will be announced on October 10.

The methodology discussed in this paper will be useful in future SERICE studies on seismic vulnerability of RC wall buildings in Iceland.

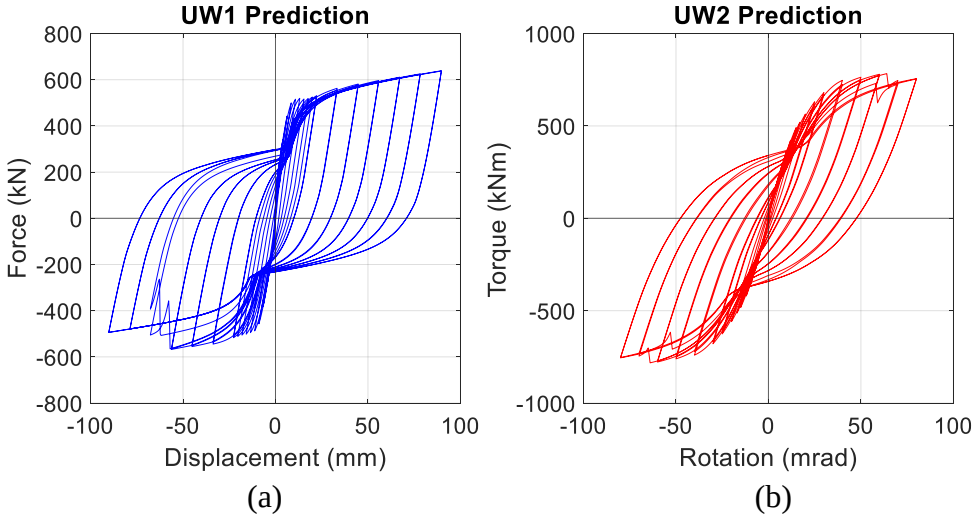

Figure 3. OpenSees Predictions: (a) UW1 subjected to pure flexure and (b) UW2 subjected to pure torsion

Table 2. Predictions for Specimens UW1 and UW2

Specimen ID	UW1 (flexure)	UW2 (torsion)
Failure mode	Flexure with buckling of longitudinal reinforcement followed by concrete failure	Flexure with compression failure of concrete, without buckling of longitudinal reinforcement
Peak response	+611kN / -567.6kN	782.6kNm
Ultimate deformation	-57.37mm	0.065rad
Deformation at first excursion attaining 0.75 peak response	+7.08mm / -7.84mm	0.022rad

References

Beyer, K., A. Dazio, and M. J. N. Priestley, Quasi-static cyclic tests of two U-shaped reinforced concrete walls, *J. Earthquake Eng.* **12**, 1023-1053, 2008.

Hoult, R., J. Almeida, and C. Doneux, A blind prediction of the seismic and torsional performance of RC U-shaped core walls, In *Proc. of the 3rd European Conference on Earthquake Engineering & Seismology*, Bucharest, Romania, 2022.

Kolozvari, K., K. Kalbasi, K. Orakcal, and J. Wallace, Three-dimensional model for nonlinear analysis of slender flanged reinforced concrete walls, *Engineering Structures* **236**, doi:10.1016/j.engstruct.2021.112105, 2021.

McKenna, F., G. L. Fenves, M. H. Scott, and B. Jeremic, Open system for earthquake engineering simulation (OpenSees), Pacific Earthquake Engineering Research Center, University of California, Berkeley, CA, USA 2000.

NORTHQUAKE 2022 - The 4th International Workshop on Earthquakes in North Iceland
Húsavík, North Iceland, 20 October 2022

Social Resilience in the Aftermath of a Natural Disaster

Tinna K. Halldórsdóttir[1]

[1]*Austurbru (AB). Iceland (tinna@austurbru.is)*

In December 2020, large landslides fell on a part of the settlement in Seyðisfjörður, East Iceland and caused property and environmental damage. This study uses demographic data, questionnaires, and interviews with residents and (first) responders. The aim is to examine the disaster's impact on the community and people in Seyðisfjörður, as well as to explore the factors that influence social resilience and how resilience manifests itself in the community.

The measurement tools consisted of questionnaires measuring a sense of cohesion, general health and post-traumatic symptoms, and questions regarding disaster awareness and experience. The main results indicate high community cohesion, and general health results indicate some difficulties and post-traumatic stress. The population is relatively aware of natural hazards in the area; they prefer to receive information directly from the authorities and state all instructions from them need to be very open and precise.

Those who suffered property damage felt, in part, they had received little resolution of their issues, and a quarter reported having no compensation yet. A few find it likely that they will move away in the next ten years, and there is a correlation between reporting lower general health, higher trauma, and higher intentions of moving away in the next few years. Residents found most of the first responses and aftermath to be very professional. However, in the days leading up to the incident and the moments after the mudslides, some needed more clarity and more precise instructions from the authorities. But overall, the residents are very grateful for the first responders and the support that followed directly after the landslides. Many mentioned that the community came together and showed great strength and compassion at this time.

The aftermath has included a long wait for a risk assessment which is a concern for residents, and many people feel uncertain about it, and its impact on the future.

Residents agree that more time is needed to assess whether the community will regain balance and if they will regain balance. Most seem to be optimistic about the future of Seyðisfjörður and see many possibilities and opportunities in the town. The results indicate a resilient community with a strong sense of cohesion. However, re-evaluation a few years from now regarding general health and trauma effects is needed.

Figure 1. Seyðisfjörður, December 2020. to July 2021.

Figure 2. Seyðisfjörður, July 2021.

Introducing MEDiate Horizon 2021 project in Iceland for Disaster-Resilient Society 2021 and the unique system dynamics approach to multi-hazard risk management.

Sólveig Þorvaldsdóttir[1]

[1]*University of Iceland and Rainrace Consultancy, Iceland, solvth@hi.is, solveig@rainrace.com*

The MEDiate Project (HORIZON-CLS-2021) focuses on the development of web-based disaster-risk management Decision Support Systems (DSS) for municipalities, businesses and citizens facing multiple interacting natural hazards and cascading impacts. The DSSs will model damage and consequence scenarios, which will allow stakeholders to test their policies on risk management, in particular policies on mitigation and preparedness for disaster operations. The results will allow stakeholders do design their disaster-risk management governance structures. The MEDiate DSS Concept model is shown in Figure 1. A key factor within the Concept Model is the aspect of dynamics, i.e. how things change with time.

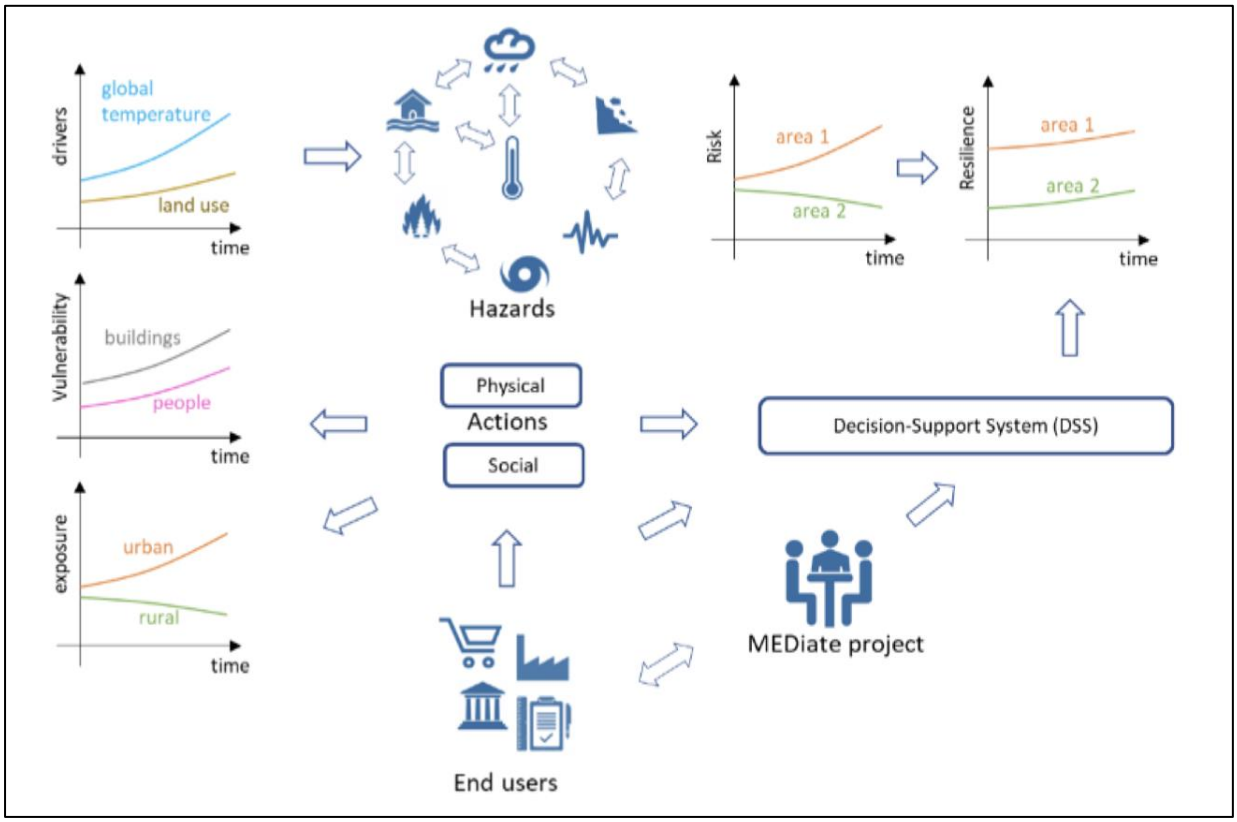

Figure 1. MEDiate DSS Concept Model.

The contribution from the University of Iceland focuses on research to support the scientific development of DSS systems for the municipality level. The work will involve applying a new and unique System Dynamics web-based resiliency model (*Thorvaldsdóttir and McDonald*, in review

process) to the context of four municipalities in Iceland, which all face the risk of natural disasters stemming for geophysical and meteorological threats, mainly earthquakes and mudslides. Two of the municipalities have recently experienced significant events, Árborg and Múlaþing, and two of the municipalities have experienced minor events (Norðurþing (Húsavík) and Fjallabyggð (Ólafsfjörður)).

The System Dynamics model is developed based on disaster-related methodology found in prior publications. For example, the premise of the model is that it is modelling a management system as defined by *ISO* (2013), meaning that its fundamental components are objectives and procedures to meeting an organization's goal. Herein the organization is a municipality. The goal is a reversed definition of a problem statement, where the problem statement is the definition of a disaster (*UNISDR* 2009): A serious disruption of the functioning of a community or a society involving widespread human, material, economic or environmental losses and impacts, which exceed the ability of the affected community or society to cope using its own resources. The goal therefore becomes: Having a well-functioning community or society with a low risk of serious disruptions to the functioning of a community or a society involving widespread human, material, economic or environmental losses and impacts and to cope with such events using a society's own resources if they occur (*Thorvaldsdóttir,* 2016). To reach this goal, the set of objectives in Table 1 are used (*Thorvaldsdóttir and Sigbjörnsson,* 2014). The objectives are the basis for a set of management functions that operate within three different phases. In order to meet the objectives, 4-5 procedures are defined for each objective, and various inter-objectives are procedures are also defined, leading to a total of 58 procedures (*Thorvaldsdóttir,* 2016).

Table 1. Disaster-related objectives, disaster functions and phase.

Objective	Management Function	Phase
1. To understand disaster risk	Analyze risk	I. Pre-Operations (the disaster-risk management activities)
2. To measurably reduce known disaster risk.	Mitigate Risk	
3. To prepare now for possible future operations.	Prepare for Operations	
4. To control damaging processes and threatening situations.	Impact Operations	II. Disaster Operations
5. To save lives	Life-saving Operations	
6. To relieve suffering of those affected.	Relief Operations	
7. To return a community to normalcy, same or improved.	Recovery Operations	
8. To improve systems and procedures based on experience	Learning	III. Post-Operations activities

System Dynamics methodology is used to understand the causal relationships between the objectives and the procedures. The causal relationships are depicted in Causal Loop Diagrams. Based on the feedback loops in the Causal Loop Diagrams, the formal System Dynamics model for key objectives and procedures for the municipality level was created (*Thorvaldsdottir and McDonald*, in review process). The results from the model depict how resiliency changes based on different policies, as shown in Figure 2.

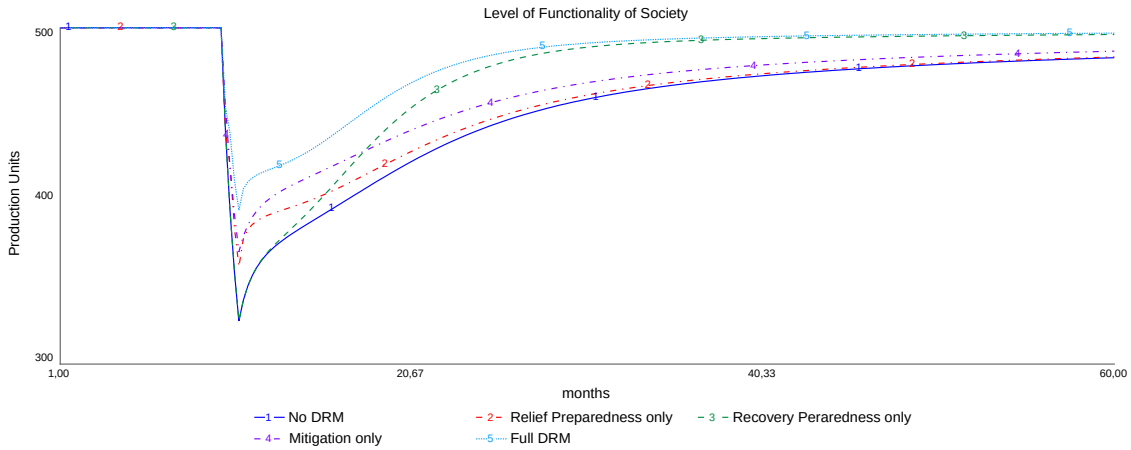

Figure 2. Calculated resiliency for a given risk level based various risk management policies: 1. None, 2. Relief preparedness only, 3. Recovery only, 4. Mitigation only, and 5. Relief preparedness, recovery preparedness and mitigation.

During the MEDiate application, staff from the four municipalities will be asked to provide input into the System Dynamics model through a web-based interface, which in turn will produce a context specific resiliency model. The results from each municipality will be shared and discusses with all four municipalities. Key research questions will be used to underpin the discussions and further develop the understanding of the elements required in of a disaster- risk management DSS for the municipality level. Research questions include:

1. Which decisions are important?
2. What is data and information needed for those?
3. What is the impact of the those decisions on other parts of the system?
4. What is the level of accuracy needed?
5. Can stakeholder decide acceptable risk level of damages and consequences?
6. How does the model increase understanding and/or interest of municipalities?
7. Are the municipalities inspired to further action?

The results will be shared with the municipalities participating in the project and through a report for wider distribution to municipalities in Iceland and other countries.

References

ISO. International Organization for Standardization. Retrieved from http://www.iso.org/iso/home/standards/management-standards.htm, 2013.

Thorvaldsdottir, S., and R. McDonald. In peer review at Natural Hazards Review, American Society of Civil Engineers.

Thorvaldsdottir, S., PhD disseration, Towards a Theoretical Foundation for Disaster-Related Management Systems: A System Dynamics Approach, 2016.

Thorvaldsdóttir, S., and Sigbjörnsson, R., Disaster-function management: Basic principles. *Natural Hazards Review*, ***15***(1), 48–57, 2014.

UNISDR. United Nations International Secretary for Disaster Reduction. *Terminology on disaster risk reduction*. Geneva: UN Retrieved from http://www.unisdr.org/files/7817_UNISDRTerminologyEnglish.pdf, 2009.